THE SLIDING WEAR OF UHMWPE AGAINST STEEL

by

A.I.G. LLOYD

A thesis submitted to the Faculty of Engineering,
University of Cape Town in fulfilment of the degree
of Master of Science in Applied Science

Department of Materials Engineering,
University of Cape Town

APRIL 1986

ACKNOWLEDGEMENTS

I would like to thank all the people who assisted me in this project and contributed to its final completion.

In particular, I wish to thank Mr Robert Noël, my supervisor, for his keen interest, unlimited advice and expert direction throughout my research.

I am very grateful to Mr Nicholas Dreze and Mr Andrew Rapley for their assistance in the assembly and maintenance of the experimental apparatus.

Mr Bernard Greeves is thanked for his photographic expertise.

I also wish to thank Mrs Helgard Böhm and Mrs Sue Betz for their help in the laboratory and in the preparation of the manuscript.

Miss Tracey Leveton is thanked for her speed and efficiency in the typing of the manuscript.

Finally, I would like to thank the staff and students of the Department of Materials Engineering for their friendship and support.

I am also grateful to the CSIR for the bursaries awarded during my postgraduate studies.

This thesis was based on the results of the colloborative programme of work undertaken as part of the research and development programme of the Research Organisation of the Chamber of Mines of South Africa.

ABSTRACT

This project has been undertaken in order to investigate the wear of polymeric sliding components in newly developed hydraulic stoping machines used in the South African gold mining industry.

The wear mechanisms causing the degradation of these components underground were identified during an extensive microscopic examination of worn components taken from in-situ stoping machines. Scanning electron microscopy (SEM) and energy dispersive X-ray analysis (EDS) techniques were used to determine the composition, size and distribution of abrasive particles embedded in the surfaces of worn components.

Abrasive wear by quartzite particles trapped between the sliding surfaces was identified as the primary wear process leading to degradation of the in-situ components. Wear also resulted from the reciprocating action of the sliding steel counterfaces whose surface roughnesses varied considerably.

Furthermore, a reciprocating sliding wear testing machine was designed which effectively simulates the sliding action of a polymer seal against a steel piston in a hydraulic cylinder.

The wear behaviour of UHMWPE sliding against AISI 431 martensitic stainless steel, in the absence of abrasive particles, was investigated during a series of laboratory tests in which the sliding velocity, normal load and counterface roughness was varied systematically over a wide range. More importantly, the effect of changing the lubricating medium from a 5:95 oil/water emulsion to plain tap water was carefully monitored. The specific wear rate, coefficient of friction and surface temperature-rise data were recorded during each test. The worn surfaces were then examined in the SEM in order to identify the wear mechanisms and to compare the surface morphologies with those of the in-situ components.

The laboratory wear tests showed that the wear rate of the polymer was significantly lower during tests in 5:95 as compared with those conducted under water lubrication.

An increase in sliding velocity caused the wear rates in both lubricating media to increase. The wear rate also increased with counterface roughness and a change in the mode of material removal was observed at a surface roughness of approximately 0,3 micrometers c.l.a. The specific wear rate was found to be independent of the normal applied load.

GLOSSARY

z : Vertical deviation of a surface profile from a datum line
L : Sample length of a surface profile
R_a : Roughness average
c.l.a. : Centre line average roughness
σ : Stress
ϵ : Strain
τ : Shear stress
$\dot{\epsilon}$: Rate of strain
t : Time
E : Elastic modulus
η : Viscosity
μ : Coefficient of friction
W : Normal load
ρ : Density
v : Sliding velocity
V : Vertical velocity
h : Thickness of the lubricant film
U : Horizontal velocity
p : Pressure
M : No. of asperity contacts
A_o : Nominal area of contact
A_r : Real area of contact
p_o : Yield Pressure
s : Shear Strength
F : Friction force
θ : Semi-apex angle of a conical indenter
Ag : Area of an abrasive groove
$\bar{p}$: Mean pressure per asperity
m : Mass
C_s : Spring constant
C_d : Damper constant
x : Sliding distance
K_o : Specific wear rate
φ : Mean surface temperature
R : Thermal resistance

CONTENTS

PAGE

CHAPTER 1

GENERAL INTRODUCTION

For a little under two decades, the Research Organisation of the Chamber of Mines of South Africa has been involved in a collaborative research and development programme for the gold mining industry which is concerned with the improvement of profitability and productivity by providing more advanced mining technology, improved underground working conditions and optimum utilisation of the labour force.

The development of hydraulically powered rockdrills which can be held and controlled manually, and hydraulic impact hammers for non-explosive rock breaking are challenging problems facing the mechanisation programme. Hydraulic power, which until recently had only limited application in gold mining, has gradually replaced the more traditional forms of power used underground on account of it's ability to produce high, readily controlled forces in small packages. This is particularly relevant in the South African gold mines because of the exceptionally high rock strengths and the constraint of narrow working areas. Originally it was decided on economic, technical and environmental grounds that dilute, water-based fluids rather than mineral oil, would be used as the hydraulic power medium, and that fluids containing typically 95% water and 5% additives to confer a degree of lubricity and corrosion protection would be employed. The engineering obstacles associated with the use of this type of fluid were identified and prototype versions of the rockdrill were tested both in the laboratory and underground. This led to full-scale production trials of the rockdrills built to commercial manufacturing standards. Similarly, the performance of the impact hammers was evaluated during experimental service underground. In both cases hydraulic power was supplied from centralised pumping stations situated remotely from the face.

The environmental conditions in South African gold mining stopes are extremely harsh, and are deleterious to all types of engineering equipment. The reliability of hydraulically powered mining systems, in particular, is

adversely affected by wear problems related to the stoping environment. Hard, sharp quartzite rock particles, which are too small to be filtered by conventional methods, are entrained in the hydraulic fluid and cause severe wear of internal components sliding under load or with a given clearance.

A new concept, named hydro-power, is currently under investigation for the purpose of powering stoping machinery. The concept involves the pumping of chilled and treated mine service water in a continuous pipeline from the surface to a deep level stope where the hydrostatic pressure head is used to power stoping machinery without the need for pumps. The transition from the use of water-based fluids to that of treated mine service water holds several attractions. The cost, maintenance time and unreliability of electro-hydraulic equipment would be eliminated, the design of the power supply system considerably simplified and the machinery could be powered and the mines cooled simultaneously. In addition, both filtration and water-treatment processes would be simplified as these are more feasible on the surface. Initial investigations have shown that there is no fundamental reason why equipment now operating on dilute, water-based fluids cannot be converted to operate on mine service water, even allowing for the poor lubricating properties of the latter. The use of water-based fluids is thus viewed as an intermediate stage in the progress towards the use of water alone.

Corrosivity represents the area of maximum difference between water and water-based fluids. The mine service water used in South African gold mines is extremely corrosive. The quality is very variable but it often contains a high concentration of dissolved solids, with sulphate and chloride ions predominating. The problem of overcoming corrosion is being tackled in two different ways. One approach is to reduce the aggressiveness of the environment by improving the quality of the mine service water. To date, good progress has been made in this field and includes both preventative and treatment methods. The second approach is based on the development of appropriate corrosion resistant engineering materials. A new range of alloys has been developed, the properties of which can be varied to meet the requirements for particular applications, but which have in common the properties of corrosion resistance, wear resistance, strength, adequate workability and weldability (Chamber of Mines Research Organisation Annual Report, (1982)).

The introduction of the hydro-power system can, therefore, only be realised if the complex materials engineering problems presented by corrosion and wear are successfully resolved. If the advances made in the selection of corrosion and wear resistant engineering materials are supported by better design and the improvement in the quality of the mine service water then the implementation of this concept into the gold mining industry could become a reality.

CHAPTER 2

IDENTIFYING THE PROBLEM

The degradation of internal sliding components, particularly the polymeric seals and bearings in the experimental rockdrills and impact hammers, is an area which requires further research before the transition is made from high water-based fluids to mine service water as the hydraulic power medium.

Thus a research project, aimed at finding a solution to this problem, was initiated by the Engineering Materials Branch (M.A.B.) of the Chamber of Mines Research Organisation. In order to achieve this aim it was necessary (i) to become familiar with the in-situ operation of the hydraulic hammers and drills, including the materials used for the various components, their function and the operating conditions to which they are subjected during normal operation; (ii) to identify the factors causing degradation of these components underground. These include wear processes resulting directly from the sliding process and, more importantly, wear caused by the intrusion of foreign elements from the external environment; (iii) to develop a laboratory research programme which would alleviate these problems and enhance our understanding of the mechanisms responsible for the wear of the components so that future selection of materials could be placed on a firm scientific foundation.

2.1 THE HYDRAULIC IMPACT HAMMER

The hydraulic impact rockbreaking machine consists of a chisel-shaped impacting hammer mounted on a machine frame which houses hydraulic power generation systems, control mechanisms and actuators. These, in turn, are mounted on and move along a guide rail linked to a rockhandling conveyor. The hammer is capable of delivering blows of approximately 3000 Joules at a frequency of 5 Hertz (300 blows per minute). The percussion mechanism operating in the hammer is based on the struck bit principle whereby the impacting tool is held in contact with the rock and struck by a moving impact head within the body of the machine, as

illustrated in Figure 2.1. The stroke of the impact head is 85 mm and maximum sliding velocities of 10 $m.s^{-1}$ are reached during the firing stroke. (The maximum sliding velocity reached on the return stroke is approximately 0,9 $m.s^{-1}$). In addition, fluid pressures of up to 18 MPa are reached during each impacting cycle.

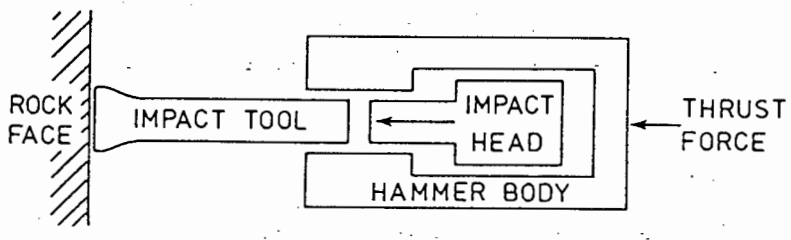

FIGURE 2.1 : The struck bit percussion mechanism operating in the hydraulic impact hammer

During the return stroke of an impacting cycle, water, at high pressure, causes a valve mechanism within the impact head to close. This action causes the impact head to slide backwards, compressing hydraulic fluid in a cavity and gas behind an accumulator piston. The subsequent release of this pressure provides the thrust force during the firing stroke of the cycle. Figure 2.2 shows the location of the seals and bearings of the impact head in a hydraulic impact hammer.

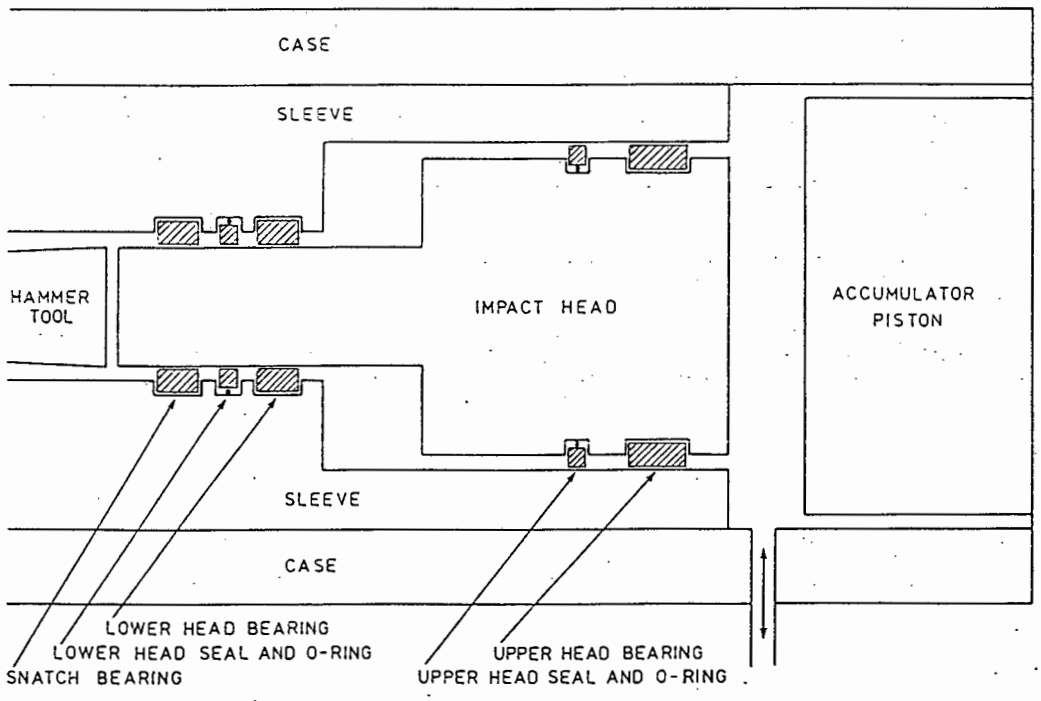

FIGURE 2.2 : A schematic representation of the seal and bearing arrangement of the impact head

Table 2.1 shows the materials comprising a few selected sliding couples in the impact hammer and Table 2.2 the operating conditions to which each is subjected.

TABLE 2.1 : Typical materials specifications for selected components from a hydraulic impact hammer operating on 5:95

	IMPACT HEAD	SNATCH BEARING	LOWER HEAD SEAL	LOWER HEAD BEARING
Material	817M40 Quenched & Tempered	Delrin 500 (Polyacetal homo-polymer)	ME 106 (UHMWPE)	Delrin 500
Hardness	30-40 HRC Front end induction hardened to a depth of ± 25 mm -44 HRC			
Surface Roughness	0,8 micrometers c.l.a. (sometimes Cr-plated: roughness-0,3 micrometers c.l.a.)		± 1,8 micrometers c.l.a.	

TABLE 2.2 : Operating conditions encountered by the above mentioned sliding components during normal operation of the hammer

	OPERATING CONDITIONS		
	SNATCH BEARING	LOWER HEAD SEAL	LOWER HEAD BEARING
Impact Head	Bearing is stationary. Impact head runs nominally dry against it at a maximum sliding velocity of 10 $m.s^{-1}$	Stationary fluid/atmosphere seal. Sees pressures of up to 18 MPa. Maximum sliding velocity of impact head is 10 $m.s^{-1}$	Bearing is stationary. Impact head runs against it at a maximum sliding velocity of 10 $m.s^{-1}$. Lubricated with 5:95 emulsion

Figure 2.3 shows the variation in velocity and displacement, as a function of time, of the impact head sliding against the lower head seal during a full impacting cycle in a hydraulic hammer.

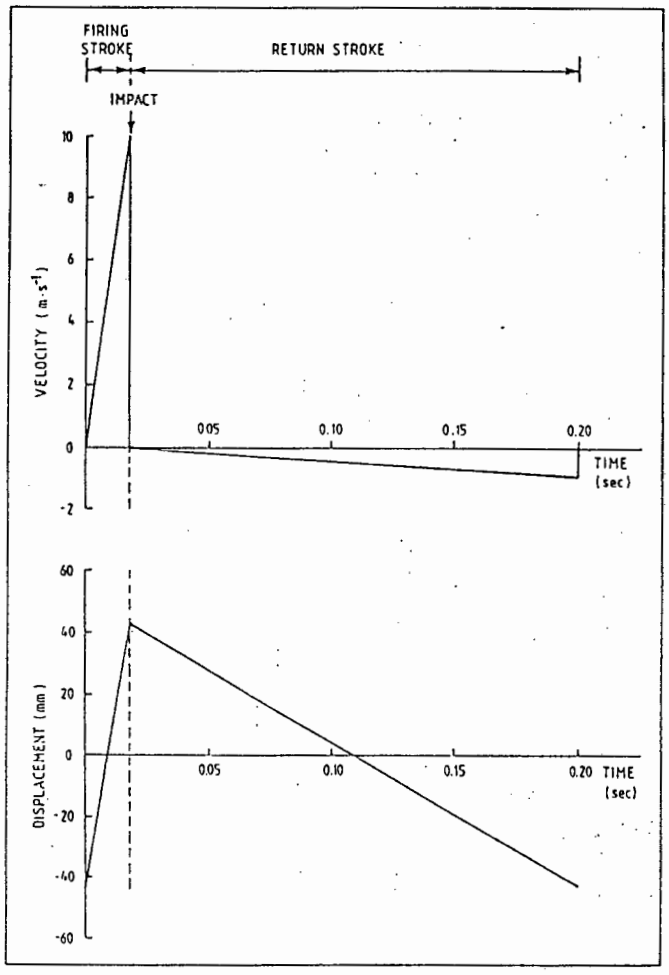

FIGURE 2.3 : Velocity/time and displacement/time curves for the sliding of the impact head against a lower head seal in the hydraulic impact hammer

Worn polymer seals and bearings, taken from impact hammers used in the underground production trials, were examined in the scanning electron microscope (SEM) in order to determine the mode of wear and to estimate the size and distribution of foreign particles embedded in the surface. Furthermore, energy dispersive X-ray spectrometry (EDS) was used to determine the compositions of these particles. Limited information regarding the service life of the machines was available except that all had operated on the high water-based hydraulic fluids.

The investigation revealed that abrasive wear by hard, sharp quartzite particles was the primary process causing degradation of polymeric components underground. The origin of these particles was twofold. Most entered the internal workings of the machines directly from the external environment. These particles ranged from a few micrometers up to one millimeter in size. Quartzite abrasives were also introduced via the

hydraulic fluid which is estimated to contain approximately 100 ppm particles smaller than 20 micrometers in size. Figure 2.4 shows quartzite particles, less than 100 micrometers in size, embedded in the lower head seal.

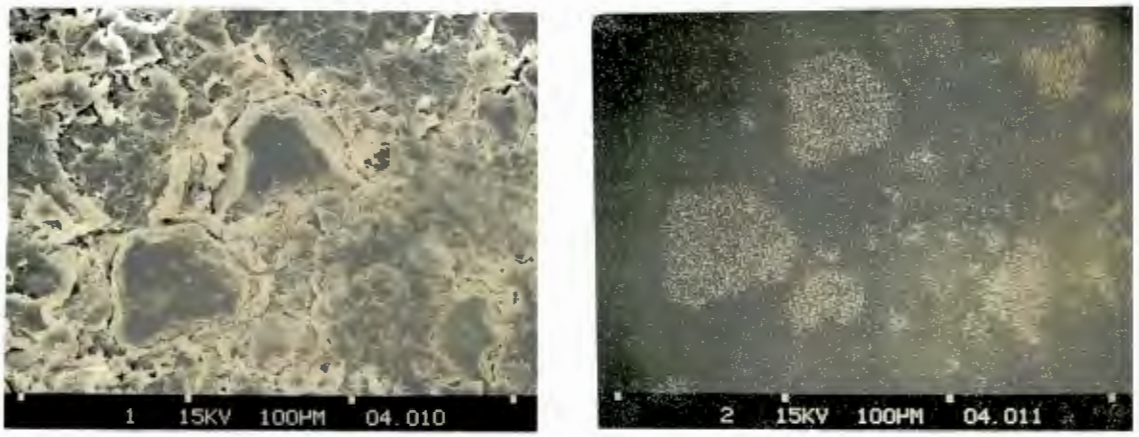

FIGURE 2.4 : A SEM micrograph and corresponding X-ray map showing quartzite particles embedded in the lower head seal

Metallic particles, some more than one millimeter in size, were observed embedded in a number of polymeric components as shown in Figure 2.5. EDS analysis revealed that the compositions of these particles were similar to those of the counterfaces against which sliding had taken place.

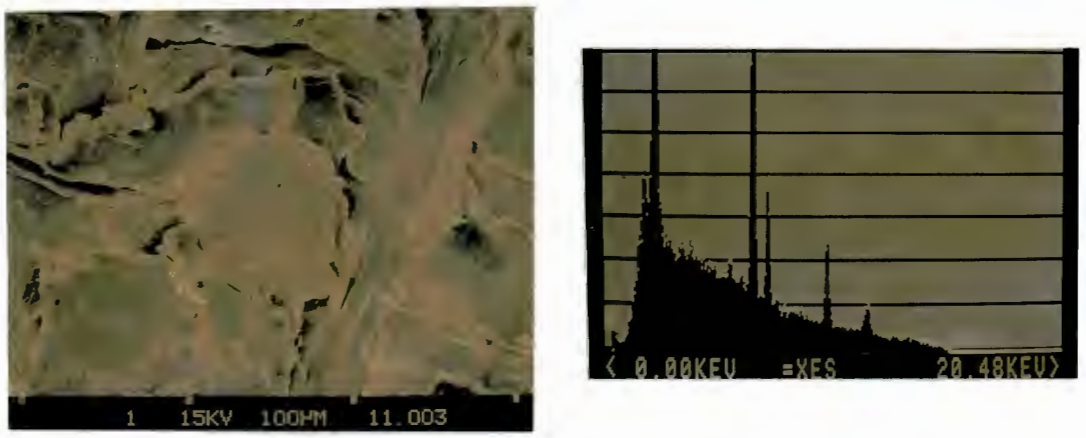

FIGURE 2.5 : EDS analysis of a metallic particle embedded in the upper head seal. (The Au peak is from the Au/Pd coating)

The bearings of the impact head and poppet were manufactured from a polyacetal homopolymer and the seals from ultra-high molecular weight polyethylene (UHMWPE). The relatively soft UHMWPE seals generally acted as filters to the abrasive particles by allowing them to become embedded in the sliding surface. However, the particles were unable to embed fully within the seals and generally tended to protrude above the seal surface. Figure 2.6 shows some abrasive particles embedded in a seal and exposing a flat face flush with the seal surface. A combination of wear by the reciprocating steel counterface and re-orientation of the particles by the high pressures occurring at the interface are probably the cause of the so-called "wear flats". These embedded particles actually reinforced the seal material by acting as fillers and limiting the amount of wear of the polymer material itself. However, the embedding process, coupled with the stresses occurring during sliding, led to embrittlement of the seals by the initiation and propagation of numerous cracks between and around the embedded particles as illustrated in Figure 2.6.

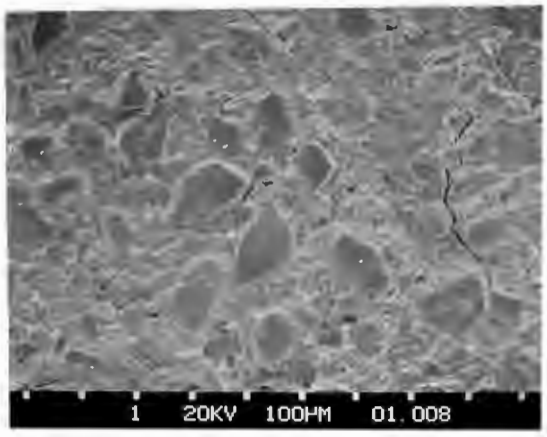

FIGURE 2.6 : Embedded quartzite particles in the lower head seal displaying the characteristic "wear flats"

Figure 2.6 also shows that the embedded particles often became dislodged from the seal surface during subsequent sliding. These loose particles caused serious abrasive wear of the seal surface before re-embedding elsewhere in the seal. Figure 2.7 shows that the wear damage was usually in the form of long, thin abrasive grooves in which tearing and cutting were the predominant material removal processes. Sliding, or adhesive, wear was also evident in some places, but was usually masked by the

abrasive processes which were occurring simultaneously at the interface.

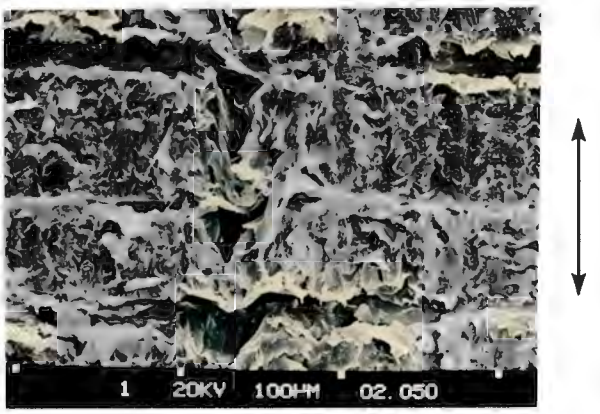

FIGURE 2.7 : Abrasive wear damage of the upper head seal. The arrow indicates the sliding direction

Examination of the worn bearings of the impact hammer, which are made from the harder, less ductile polyacetal polymer, showed that completely different mechanisms were responsible for the wear of these components underground. The function of these bearings is simply to support the weight of the sliding counterface. They are, therefore, not subjected to the extremely high pressures encountered by the seals. They run with a given clearance at speeds of up to 10 $m.s^{-1}$. The bearings are usually lubricated with 5:95 fluid although some are required to run dry.

The number and size of the particles embedded in the bearings was dramatically reduced. The particles, both quartzitic and metallic, were only lightly embedded in the bearing surface and were all smaller than 100 micrometers in diameter. Unlike the particles in the seals, these particles were sharp, angular and relatively unworn which indicates that they were only in sliding contact for short periods of time before leaving the surface. Instead of becoming embedded, deep grooves were ploughed across the bearing surfaces by the particles trapped between the bearing and the piston running with a given clearance. The abrasives acted as plough shears, driving up crests of deformed material ahead of, and to the sides of the advancing particle. Figure 2.8 shows abrasive wear of the snatch bearing by a quartzite particle.

FIGURE 2.8 : A quartzite particle in the process of ploughing out an abrasive groove in the snatch bearing. The arrow indicates the sliding direction

Therefore, in contrast with the damage resulting from the mass embedding of particles in the UHMWPE seals, deterioration of the polyacetal bearings resulted from the more conventional abrasive wear processes of ploughing and microcutting as illustrated in Figure 2.9.

FIGURE 2.9 : Abrasive wear damage on the surface of the upper head bearing. The arrow indicates the sliding direction

In addition to abrasion, evidence of sliding or adhesive wear was observed on some bearing surfaces. The polymer material was plastically strained in the sliding direction and subsequently smeared flat by the sliding counterface. Figure 2.10 shows adhesive wear of the upper head bearing.

FIGURE 2.10 : Adhesive (sliding) wear of the surface of the upper head bearing. The arrow indicates the sliding direction

2.2 THE HYDRAULIC HAND HELD ROCKDRILL

A number of worn UHMWPE piston seals taken from hand held rockdrills used in the production trials, were also examined. Figure 2.11 is a schematic diagram of the piston and piston seal assembly in the rockdrill.

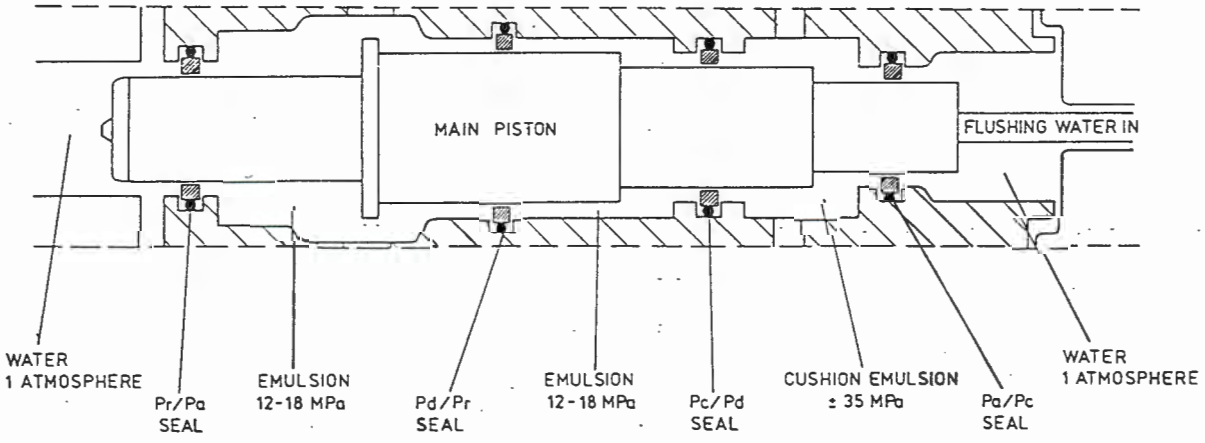

FIGURE 2.11 : The main piston and piston seals in the actuator assembly of the hand held rockdrill

The struck bit principle is also utilised in the rockdrills. The drills have a stroke of 23 millimeters and operate at a frequency of 50 Hertz. Maximum sliding velocities of 10 $m.s^{-1}$ are attained during the firing stroke of the cycle but the velocity decreases to 3 $m.s^{-1}$ on the return stroke. The piston seals see pressures as high as 35 MPa during an impact cycle. However, apart from their sealing function, they are also required to serve as bearings, locating and supporting the reciprocating piston. Tables 2.3 and 2.4 show the materials used and the operating conditions prevailing in the piston assembly of a hand held drill operating on 5:95.

TABLE 2.3 : The materials comprising the sliding couples in the piston assembly of the hand held rockdrill

	MAIN PISTON	PISTON SEALS
Material	835M15 - Carburised and case hardened	ME 106 (UHMWPE)
Hardness	Case : 2,5 - 3 mm thick Hardness : 60-63 HRC	
Surface roughness	Cr plated and liquid honed surface roughness : n4 (± 0,2 micrometers c.l.a.)	± 1,8 micrometers c.l.a.

TABLE 2.4 : The operating conditions seen during the sliding of the piston against the piston seals in a hand held rockdrill

	OPERATING CONDITIONS			
	Pr/Pa Seal	Pd/Pr Seal	Pc/Pd Seal	Pa/Pc Seal
Main Piston	Stationary fluid/atmosphere seal. Seals flushing water at 1 atmosphere from emulsion at 12-18 MPa. Maximum sliding velocity of piston - 10 $m.s^{-1}$	Stationary fluid/fluid seal. Seals emulsion at pressures of 12-18 MPa on either side. Maximum sliding velocity of piston - 10 $m.s^{-1}$	Stationary fluid/fluid seal. Seals emulsion at 12-18 MPa from cushion. Emulsion at 35 MPa. Maximum sliding velocity of piston 10 $m.s^{-1}$	Stationary fluid/atmosphere seal. Seals cushion emulsion at 35 MPa from flushing water at atmospheric pressure. Maximum sliding velocity of piston - 10 $m.s^{-1}$

Figure 2.12 shows the velocity/time and displacement/time curves for the piston sliding against the piston seals during normal operation of the hand held rockdrill.

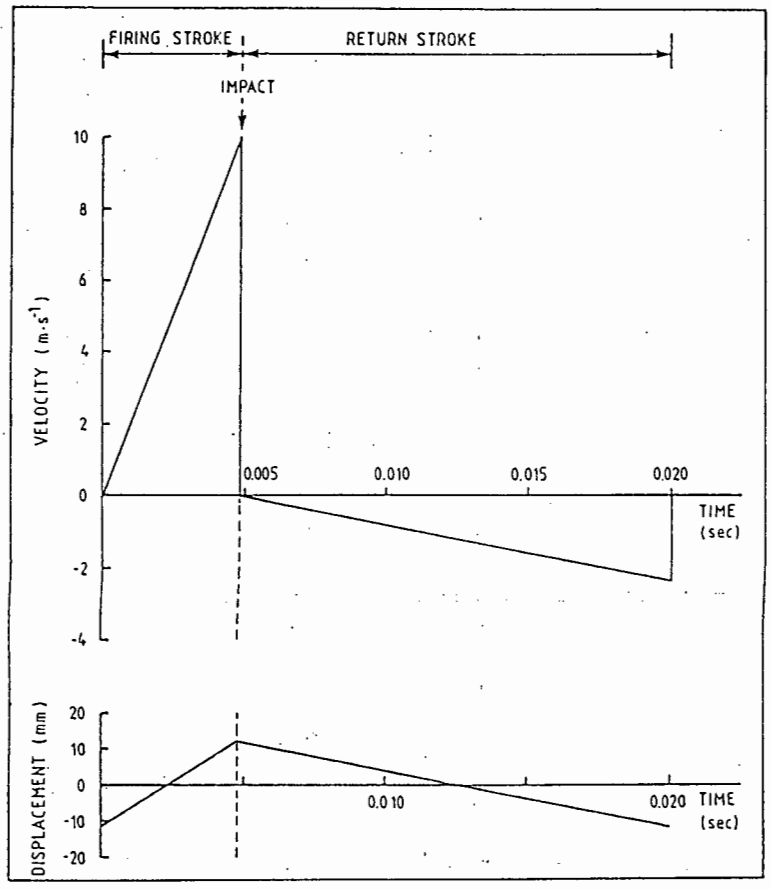

FIGURE 2.12 : Variations in velocity and displacement, as a function of time, of the piston sliding against the piston seals in a hand held rockdrill

The average operating life of a piston seal was estimated to be approximately 1500 minutes, which is equivalent to 500 drilled holes or a total sliding distance of 200 km. The piston seals are fluid/fluid seals, separating cavities containing emulsion at different pressures. However, some are required to seal emulsion at high pressure from flushing water at atmospheric pressure and it was reported that these seals, designated Pa/Pc and Pr/Pa respectively, were the most severely worn underground, resulting in their service lives being unacceptably short (Manager MAB, (1984)). A detailed SEM investigation revealed that typical abrasive wear processes, especially ploughing by quartzite particles, introduced via the flushing water, were responsible for the degradation of the seal surfaces as illustrated in Figure 2.13.

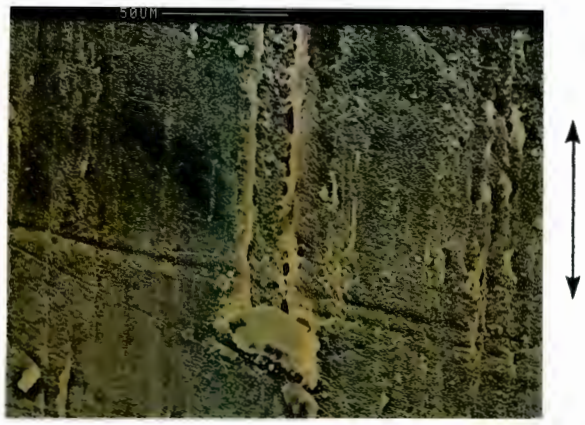

FIGURE 2.13 : Abrasion of a Pa/Pc piston seal by a quartz particle in a hand held rockdrill. The sliding direction is indicated by the arrow

The worn surfaces of some seals, the Pr/Pa seals in particular, were identical to those of the head seals taken from the impact hammer. Numerous quartz particles, all smaller than 100 micrometers in diameter, were deeply embedded in the seal surfaces. The associated wear flats and polymer embrittlement were also in evidence. These can be seen in Figure 2.14.

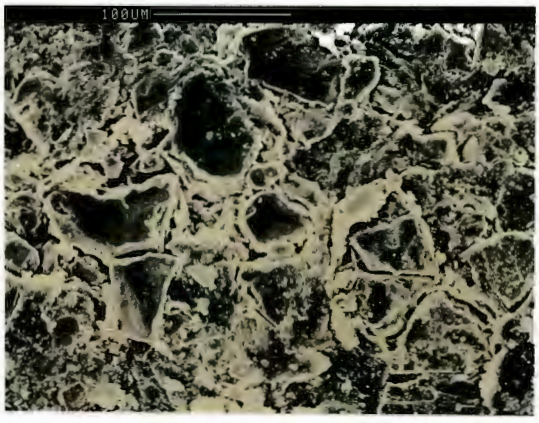

FIGURE 2.14 : Quartzite particles displaying "wear flats", embedded in an embrittled Pr/Pa piston seal.

In comparison, the Pd/Pr and Pc/Pd seals were relatively unworn. The only damage was caused by the embedding of a few quartz particles.

However, these particles were too large to have been entrained in the hydraulic fluid. They probably originated from the flushing water and entered the emulsion cavities via the Pr/Pa and Pa/Pc seals, respectively. The particles embedded without causing any prior abrasive damage to the seal surface. They were simply pressed into the surface by the extremely high fluid pressures prevailing in the emulsion cavities. Figure 2.15 shows quartzite particles pressed into the surface of a Pd/Pr seal.

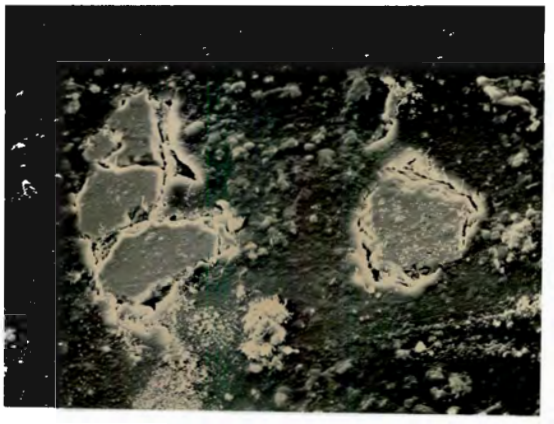

FIGURE 2.15 : Quartzite particles embedded in a Pd/Pr piston seal

2.3 THE AIM OF THIS PROJECT

The wear of internal sliding components in newly developed hydraulic stoping machines, such as the hydraulic impact hammer and hand held rockdrill, presents a major problem facing the mechanisation programme of the Chamber of Mines Research Organisation. The proposed transition from the use of high water based hydraulic fluids to pure water further compounds the problem by introducing the undesirable effects of corrosion and poorer lubricity. A collaborative research programme, encompassing design, water treatment and materials selection disciplines, was thus initiated to alleviate these problems.

A detailed examination of worn polymer seals and bearings from the experimental stoping machines operating on 5:95 was undertaken. The

investigation revealed that wear of these components underground was largely due to abrasion by quartzite particles which entered the internal workings of the machines directly from the external environment or were entrained in the hydraulic fluid. It is envisaged that through careful design and improved filtering methods the size and concentration of these abrasives could be considerably reduced.

The development of a laboratory wear testing machine which simulates, as closely as possible, the action of a steel piston running against a polymer seal in a hydraulic cylinder was considered to be of paramount importance aiding the study of sliding wear mechanisms and the resulting selection of wear resistant materials. Furthermore, the findings and knowledge gained from this study could be extended to various other sliding applications within the mining industry. The experimental rig, therefore, had to be extremely versatile in order to facilitate the testing of various sliding couples, under a wide range of operating conditions, including the addition of abrasive particles.

Clearly this project was not able to cover all the possible combinations of operating conditions required of a research programme of this nature. However, the development of the test facility, capable of good reproducibility, was useful in the study of the effects of sliding velocity, normal load, counterface roughness and, most importantly, type of lubricant on the wear of UHMWPE.

This investigation will serve as a solid basis for future testing which should include a comparison of these results with those resulting from the introduction of abrasive particles, as well as the testing of new materials and sliding couples. It is intended that the results obtained from the laboratory tests serve as a guide to the selection of materials for use in the stoping machines designed to operate in hydro-power systems.

CHAPTER 3

LITERATURE REVIEW

3.1 DEFINITION AND SCOPE OF TRIBOLOGY

Tribology is officially defined as: "The science and technology of interacting surfaces in relative motion and of related subjects and practices". The term was first defined by a British committee in 1966 from the word "tribos" which means "rubbing" in classic Greek. It is a study of the friction, lubrication, and wear of engineering surfaces and embraces all aspects of moving surfaces as well as the transmission and dissipation of energy and materials in mechanical systems (Czichos, (1978)). Thus, the work of the tribologist is truely interdisciplinary, embodying physics, chemistry, mechanics, thermo-dynamics, and materials science, and encompassing a large, complex, and intertwined area of machine design, reliability, and performance where relative motion between surfaces is involved (Moore, (1975)).

The technical function of numerous engineering systems depends on the process of motion. A feature common to all processes of motion is the occurrence of effects of "resistance to motion", i.e. the occurrence of friction in one form or another. As a consequence of friction the dynamic behaviour of the whole system is disturbed and some part of the energy of motion is dissipated. Further, if in a dynamic system one moving component consists of a solid body, the effect of friction is accompanied by wear: "The progressive loss of substance from the operating surface of a body occurring as a result of relative motion at the surface" (Czichos, (1978)).

In 1966 a study of the cost to Great Britain arising from poor tribological practice suggested that no less than £515 million per annum could be saved by improved application of existing knowledge (Halling, (1976)). This enormous sum arises from constituent savings shown in Figure 3.1.

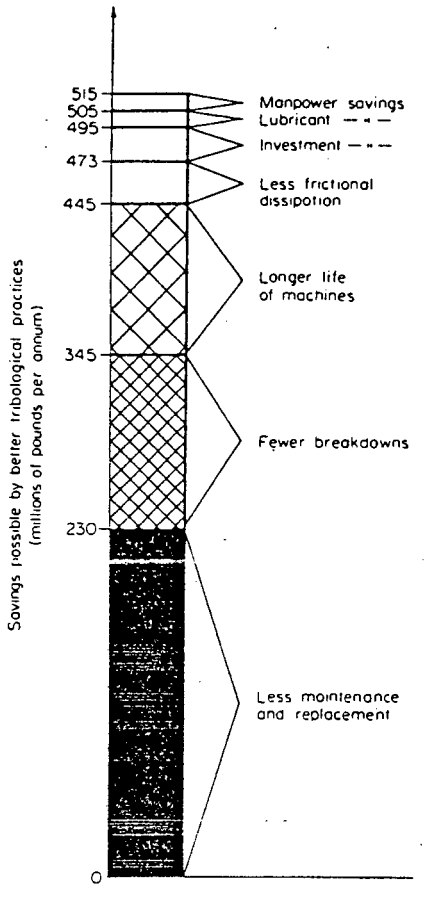

FIGURE 3.1 : Savings achievable in Britain each year due to better tribological practice (after Halling, (1976))

3.2 THE SURFACE TOPOGRAPHY

The geometric texture of ordinary surfaces is controlled by the characteristics of the finishing process by which they are produced. Close examination of these surfaces, even after the most careful finishing, shows that they are still rough on a microscopic scale. Figure 3.2 shows the various geometric components of a solid surface. The roughness is formed by random fluctuations in the surface, of short wavelengths (microroughness), characterised by hills, or asperities, and valleys of varying amplitude and spacing. On many surfaces a longer wavelength roughness called waviness is also observed and is often referred to as macroroughness whilst errors of form, in which the surface deviates from the desired shape, may occur due to errors inherent in the manufacturing process (Halling, (1975)).

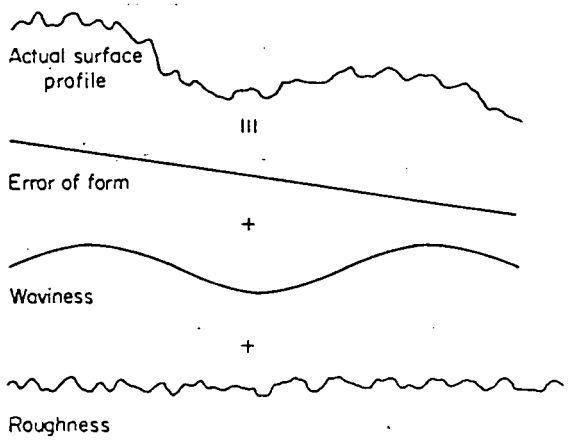

FIGURE 3.2 : The constituent geometric components of a solid surface (after Halling, (1976))

Surfaces which have been submitted to directional methods of processing exhibit a definite orientation of asperity distribution. It has also been shown that for such surfaces the heights of the peaks of the profile are distributed according to some statistical law i.e. Gaussian or exponential (Greenwood and Williamson, (1966); Whitehouse and Archard, (1970) as cited in Archard (1974)). Figure 3.3 shows a typical asperity height distribution curve for a ground surface and the method by which it is derived. It involves measuring the vertical ordinates z of the profile from some datum line along a representative length of the profile and summing the number of ordinates occurring at any given horizontal level in the profile.

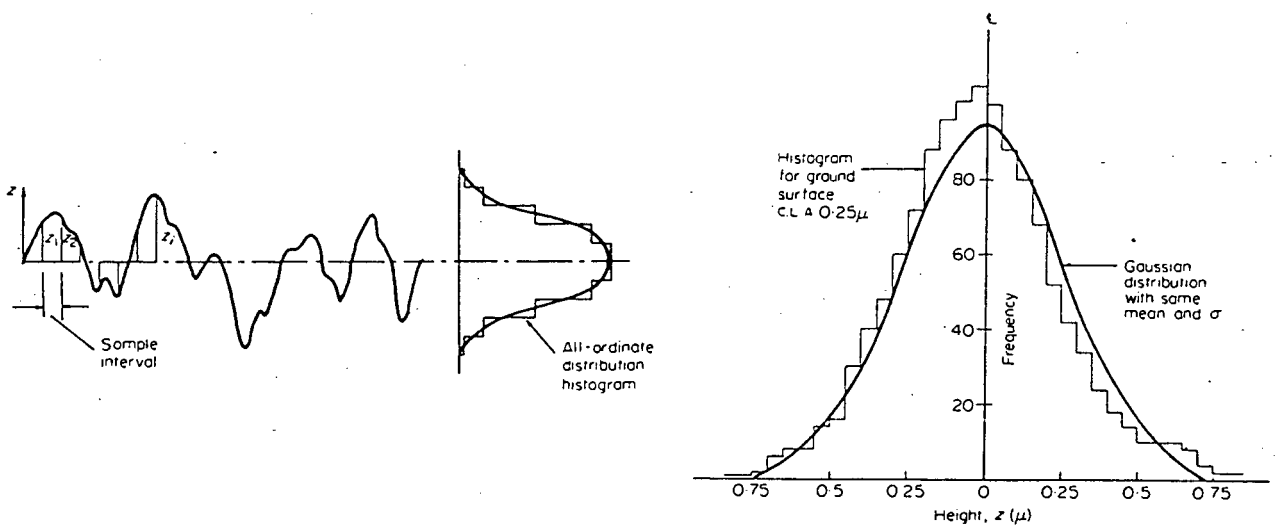

FIGURE 3.3 : The method of deriving the asperity height distribution of a ground surface (after Halling, (1975))

The problem becomes one of being able to measure the surface texture and to give it a value which is meaningful. Quantitative assessment of the topographic features of surfaces is of vital importance for solving a wide variety of problems in tribology. Measurements of these features will, therefore, prove indispensable in the study of all kinds of surface contact phenomena.

In order to make a quantitative assessment of the topographical features of a surface, three-dimensional maps are needed. Unfortunately, simple methods of reproducing these maps have not yet been developed. We must, therefore, rely on a two-dimensional profile of the surface together with observations using various microscopic techniques (Falkner, (1980)).

Profilometry is the most acceptable way of obtaining surface finish readings. The best known profilometry method is the stylus method, in which a fine diamond stylus traverses the surface irregularities and its vertical movements are amplified and recorded, usually by electrical systems. The higher vertical magnification, although useful in giving greater emphasis to the height characteristics of the surface, does mean that the resulting record is distorted. The surface asperities are undulations rather than sharp peaks and the appreciation of these gentle slopes occurring on machined surfaces is of great importance in tribology This is illustrated in Figure 3.4 which compares the actual surface profile with the distorted record produced by a profilometer. The datum from which this surface is measured is usually generated by a skid immediately succeeding the stylus. The major limitation of profilometers is that they are restricted to a single line sample which may not be representative of the whole surface. Another limitation arises from the size limitation of the stylus where it's finite size precludes it from complete penetration of all the valleys (Halling, (1975)).

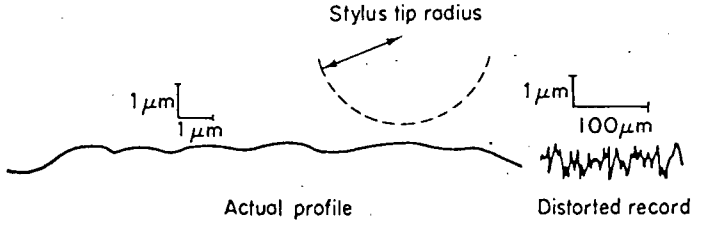

FIGURE 3.4 : The actual profile of a surface compared with the surface record obtained from a profilometer (after Halling, (1975))

The universally recognised parameter of surface roughness is the roughness average R_a or centre line average c.l.a. in which a centre line is drawn through the surface profile in such a position that the sum of the enclosed areas above and below the line are equivalent. The c.l.a. value is defined as the arithmetic average value of the vertical deviation of the profile from the centre line. In mathematical form this can be written as:

$$\text{c.l.a.} = \frac{1}{n_i} \sum_{i=1}^{n} |z_i|$$

where n is the number of points on the centre line at which the profile deviation z_i is measured. The centre line average is normally determined as the mean results of several consecutive sampling lengths L (Halling, (1975)).

Figure 3.5 illustrates the calculation of the c.l.a. surface roughness parameter.

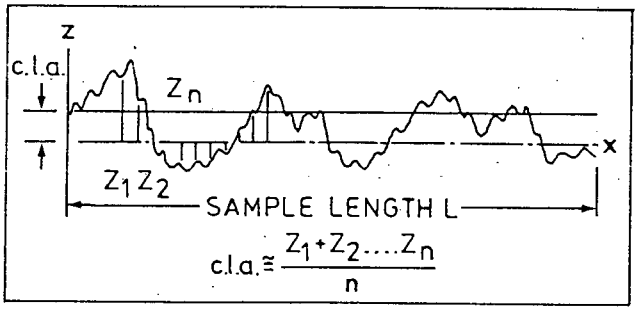

FIGURE 3.5 : The calculation of R_a/c.l.a. (after Yust, (1985))

These parameters are seen to be primarily concerned with the relative departure of the profile in the vertical direction only, they do not provide any information about the slopes, shapes and sizes of the asperities or about the frequency and regularity of their occurrence. It is possible therefore, for surfaces of widely differing profiles to give the same c.l.a. values as illustrated in Figure 3.6 (Falkner, (1980)).

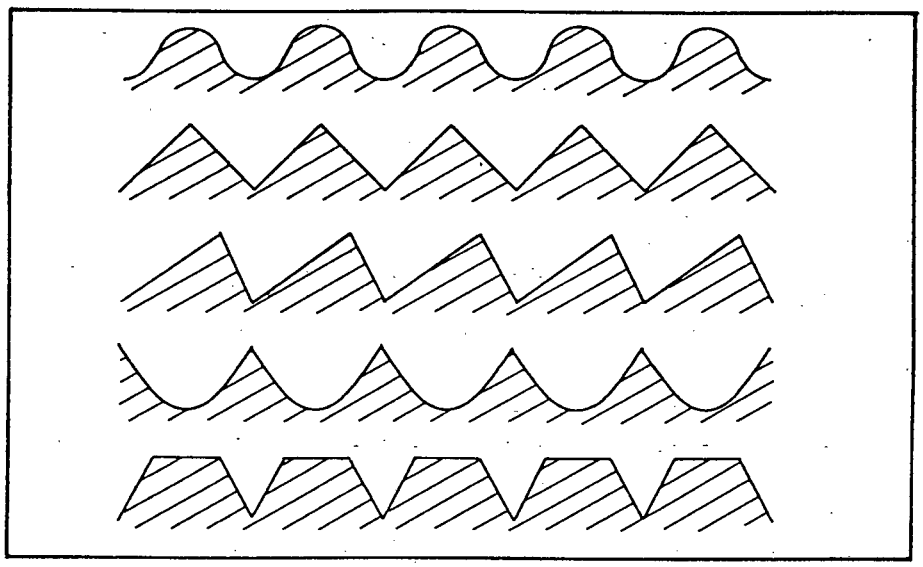

FIGURE 3.6 : Geometric profiles having the same c.l.a. value (after Falkner, (1980))

3.3 VISCOELASTICITY

The term viscoelasticity is commonly applied to materials which are neither ideal elastic solids nor viscous liquids, but in fact possess characteristics which are typical of both.

In a perfectly elastic (Hookean) material the stress σ, is directly proportional to strain ε and , for uniaxial stress and strain, we may write:

σ = constant x ε

where the constant refers to the elastic modulus E of the material.

In a perfectly viscous (Newtonian) fluid the shear stress τ, is directly proportional to the rate of strain $\dot{\varepsilon}$:

τ = constant x $\dot{\varepsilon}$

where the constant refers to the viscosity η of the fluid (Powell, (1983)).

These catagories are idealizations and any real solid shows deviations from Hooke's Law and any real liquid does not obey Newtons Law directly. There are two important types of deviations. Firstly, the strain (for a solid) or rate of strain (for a liquid) may not be directly proportional to stress, but may depend on stress in a more complicated manner, especially when the elastic limit of the solid is exceeded. Secondly, the stress may depend on both strain and rate of strain. Both these deviations are classified as viscoelastic. Thus, for viscoelastic materials the stress is a function of strain and time and so may be described by an equation of the form:- $\sigma = f(\varepsilon, t)$. (Moore, (1972)).

The most characteristic features of viscoelastic materials is that they exhibit a time dependant strain response to a constant stress (creep) and a time dependant response to a constant strain (relaxation). In addition, when the applied stress is removed, the materials have the ability to recover slowly over a period of time (Moore, (1972)). Figure 3.7 is a schematic representation of creep behaviour in viscoelastic materials. In a creep test a constant load is applied to the material and the variation of strain with time is recorded.

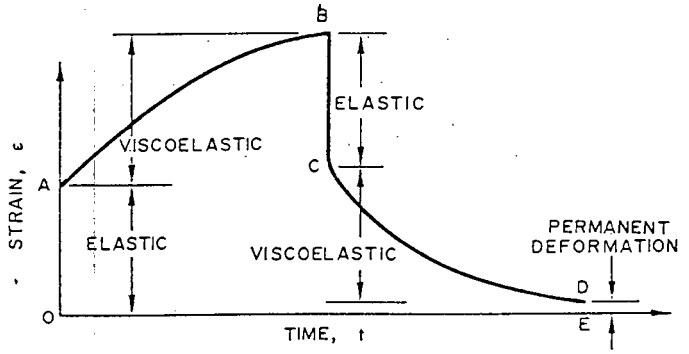

FIGURE 3.7 : A schematic representation of creep behaviour in viscoelastic materials (after Moore, (1972))

Upon application of the stress there is an instantaneous strain to point A, which is an elastic response. The sample then creeps viscoelastically to B. If the load is removed at this point there is an immediate elastic recovery to C followed by a final gradual viscoelastic recovery to D, leaving a permanent deformation D E.

The viscoelastic behaviour (creep and recovery) of polymeric materials can be simulated by mechanical models consisting of some suitable

combination of springs which obey Hooke's Law and viscous dashpots which follow Newtons Law (Crawford, (1981)). One such model is the Maxwell-Voigt model, consisting of Maxwell and Voigt elements in series as illustrated in Figure 3.8. One of the springs assumes the role of retarded elasticity and the other that of instantaneous elasticity - these being typical characteristics of viscoelastic performance.

The exponential responses predicted by these models are not a true representation of the complex viscoelastic response of polymeric materials. However, the simulation can be greatly improved by the addition of more elements to the model.

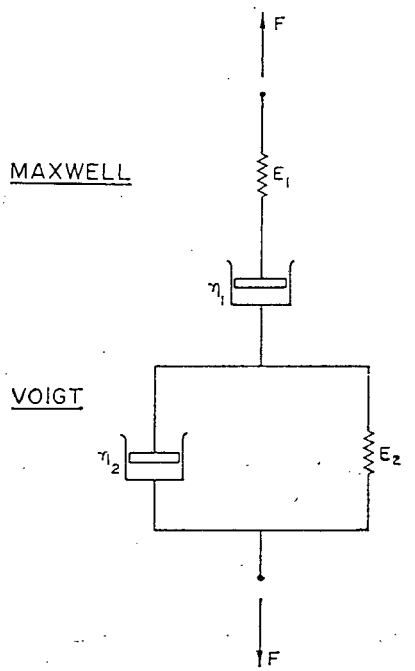

FIGURE 3.8 : The Maxwell-Voigt model used to simulate the viscoelastic creep behaviour of polymeric materials. E - Elastic modulus; η - viscosity

A knowledge of the fundamentals of viscoelasticity is important in this study as the modern concept of polymeric friction recognises the viscoelastic nature of its principal components (adhesion and deformation). When sliding occurs, it is no longer possible to identify unambiguously the separate contributions of adhesion and deformation to friction; both processes are influenced by the viscoelastic properties of the polymers in a similar way (Evans and Lancaster, (1979); Ludema and Tabor, (1966)).

3.4 LUBRICATION

Tribological processes, i.e., contact, friction and wear processes are, in general, related to direct physical interactions between relatively moving surfaces. All these processes can be influenced or modified by the process of lubrication. The purpose of lubrication is to seperate two surfaces moving relative to each other by a fluid film which can be easily sheared with low resistance without causing any damage to the surfaces. Depending on the thickness h of the lubricant film, the materials, the interfacial height distribution of the film, the operating conditions and the degree of geometrical conformity, different lubrication modes can be distinguished. These modes can be distinguished using the Stribeck curve which represents the general characteristic of lubricated moving surfaces as a function of the lubricant viscosity η, the sliding velocity v, and the normal load W (or pressure p) as illustrated in Figure 3.9. Thus, the friction coefficient μ is plotted as a function of the parameter $\eta.v.W^{-1}$ where η is the viscosity at the operating temperature. The three main lubrication regimes are (Czichos, (1978)):

I Hydrodynamic lubrication (and Elastohydrodynamic, EHD, lubrication)
II Partial EHD or mixed lubrication
III Boundary lubrication

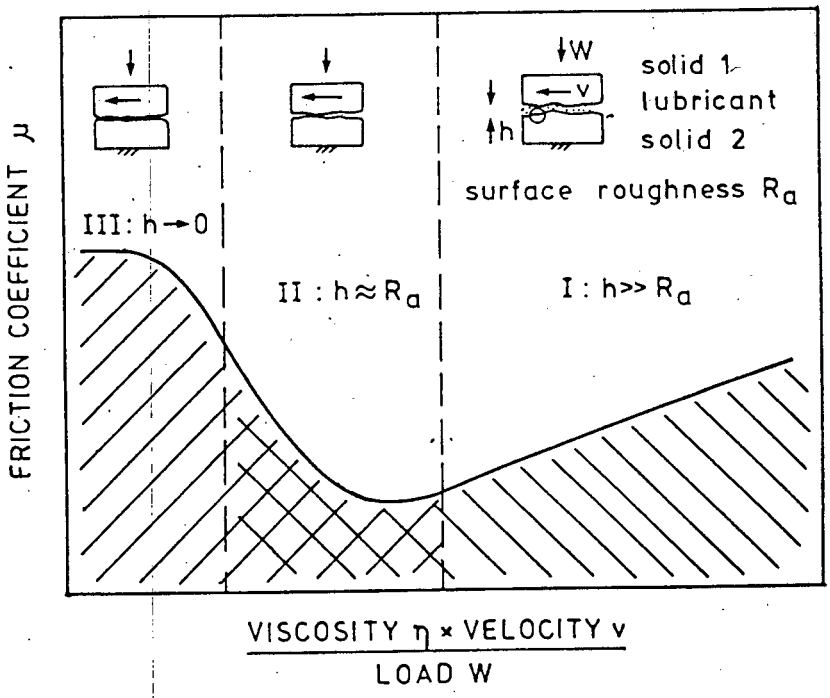

FIGURE 3.9 : The Stribeck curve showing the different lubrication regimes (after Czichos, (1978))

In regime I, the rigid surfaces are seperated by a continuous lubricant film, whose thickness h is much larger than the combined surface roughness measure R_a of the surfaces. Since in this regime no direct physical contact interactions between the surfaces occur, wear processes cannot take place (except surface fatigue wear, cavitation wear or fluid erosion). The tribological behaviour of the system is then mainly determined by the two following features:

i) The resistance to motion is given by the "internal friction" of the fluid, i.e, the shear resistance or viscosity of the fluid film.

ii) The effects of wear are eliminated if the geometry of the surfaces is such that a load-carrying pressure is set up in the lubricant film during the motion of the surfaces leading to a complete seperation of the surfaces (Czichos, (1978)).

3.4.1 Hydrodynamic Lubrication : Regime I

A simple definition of hydrodynamic lubrication is the pressure built up in the continuous fluid film by the wedging action produced by two non-parallel surfaces having relative motion which is sufficient to support an applied load without causing metal-to-metal contact. The load capactity will be greater at higher speeds and with higher values of viscosity (Deutschman et al (1975)).

The mathematical foundations of all hydrodynamic lubrication theory were laid in 1886 by Osborne Reynolds in deriving the equations named after him which are the basis on which all subsequent lubrication theory has been based. The derivation of the Reynolds' equation can be found in any standard reference (Deutschman et al, (1975); Halling, (1975)).

In its most general form, the Reynolds' equation is as follows:

$$\frac{\partial}{\partial x}\left[\frac{\rho h^3}{\eta}\cdot\frac{\partial p}{\partial x}\right]+\frac{\partial}{\partial y}\left[\frac{\rho h^3}{\eta}\cdot\frac{\partial p}{\partial y}\right] \equiv$$

$$\underbrace{6(U_1 - U_2)\frac{\partial(\rho h)}{\partial x}}_{\text{(wedge term)}} + \underbrace{6\rho h \frac{\partial}{\partial x}(U_1 + U_2)}_{\text{(stretch term)}} + \underbrace{12\frac{\partial(\rho h)}{\partial t}}_{\text{(squeeze term)}}$$

where U_1 + U_2 are horizontal velocities of the upper and lower surfaces respectively, V is the vertical velocity of the upper surface, and p is the local pressure within the film. The coordinates x and z are considered to be mutually perpendicular and in the plane of the lubricating film, with x taken in the direction of the velocities of U_1 and U_2. ρ and η are the density and absolute viscosity of the lubricant and h = h(x, z, t) describes the local instantaneous film thickness, as shown in Figure 3.10.

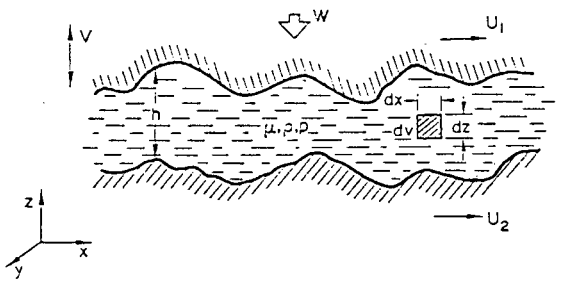

FIGURE 3.10 : The notation for Reynolds' Equation (after Moore, (1972))

For liquids, density variations are small and ρ can be eliminated entirely from the equation. Since horizontal relative velocity between the surfaces is significant and not the absolute magnitude of each component velocity, we can consider U_2 = 0 and the upper surface to move with velocity U.

With these substitutions, the generalised Reynolds equation becomes:-

$$\frac{\partial}{\partial x}\left[h^3 \frac{\partial p}{\partial x}\right] + \frac{\partial}{\partial y}\left[h^3 \frac{\partial p}{\partial y}\right] = 6\eta U \frac{\partial h}{\partial x} + 6\eta h \frac{\partial U}{\partial x} + 12\eta V$$

The physical significance of Reynolds' equation is that the generation of hydrodynamic pressure within the film is a function of three terms which have been called the wedge, stretch and squeeze

contributions to load support. In most common applications where the interacting surfaces are assumed to be smooth, rigid and inflexible, the stretch and squeeze terms may be neglected and load support may be attributed to the wedge effect, the latter being a consequence of non-parallel or converging surfaces in relative motion. However, if one or both sliding members has viscoelastic properties, it is clear that relative stretching of the material causes an additional increment in load support, although this effect is generally small compared to the wedge term. The squeeze contribution is due to normal approach of the surfaces, whether or not sliding motion occurs between them. This effect can be caused by impact, slow-speed squeezing or more commonly relative normal vibration between the surfaces (Moore, (1972)). Table 3.1 shows how the wedge, stretch and squeeze terms contribute separately to pressure generation in the film and hence load support.

TABLE 3.1 : Sources of load support using smooth surfaces (after Moore, (1972))

Description of system†	Schematic representation	Hydrodynamic equation
1. *Plane, smooth, rigid, inclined* surfaces. No vertical motion	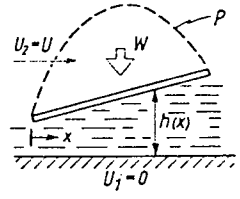	*Wedge Term:* $\frac{d}{dx}\left[h^3\frac{dp}{dx}\right]=6\mu U\frac{dh}{dx}$
2. *Plane, smooth parallel* surfaces. Lower surface *rigid* and *fixed*. Upper surface *flexible* and held at one end	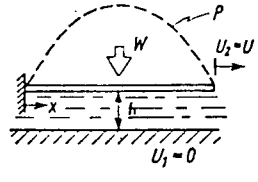	*Stretch Term:* $\frac{d}{dx}\left[h^3\frac{dp}{dx}\right]=6h\mu\frac{dU}{dx}$
3. *Plane, smooth parallel, rigid* surfaces. No side motion, lower surface fixed. Upper surface reciprocates vertically	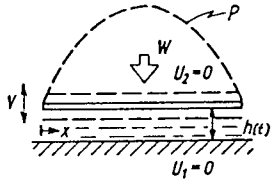	*Squeeze Term:* $\frac{d}{dx}\left[h^3\frac{dp}{dx}\right]=12\mu V$

† Incompressible, isoviscous liquid. Two-dimensional models.

If under conditions of hydrodynamic or EHD lubrication, the lubricant viscosity or the velocity decreases or the load increases, the lubricant film gets "thinner" and the separation of the surfaces decreases. If then the first asperity contact interactions occur, region II of partial EHD lubrication or mixed lubrication is reached. Refer to Figure 3.9. Similar conditions exist during lubrication of the soft and flexible surfaces of viscoelastic and elastomeric materials where the elastic deformation of the surfaces and the pressure dependance of the lubricant viscosity must also be taken into account. These effects drastically change the geometry of the lubricating film which in turn alters the pressure distribution of the contacts. Therefore, the hydrodynamic pressure generation must be matched with the elastic pressures. The load is now carried partly by the fluid film and partly by the contacting asperities. Thus, the friction resistance is due partly to the shearing of the lubricant film and partly to the asperity interactions. All types of wear are possible in this regime but are obviously modified by the action of the lubricating film.

3.4.2 Partial Elastohydrodynamic or Mixed Lubrication : Regime II

Consider the case where a thin lubricant film exists between the surfaces of a rough, rigid base and an elastomer, sliding with velocity U, as illustrated in Figure 3.11. ρ is constant, the squeeze term is zero, and the stretch term can be initially disregarded.

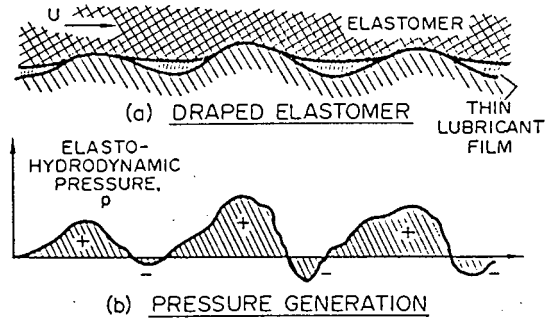

FIGURE 3.11 : The elastohydrodynamic seperating effect in lubricated sliding of elastomers (after Moore, (1972))

There is a hydrodynamic pressure wedge effect in the converging parts of the lubricant film which tends to lift the elastomer from the surface. This effect is partially resisted by the elasticity of the flexible surface, and a compatibility condition must eventually exist between the hydrodynamic and the elastic pressure distributions. This equilibrium produces a steady-state distortion effect in the surface of the elastic body. As a result, the normal flow pattern of the elastic body past the rigid base is affected by the creation of positive pressure increments on the peaks of the asperities and negative increments in the valleys. The summation of the positive increments far out weighs the negative ones, thus producing a net separating effect (Moore, (1972)).

If the lubricating conditions, operating in Regime II, change even further to the left of the Stribeck curve, the amount of asperity interactions increases, and the film thickness decreases down to some monolayers or below. Under these conditions boundary lubrication processes prevail (Czichos, (1978)). Refer to Figure 3.9.

3.4.3 Boundary Lubrication : Regime III

In this regime the bulk rheological properties of the lubricant are of less importance and the load is carried almost entirely through the deformation of the asperities. The physico-chemical interactions of the solid/lubricant/solid interface determine the friction and wear behaviour of the system. The processes which determine the tribological behaviour of solid surfaces are valid likewise under boundary lubrication conditions although they are modified by the boundary lubricant to some extent. The main purpose of a boundary lubricant is to interpose between the moving surfaces a film that is able to reduce the amount of direct solid/solid interaction and that is itself easily sheared. This is provided best by an interfacial film consisting of long chain molecules which attach themselves to the solid surfaces by adsorbtion processes (physical and chemical) or by chemical reaction (Czichos, (1978)).

3.5 FRICTION

3.5.1 The Real Area of Contact

For the contact between rough surfaces two terms must be distinguished as illustrated in Figure 3.12 (Czichos, (1978)).

i) The nominal area of contact A_o, i.e. the apparent area of overlap.
ii) The real area of contact A_r, i.e., the sum of the seperate microscopic areas at which the asperities are in contact.

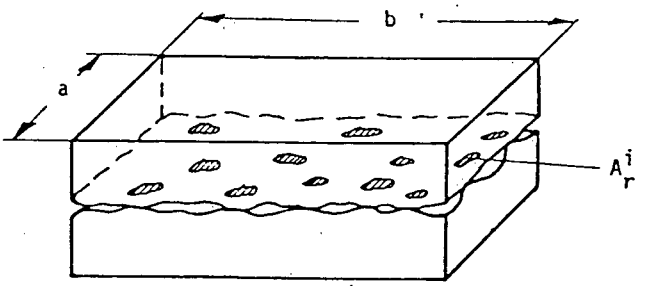

$$A_o = a \cdot b \gg A_r = \sum_{i=1}^{n} A_r^i \quad \text{(n: number of contacts)}$$

FIGURE 3.12 : Nominal and real area of contact (after Czichos, (1978))

The surface asperities of solid bodies in static contact are deformed elastically, plastically and viscoelastically and the area of contact is determined by the deformation properties of the materials and the detailed topography of the surfaces (Tabor, (1981)).

If two metal surfaces are brought into contact under the action of an applied load W, physical contact between asperities is established in at least three locations.

$$\text{Thus,} \quad W = \sum_{i=1}^{M} A_i \, p_i \quad (M \geq 3)$$

where A_i and p_i are the area and pressure produced by the contact at the "i'th" location.

Initially, the summation of the individual contact areas is too small to carry the load W. As a result, the pressure on the larger asperities increases rapidly to the plastic flow or yield pressure p_o of the softer surface. The load is therefore carried by these plastically deformed apserities and also by lesser asperities where the pressure is still elastic.

$$W = p_o \sum_{i=1}^{M_1} A_i + \sum_{j=1}^{M_2} p_j A_j$$

The second term, due to elastic contact, is negligible and may be ommitted from the equation.

$$\text{Thus} \quad W = p_o \sum_{i=1}^{M_1} A_i = p_o A_r$$

Plastic flow at the asperity peaks increases the size of the individual contact areas and the total area adjusts itself to match the applied load W. As W increases there is a proportional increase in A_r as illustrated in Figure 3.13. At the same time, the number of contacting asperities M increases so that the average contact area (A_r/M) remains virtually constant. Thus, for the situation where contact is wholly plastic, the actual contact area A_r is directly proportional to the first power of the load, i.e. $A_r \propto W$ (Moore, (1972)).

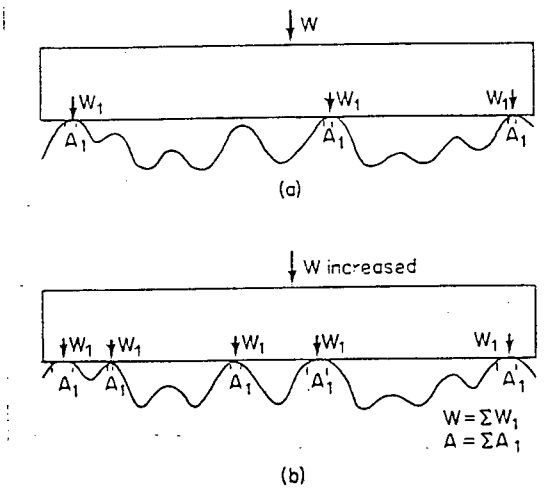

FIGURE 3.13 : The effect of increasing the load on the contact between a smooth, rigid surface and a rough surface having asperities of varying heights (after Halling, (1976))

However, during loaded contact between a rough surface and an elastomer, a situation develops in which the elastomer drapes physically about the major asperities of the support surface, and elastic pressures develop in the elastomer over the areas of contact. Hertz has shown that, for hemispherical asperities, the load vs. area relationship is:

$$A_r = K\, W^{2/3}$$

where K is an elastic constant. Thus, for elastic contact the real area of contact varies with the $^2/_3$ power of the load (Moore, (1972)).

For metal-on-metal applications the contact conditions can be described as elasto-plastic and in this case the load index lies between $^2/_3$ and unity, i.e., $A_r \propto W^n$, where $n = {}^2/_3\text{-}1$. Thus, during the initial contact of most metal surfaces prepared with an engineering finish the deformation will be mainly plastic and the true area of contact will be $A_r = W/p_o$. With repeated loading-unloading-loading of the same asperties, plastic deformation will change the shape of the asperities and the deformation will become elastic. The area of contact then becomes $A_r = W/p$ where p is some average value of contact pressure. Experimentally p has a values of the order 0,1 to 0,3 p_o. With polymers viscoelastic damping will introduce time and temperature dependant behaviour but, as a first approximation, the above models are satisfactory particularly for multiple asperity contacts (Tabor, (1981)).

Unfortunately, there is not a really satisfactory method of determining experimentally the area of contact while the surfaces are still in contact, particularly while sliding is taking place.

3.5.2 The Laws of Sliding Friction

The "friction force" is the resistive force, parallel to the direction of motion, which is experienced whenever one solid body slides over another. The tangential force required to initiate

sliding is the "static" or "initial" friction force whilst that required to maintain sliding is the "kinetic" (or dynamic) friction force (Moore, (1975)).

The classic laws of friction as they evolved from the early work of da Vinci, Amoutons and Coulomb may be summarised as follows:-

1) The friction force F is proportional to the applied load W, i.e. $F = \mu W$. Thus the coefficient of friction $\mu = F/W$.

2) F is independant of the apparent geometric area of contact A_0.

3) The static coefficient is greater than the kinetic coefficient.

4) The coefficient of friction is independant of sliding speed.

In the light of recent advances, however, most of them have been found to be incorrect and are now regarded only as rough empirical laws of limited validity (Tabor, (1981)).

The first law is correct except at high pressures when A_r approaches A_0. The second law appears to be valid only for materials possessing a definite yield point (such as metals) and it does not apply to elastic and viscoelastic materials (such as polymers and rubbers). The third law is not obeyed by any viscoelastic material whilst the fourth law is not valid for any material (Moore, (1972)).

3.5.3 Metallic Friction

A number of general theories have been proposed to explain the nature of dry friction between two metal surfaces. These include (Moore, (1975)):

Mechanical Interlocking :

Amontons and De La Hire in 1699 proposed that metallic friction

can be attributed to a mechanical interlocking of surface roughness elements.

Molecular Attraction :

Tomlinson in 1929 and Hardy in 1936 attributed friction forces to energy dissipation when atoms of one material are "plucked" out of the attractive range of their counterparts on the mating surface.

Electrostatic Forces :

According to this theory presented as early as 1961 stick-slip phenomena between rubbing metals can be explained by the initiation of a net flow of electrons, which produce clusters of charges of opposite polarity at the interface. These charges are assumed to hold the surfaces together by electrostatic attraction.

Welding, Shearing and Ploughing :

This most recent theory proposed by Bowden in 1950 is now widely accepted for metal friction. High pressures developed at individual contact spots cause local welding and the junctions thus formed are sheared subsequently by relative sliding of the surfaces. Ploughing by the asperities of the harder surfaces through the matrix of the softer material contributes the deformation component of friction (Moore, (1972)). Thus, friction occurs through asperity interactions, i.e. through a dissipative process involved in the joining and separation of micro-contacts as illustrated in Figure 3.15 (Czichos, (1978)).

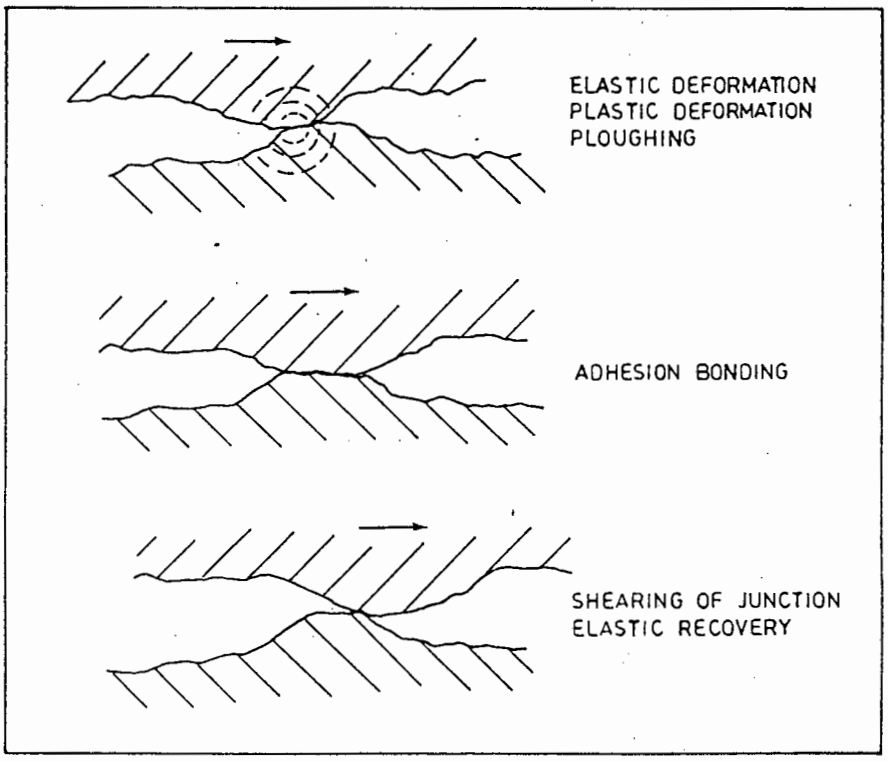

FIGURE 3.15 : A schematic representation of a unit event in the friction process (after Czichos, (1978))

The macroscopic friction force is the sum of the microscopic forces at the individual contact areas, and the energy dissipated may be expressed as the sum of the corresponding elementary dissipative processes. In the different stages of the formation and separation of a micro-contact, the following main processes are involved (Czichos, (1978)).

1) Elastic asperity deformation
2) Plastic asperity deformation
3) Ploughing
4) Shearing of adhesive junctions

For unlubricated surfaces in relative motion the different contributions to the overall friction may be broadly classified into two groups:

1) Adhesion processes
2) Deformation processes

As a first approximation: $F = F_{adhesion} + F_{deformation}$

There is a considerable amount of interaction between the frictional processes belonging to each group but by careful selection of experimental conditions it is possible to seperate the two terms (Czichos, (1978)).

3.5.3.1 The Adhesion Component of Friction

When two clean, smooth metal surfaces are brought into contact under load, local welding or adhesion bonding occurs at the tips of the major asperities. The welding process occurs through the action of surface forces (Czichos, (1978)).

1) Long-range or van der Waals forces, acting between any combination of materials down to a seperation of about one nanometer.

2) Short-range forces of metallic, ionic or covalent type, depending upon the nature of the materials in contact, acting at separations less than one nanometer.

In an ideal elastic-plastic material $W = A_r\ p_o$. For sliding to occur, the friction force F is needed to shear the weakest tangential planes at the areas of actual contact. Thus, neglecting the effects of junction growth, we may write:-

$$F_{adhesion} = A_r s$$

where s is the mean shear strength of the weaker material.

Thus, the coefficient of friction is:

$$\mu = \frac{F}{W} = \frac{A_r s}{A_r p_o} = \frac{S}{p_o}$$

This relationship defines the simple theory of adhesion for metals (Tabor, (1981)).

For most metals s is of the order 0,2 p_o so that, on this model, μ = 0,2. In practice, however, most metals in air give μ of the order unity. This discrepancy can be explained by the process of junction growth and is illustrated in Figure 3.16. Under the combined action of a normal and tangential force, the plasticity conditions in the junctions are exceeded. The area of contact therefore increases until the plasticity conditions are again satisfied. The junction area grows according to an empirical law of the form: $A = A_r [1 + \alpha (F/W)^2]^{\frac{1}{2}}$ where α has the value of order 9 (Tabor, (1981)).

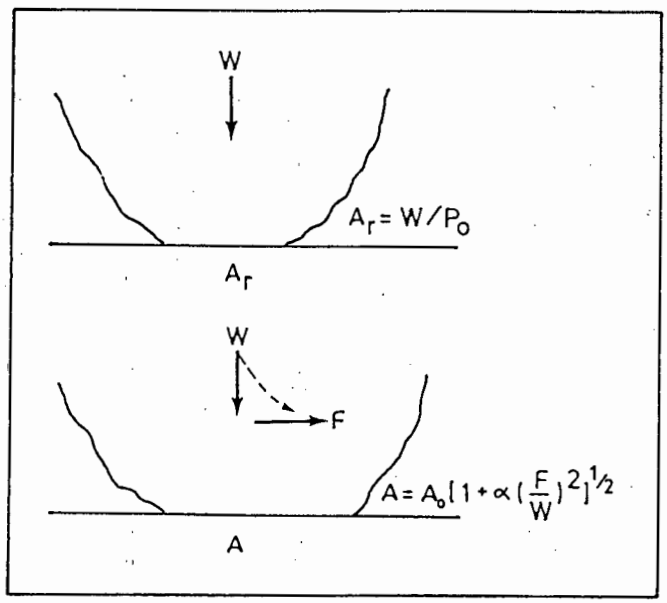

FIGURE 3.16 : The growth of an adhesive junction during sliding (after Tabor, (1981))

3.5.3.2 The Deformation Component of Friction

Recall : $F = F_{adhesion} + F_{deformation}$

$F_{deformation} = F_{ploughing}$ is that part of the total friction force caused by asperities on a hard metal penetrating into a softer metal and "ploughing" out a groove by plastic deformation. This is the major component of friction during abrasion and is also important when the adhesion term is small, as in lubricated sliding. The friction coefficient may be estimated from the forces required for plastic flow of the softer metal as illustrated in Figure 3.17.

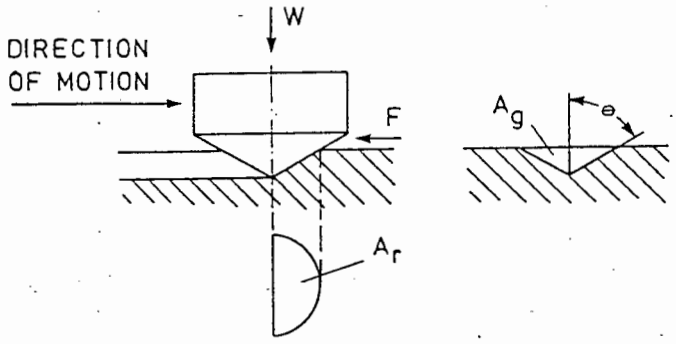

FIGURE 3.17 : The ploughing component of friction for the case of a hard conical indenter sliding over the surface of a softer material (after Czichos, (1978))

The normal load W is balanced by the yield pressure $p_{o(normal)}$ of the metal acting via the real contact area A_r :

$$W = A_r \, p_{o(normal)}.$$

The resistance to tangential motion F is balanced by the yield pressure $p_{o(tangential)}$ of the metal acting over the cross-sectional area of the groove A_g :

$F = Ag\ P_{o(tangential)}$

Assumming that the plastic-yielding is isotropic, i.e., $P_{o(normal)} = P_{o(tangential)}$, then : $\mu = \frac{F}{W} = \frac{A_g}{A_r}$

For the case of conical indenter : $\mu = 2/\pi \cot\theta$ where θ is the semi-apex angle of the indenter (Tabor, (1981)).

Similar expressions can be obtained for asperities of different shapes.

The ploughing component may be added arithmetically to that part of the friction due to adhesion. A proper treatment, however, should combine both mechanisms in a single plasticity model (Tabor, (1981)).

3.5.4 Friction in Polymers and Elastomers

There has been a dramatic increase in the utilisation of polymers, elastomers and polymer-based composite materials in a wide variety of tribological applictions. These materials, often with inherent lubricity, are increasingly replacing metallic components in engineering applications where marginal lubrication, dry conditions, corrosive and abrasive environments occur. Further, because of their elasticity, polymers are able to accommodate shock loading, shaft misalignment and bending better than metals. They also weigh less and in general, run more quietly (Thorpe, (1982)).

Lee (1974), Briscoe et al (1974) and Tabor (1974) suggest that the friction force resulting from the sliding of a polymer against a hard counterface may also be divided into two components, namely the adhesion component resulting from the shearing of adhesive bonds in the regions of real contact, and the deformation component resulting from the dragging of asperities of the counterface through the polymer surface. The relative importance of these two components is strongly influenced by such factors as the nature of the counterfaces, the load, the sliding speed, the

temperature, the environments, the thickness of the polymer and the lubricant.

Moore (1975) considered the contact between a rough, rigid surface and an elastomer loaded against it with load W. He proposed that the elastomer assumes the contour of the base surface by physically draping about its major asperities, as shown in Figure 3.18.

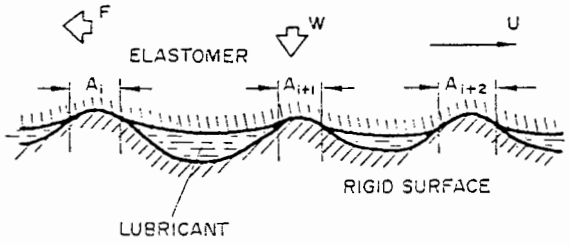

FIGURE 3.18 : Contact between an elastomer and a rigid base (after Moore, (1975))

Elastic pressures develop in the elastomer over the area of contact and the load is supported by these individual contact areas according to the relationship.

$$W = \sum_{i=1}^{M} A_i \, p_i = \overline{p} \, A_r$$

where $\overline{p}$ is the mean pressure per asperity, M is the total number of asperities over which the load W acts and the total actual contract area A_r is given by:

$$A_r = KM \, (p/E)^n$$

Here, K is a constant, E the Young's modulus of the elastomer, and the index $n \longrightarrow 1$ in most practical cases.

When a tangential force F is applied to the upper surfaces, adhesive forces develop at the contact locations, and if no relative motion occurs between the surfaces, we can write:

$$F = \sum_{i=1}^{M} F_i$$

The adhesive forces F_i are due to molecular bonding of surface atoms in both members.

Now, if F is increased until gross sliding at a steady speed occurs at the interface, the resistive force F now comprises of adhesion and deformation terms. The deformation term is due to a delayed recovery of the elastomer after indentation by a particular asperity and gives rise to what is generally referred to as the hysteresis component of friction.

Thus, for elastomers : $F = F_{adhesion} + F_{hysteresis}$ (Moore, (1975))

Figure 3.19 shows schematically the principal components of elastomeric friction. It is seen that adhesion is distinctly a surface effect and may be regarded as occurring to a depth in either surface which does not exceed molecular dimensions, whereas hysteresis is a bulk phenomenon which depends on the elastic or viscoelastic properties of the elastomer. However, both terms are a result of energy dissipation which gives rise to substantial temperature increases both at the sliding interface and within the bulk of the sliding bodies (Moore, (1972)).

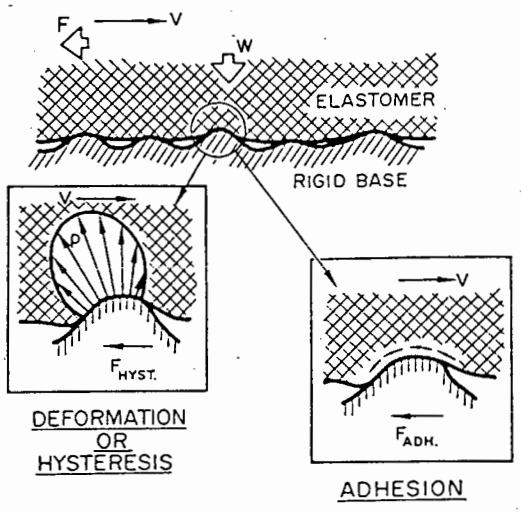

FIGURE 3.19 : The principal components of elastomeric friction (after Moore, (1972))

Friction can be considered as a macroscopic or microscopic mechanism. The microscopic or molecular mechanism can also be described as causative, since the molecular interaction of surface molecules of the sliding pair is treated in detail to establish the true cause of the friction mechanism. On the other hand, the macroscopic mechanism is often referred to as resultant, being based on a relatively crude simulation of frictional events and usually following a simple model representation.

3.5.4.1 The Adhesion Term

The exact nature of adhesion in elastomers is not certain, although it is generally recognised to consist of the making and breaking of junctions. On a microscopic scale, adhesion in elastomers is distinctly a surface effect. The process can be described as a dissipative, thermally activated molecular stick-slip mechanism. During relative sliding against a hard, rough surface, the flexible chains in the surface layer attempt to link with the molecules of the base, thus forming local junctions. Sliding action causes these bonds to stretch, rupture and relax before new bonds are formed. Thus, the elastomer molecules effectively jump a molecular distance to their new equilibrium position as illustrated in Figure 3.20 (Moore, (1972)).

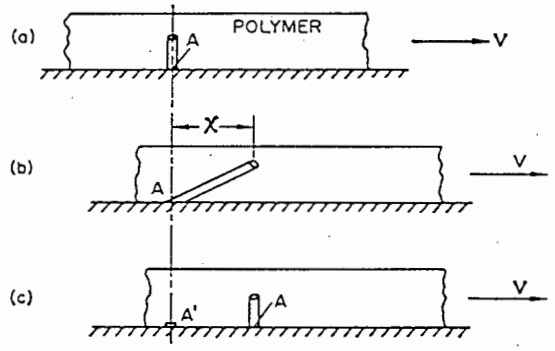

a) 'Adhesion' takes place at points A.
b) Elastomer sample moves a distance x at velocity v, and friction drag is developed. Elastic energy is stored in the element.
c) Adhesion at A fails. Energy stored in the element is returned in part to the system. New point of attachment at A.

FIGURE 3.20 : A simple micromechanism of adhesion in elastomers (after Moore, (1972))

From the macroscopic view point:

$$F_{adhesion} = \sum_{i=1}^{M} F_i = \sum_{i=1}^{M} A_i \, s_i$$

where A_i is the local macroscopic area of contact and s_i the local effective shear strength of the interface (Moore, (1972)).

The adhesion forces in polymers arise from two sources (Tabor, (1974)).

1) Electrostatic forces, i.e., the formation of an electrically charged double layer by the flow of charge at the interface between two materials of different electronic band structures

2) van der Waals forces and , if there are certain polar atoms present, from hydrogen bonding.

These forces are comparable with those existing between the polymer chains themselves so that, during sliding, shearing takes place at a short distance from the interface within the bulk of the weaker body resulting in the tearing out of polymer fragments. Thus, the adhesive friction force may be expressed in terms of the bulk shear strength of the polymer (Briscoe et al, (1974)), (Tabor, (1974)), (Rhee and Ludema, (1978)), (Tanaka and Miyata, (1977)).

Two notable exceptions are PTFE and HDPE. Here, sliding appears to occur truly at the interface and this has been attributed to the smooth molecular profile of these polymers (Pooley and Tabor, (1972)).

It is generally accepted that during the sliding of an unlubricated polymer over a hard, smooth surface the

deformation term is neglibible and the adhesion component is responsible for the major part of the friction (Briscoe et al, (1974)), (Tabor, (1974)) and (Moore, (1972)). The adhesion component is not a constant but depends on speed, temperature and contact pressure in a manner suggesting a close correlation with the bulk viscoelastic properties. This appears to be reasonably valid for rubbers but less so for thermoplastics (Tabor, (1974)), (Ludema and Tabor, (1966)). The lack of correlation in polymers is attributed to the extremely high shear strains occurring at the interface during sliding (Ludema and Tabor, (1966)).

However, if a polymer slides over a rough surface, or if sliding occurs in the presence of a good lubricant, the adhesion term is considerably reduced. In such cases the hysteresis or deformation term provides the tractive forces (Moore, (1972), (Ludema and Tabor, (1966)), (Tabor, (1974)).

3.5.4.2 The Deformation Term

The friction component due to deformation is based on a simple physical idea that energy is fed into the polymer ahead of the asperity, some of this is restored at the rear of the asperity and urges it forward, as illustrated in Figure 3.21. The net loss of energy is related to the input energy and the loss properties of the polymer at the particular temperature, contact pressure and rate of deformation of the process (Tabor, (1974)).

The deformation term involves the bulk viscoelastic properties of the polymer rather than some special surface condition and the maximum energy dissipation does not occur at the sliding interface, but at a small depth below the surface where the maximum shear stresses occur (Tabor, (1974)), (Lee, (1974)).

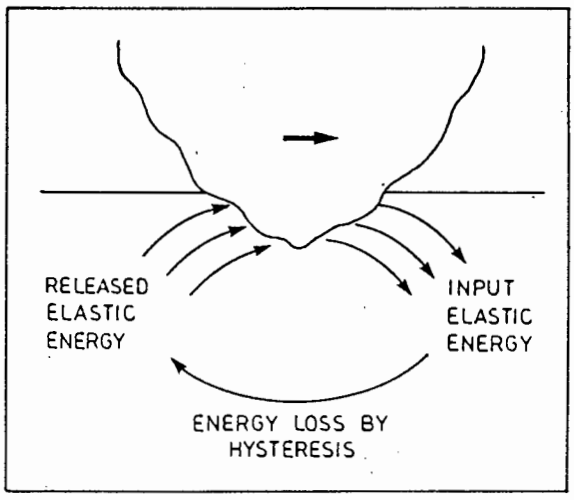

FIGURE 3.21 : A basic physical model of the loss mechanism in the deformation of a polymer by a hard asperity (after Tabor, (1974))

Deformation loss is also a collective term, including the special cases of hysteresis losses and grooving losses. Hysteresis losses occur in viscoelastic materials, where deformation energy is recovered. Grooving losses are observed with plastics and elastic materials stressed beyond their yield point, and they imply permanent deformation (Lee, (1974)). The deformation component of the friction in this study is believed to be comprised of recoverable hysteresis as well as permanent deformation resulting from ploughing or grooving processes.

The bulk or hysteresis component of friction can be visualised by Figure 3.22, which shows the pressure distribution about an individual asperity pressed into a viscoelastic plane. When there is no relative motion, the pressure distribution in the elastomer above the asperities is symmetrical, i.e., no net side forces are created at the interface and the coefficient of hysteresis friction is zero, as seen in Figure 3.22(a). However, during relative sliding, at a velocity v, a pressure effect at the leading edge of the asperity causes the viscoelastic material to "pile up" in this region whereas contact is broken higher up on the downward slope of the asperity as shown in Figure 3.22(b)

(point d). Thus, the contact arc ab moves backwards relative to the sliding direction and assumes a new position cd. This creates an unsymmetrical pressure distribution which gives rise to a net hysteresis force F_{hyst} opposing the sliding motion. As the sliding speed is further increased the degree of pressure asymmetry increases and the magnitude of the hysteresis force F_{hyst} also increases. Since the pressure p also increases with sliding velocity, the length of the contact arc at each asperity tip decreases, i.e. effective stiffening of the elastomer occurs as the velocity increases, as shown in Figure 3.22(c). The points c and d approach each other and the contact arc ef at very high speeds has a minimum value and is virtually symmetrical. The hysteresis force due to pressure asymmetry is therefore reduced (Moore, (1972)).

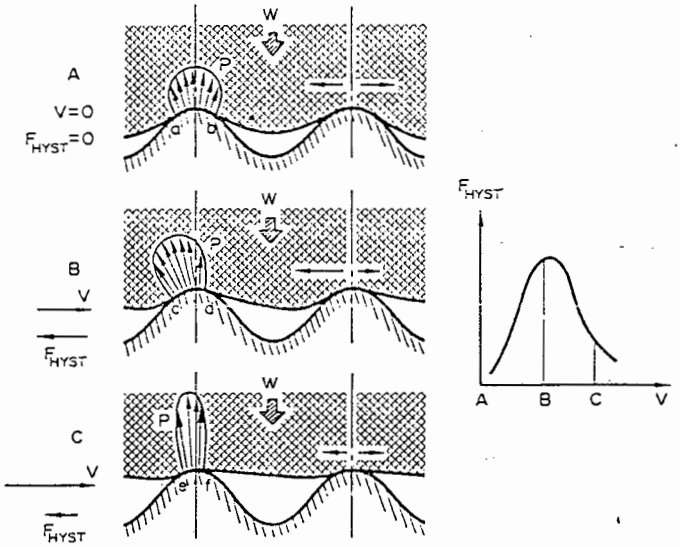

FIGURE 3.22 : Effects of asperity interaction on the hysteresis force in sliding (after Moore, (1972))

3.5.5 Stick-Slip Effects

The influences of the various tribological processes may lead to unwanted vibrations of the moving parts, and to "stick-slip"

motion. Many tribo-mechanical systems whose functional purpose is connected with the transmission of motion can be modelled in a simplified manner by the configuration shown in Figure 3.23.

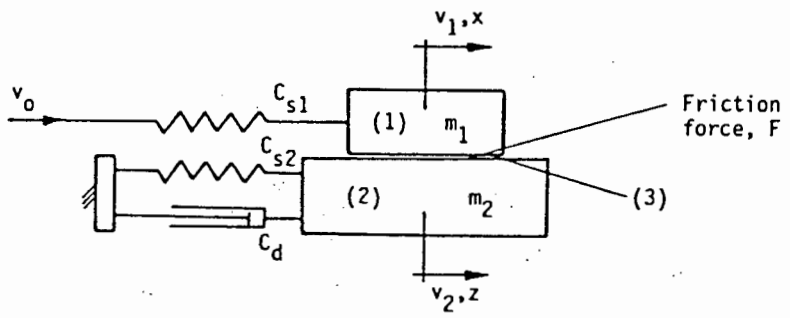

FIGURE 3.23 : A model of a tribo-mechanical system (after Czichos, (1978))

The model system consists of a body (1) of mass m_1, moving relatively to its counterpart (2) of mass m_2 fixed to the ground via a spring with a spring constant C_{s2} and a damper with a damper constant C_d. The body (1) is driven via the spring C_{s1} at a constant velocity $v_o = s/t$.

The motion of body (1) of velocity v_1 and distance x_1 relatively to body (2) of velocity v_2 and distance x_2 is influenced by the friction force F acting in the interface (3) between body (1) and body (2). The type of motion is determined by the value of the friction force at $v_{rel} = 0$ and the dependence of the friction force on the velocity $F = f(v)$. Let the initial state of the system shown in Figure 3.23 be such that the springs C_{s1} and C_{s2} are uncompressed and m_1 and m_2 are at rest. When the motion of velocity v_o is introduced there will be no movement of m_1 relative to m_2 ("stick" phase) until the driving force on m_1 is high enough to overcome the (static) friction force between m_1 and m_2. If then the motion of m_1 relative to m_2 starts ("slip" phase) the springs decompress. Thus the driving force is lowered by a certain amount. If now the driving force on m_1 falls below the (kinetic) friction force, a seond "stick" phase may evolve. This in turn leads to an increase of the driving force until the motion of the second slip phase starts, and so on (Czichos, (1978)).

Figure 3.24 show the variation of the friction force during reciprocating sliding with stick-slip.

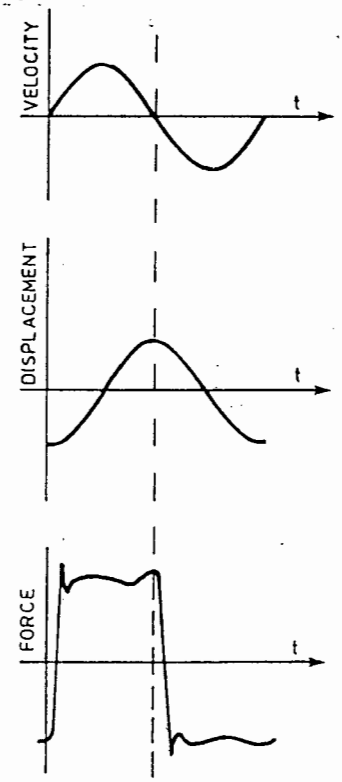

FIGURE 3.24 : Variation of velocity, displacement and friction force during reciprocating sliding with stick-slip (after, Plint and Plint, (1985))

3.6 WEAR

The most general definition of wear is taken as "the progressive loss of substance from the operating surface of a body as a result of relative motion at the surface".

It is well recognised today that wear is the predominant cause of maintanance breakdowns in industry which results in severe economic losses. There are a number of mechanisms involved in a wear process and whereas a limited understanding of these mechanisms has been developed, the general picture of wear is still missing because of the interplay of these mechanisms in any real situation (Bahadur, (1978)).

The wear behaviour of a materials couple is determined by interfacial wear processes occurring between the two partners moving under a load W with a velocity v over a distance x as shown in Figure 3.25. For an

unequivocal characterisation of wear, the following should be specified (Czichos, (1978)).

i) The type of relative motion.
ii) The properties of the interacting elements.
iii) The dominant interfacial wear mechanism.

The combination of these three characteristics specifies the "type" of wear. For a more quantitative characterisation the following should also be specified.

iv) The input work:- normal load, friction coefficient, distance of motion at stated velocity.
v) Materials properties relevant to wear.
vi) The wear rate.
vii) The appearance of the worn surface.

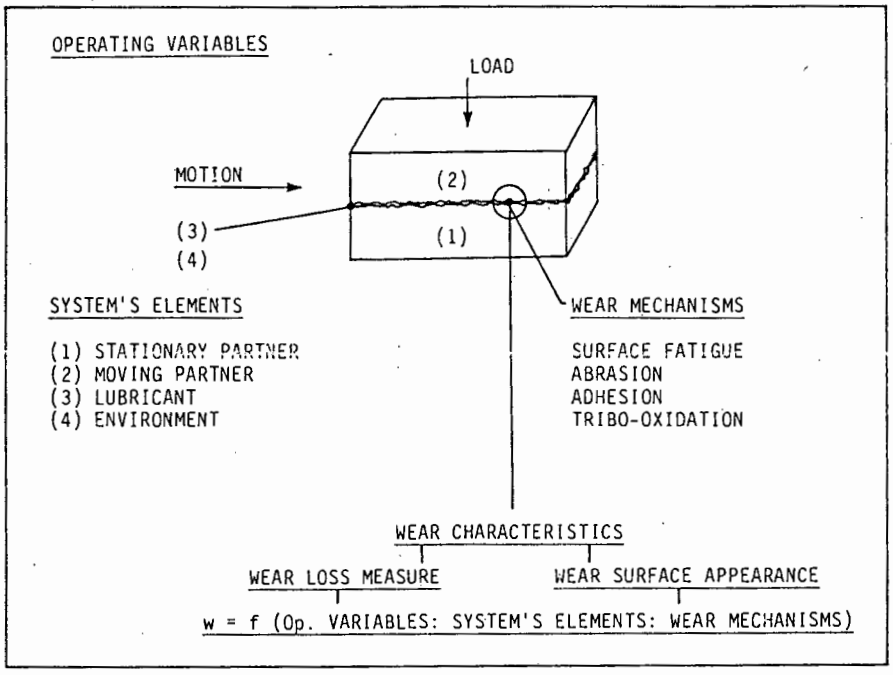

FIGURE 3.25 : Wear as characteristic of a tribological system (after Czichos, (1978))

3.6.1 The Wear of Polymers

It is generally accepted that there are four main physical mechanisms of wear occurring in polymeric materials, namely abrasive wear, adhesive wear, surface fatigue and thermal/

corrosive/oxidative degradation (Czichos, (1983); Evans and Lancaster, (1979); Tabor, (1976); Kar and Bahadur, (1978); Briscoe, (1981)).

Briscoe, (1981) further grouped these processes into two main classes named cohesive wear and interfacial wear.

i) Cohesive wear processes include those mechanisms which involve the dissipation of frictional work and its resultant damage in relatively large volumes adjacent to the interface. Abrasion and fatigue wear induced by stresses are within this category. These mechanisms are, by and large, controlled by the cohesive strength or toughness of the polymer.

ii) Interfacial wear processes involve the dissipation of frictional work in a thinner region at the interface. Transfer or adhesive wear and chemical or corrosive wear are the main processes here. The chemistry of the surfaces and the forces emanating from the surfaces are the main influencing factors.

Two difficulties arise from such a formal classification (Evans and Lancaster, (1979); Czichos, (1983); Bahadur, (1978)). Firstly, the wear mechanisms depend significantly on the mechanical properties of the material. Secondly, a very considerable degree of inter-relationship exists among the different processes that lead to failure. Figure 3.26 summarises the various wear processes occurring in polymers.

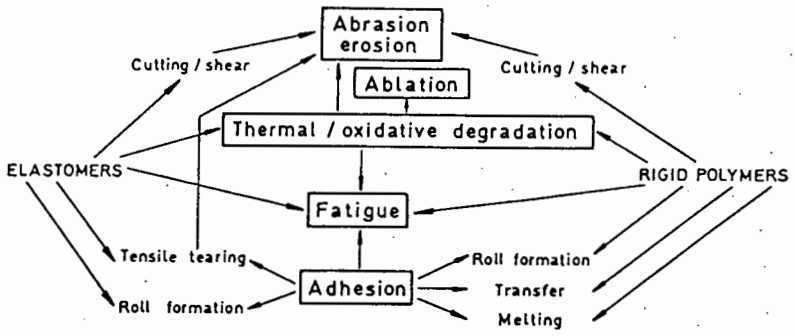

FIGURE 3.26 : A summary of wear processes for polymers (after Evans and Lancaster, (1979))

3.6.1.1 Abrasive Wear

Abrasive wear is the wear by displacement of material from surfaces in relative motion caused by the presence of hard protuberances, or by the presence of hard particles either between the surfaces or embedded on one of them (Lancaster, (1969)).

The principal processes in abrasive wear are ploughing/shearing and microcutting (Evans and Lancaster, (1979); Vingsbo (1979)). In microcutting the abrasive element acts like a microcutting tool which may, under particular tribo-conditions, lead to the removal of material from the surface by the formation of chips, shavings and fragments. Ploughing occurs when the abrasive element acts as a plough shear, forming a wear groove by plastic deformation and driving up a pair of crests in the polymer material (Vingsbo (1979); Kar and Bahadur, (1978); Tabor, (1976)).

The simplest physical picture of two-body abrasive wear in polymers is one in which a hard, conical indenter penetrates and ploughs a groove in the softer polymer material as illustrated in Figure 3.27. If the deformation is wholly or substantially plastic then the volume displaced (either by cutting or plastic deformation) is proportional to tan θ where θ is the base angle of the cone, i.e., the volume of material removed per unit sliding distance is:

$$\text{wear volume} = \frac{K \ W \tan \theta}{H}$$

where W is the normal load, H is the time dependant hardness and K is the probability of the formation of a wear particle (Evans and Lancaster (1979); Briscoe, (1981)).

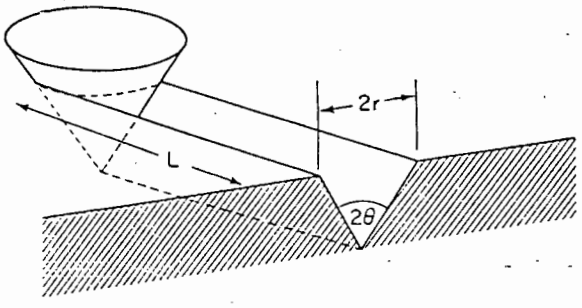

FIGURE 3.27 : Abrasive wear due to a single conical asperity (after Halling, (1976))

This equation only holds for polymers when θ is large, i.e. plastic deformation only becomes the predominant mode when the indenter is very sharp. Thus, during sliding against metals of roughnesses commonly encountered in engineering practice the deformation of polymers is partly plastic and partly elastic and the relative proportions will vary with roughness (Lancaster, (1969)).

Evans and Lancaster (1979) have shown that if s is the breaking stress of the polymer and ε is the elongation to break, the work required to complete the process of producing a wear fragment is proportional to the product $s\varepsilon$. Ignoring differences in hardness and coefficient of friction, there is a linear relationship between the wear rate of various polymers and $1/s\varepsilon$ as shown in Figure 3.28. However, the measurement of s and ε were made at conventionally low strain rates whereas those involved in wear processes must be many orders of magnitude greater. The existence of this correlation therefore implies that the magnitude of $s\varepsilon$ is either independant of strain rate or varies with strain rate in a similar way for all polymers.

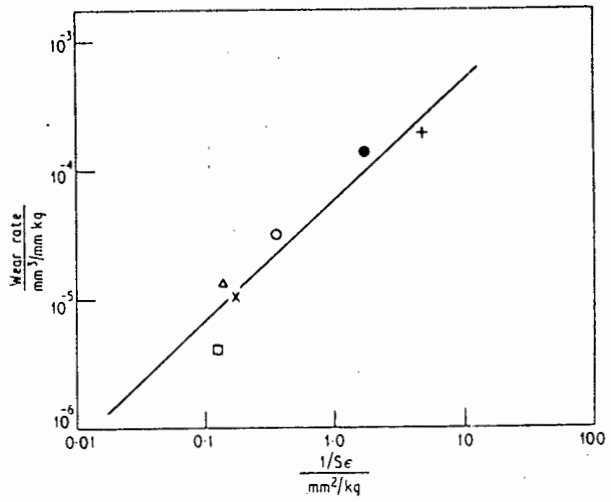

FIGURE 3.28 : The correlation between wear rates of polymers and their reciprocal of the energy parameter sε. + = polystyrene, • = PMMA, o = acetal homopolymer, △ = polypropylene, x = PTFE, □ = nylon 66 (after Lancaster, (1969))

3.6.1.2 Adhesive Wear

Adhesive wear mechanisms in polymers are mainly characterised by the formation and fracture of adhesively bonded junctions occurring because of relative motion between the mating surfaces (Tabor, (1976)).

When polymers are slid over smooth, clean counterfaces the adhesion between the polymer and the counterface is of sufficient magnitude to inhibit sliding at the original interface. Instead the junctions rupture within the polymer itself and a layer of polymer is deposited on the counterface in the form of a more or less coherent transfered layer. Subsequent traversals over this film removes the transfered layer which is ultimately removed from the contact. A further layer is deposited, the process repeats and the polymer surface is gradually worn away (Briscoe, (1981); Belyi et al

(1977)). Thus, during adhesive wear modifications to the surfaces of both the polymer and the counterface are induced by the sliding process. Figure 3.29 identifies a number of surface modifications induced during sliding of polymers against metals.

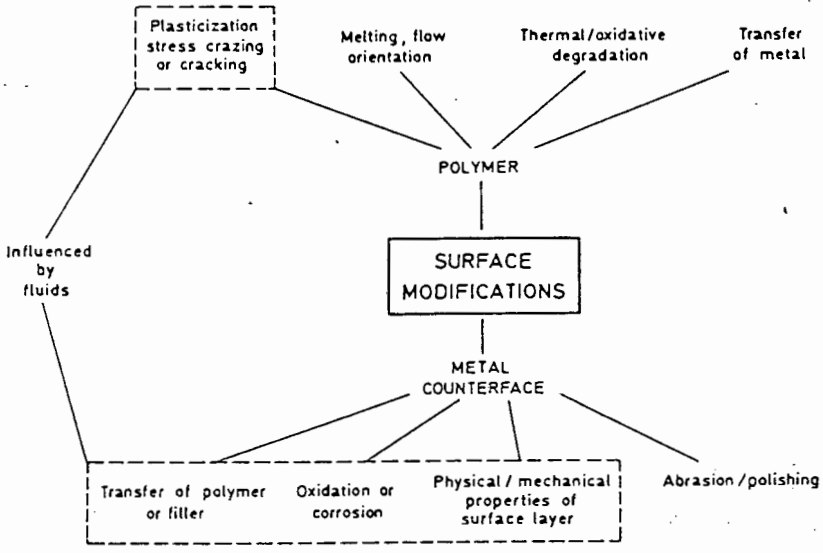

FIGURE 3.29 : Types of surface modification induced during sliding of polymers against metals (after Evans and Lancaster, (1979))

The presence of thin films of transfered polymer on the metal counterface significantly affects both friction and wear, and usually leads to a reduction in both. Transfered fragments of polymer are readily deformed during repeated contacts and thus ultimately leads to a reduction in the effective surface roughness of the counterface. Also, sliding now occurs between oriented molecular chains of polymer on both surfaces. Thus, the friction is reduced, the localised contact stresses are reduced and so, in turn, is the wear rate (Pooley and Tabor, (1972); Tanaka and Uchiyama, (1974); Tanaka, (1981); Makinson and Tabor, (1966); Eiss et al, (1979)).

Adhesive processes can sometimes initiate abrasive wear of the surfaces by the transfer of metal to the polymer during polymer/metal sliding. This occurs when the sub-surface strength of the metal falls below that of

the adhesive or mechanical interactions at the interface. The metal could be weakened locally by repeated contacts during sliding (Suh, (1973)). Also, conventional surface-finishing treatments may generate locally weakened asperities even before sliding begins. Any metal fragments transferred to the polymer will tend to become embedded in the surface layers and are then able to modify the counterface topography during subsequent sliding (Evans and Lancaster, (1976); Tabor, (1982); Vingsbo, (1979)).

3.6.1.3 Fatigue wear

Fatigue wear refers to the cyclically repeated imposition of a stress state on the surface of a component, inducing a small degree of mechanical damage in the surface and subsurface regions with each stress pulse. Ultimately, the damage accummulation leads to failure by deformation and/or fracture at the surface (Yust, (1985)). If there is a strong interfacial adhesion, the surface layers of the polymer may be detached in a single traversal - this is really adhesive wear - but often even in the presence of appreciable adhesion, several traversals of the same portion of the surface may be required before a fragment is finally detached. Sometimes failure is initiated at a surface flaw, sometimes at a subsurface flaw. Fatigue of polymers does not occur if the stresses are below a certain limit. However, although the average loading may be below this limit, individual asperities may be subjected to stresses well above their fatigue limit. The asperities are then removed and may become trapped between the sliding surfaces (Tabor, (1976)). Localised elastic deformation of a polymer during sliding becomes increasingly significant with decreasing elastic modulus and/or counterface roughness, and in these conditions fatigue processes begin to play a major role in wear.

As the roughness decreases, the amount of plastic deformation and the cutting component of the wear will decrease until, on very smooth surfaces, the deformation becomes wholly elastic. The wear process then becomes one of localised elastic fatigue, complicated by the effects of adhesion (Lancaster, (1969)). Thus, there is no rigid boundary between fatigue and abrasive/cutting wear as illustrated in Figure 3.30 (Evans and Lancaster, (1979)).

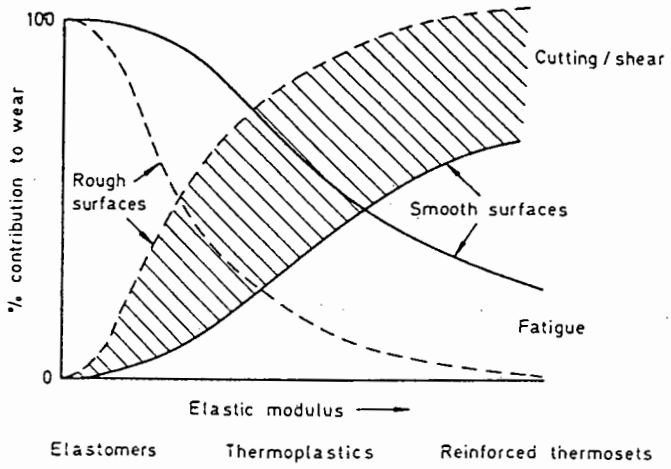

FIGURE 3.30 : Schematic variation of abrasion (cutting/shear) and fatigue wear with elastic modulus (after Evans & Lancaster, (1979))

3.6.1.4 Corrosive Wear

An element of chemical degradation is most certainly present in all wear processes. Because of the many variables which may enter into tribochemical reactions, it is difficult to generalise about this phenomenon. In some circumstances the reaction layer may serve a protective function, or may even act as a lubricant. In other cases, the chemical reaction may accelerate the wear process, i.e., thermal and oxidative degradation of the surface layers of the polymer will reduce their ductility, which can lead to enhanced abrasion as a factor in the wear process (Evans and Lancaster, (1979)).

3.6.2 Wear Testing

The ultimate technological objective of wear testing is to obtain data on the performance and reliability of specific components in service conditions. For this purpose, there is no wholly satisfactory alternative to full-scale testing of the component itself. However, by using relatively simple laboratory equipment operating in conditions more clearly defined and controlled than those likely to be encountered in service, two intermediate objectives can be satisified:- (1) to rank materials for wear resistance in conditions that simulate the essential features of an application; and (2) to obtain basic information about wear mechanisms as an aid to failure diagnosis or to the development of new materials (Evans and Lancaster, (1979)).

Therefore, in laboratory tests it is common to choose specific combinations of load, speed, contact geometry, motion, counterface material and surface finish, ambient temperature and the presence or absence of lubricant or abrasive. The number of test combinations is therefore vast, and yet it is vitally important for the correct choice to be made if the results are to be of value in predicting in-service life of the component (Anderson and Williamson, (1984)). One of the big problems with wear testing is that the different specimen configurations and test conditions used by the different workers make the comparison of results from various laboratories very difficult (Dowson et al (1974)). Thus, in order to produce data in a form which can be analysed directly when generated under different test conditions, a "specific wear rate" is commonly used. The specific wear rate K_0 is defined as the volume of wear per unit applied load per unit sliding distance and is proportional to the slope of the volume loss-sliding distance curve (Evans and Lancaster, (1979)).

$$\text{Specific Wear Rate } K_0 = \frac{\text{Volume Loss}}{\text{Normal Load . Sliding Distance}} \quad \frac{mm^3}{N.m}$$

The concept of specific wear rate presupposes that variations in load, speed, and sliding distance are not accompanied by

significant changes in any other variables that affect wear such as temperature or the topography of the sliding surfaces (Evans and Lancaster, (1979)).

3.6.3 The Wear of Ultra-High Molecular Weight Polyethylene (UHMWPE) Sliding Against Stainless Steel

The friction and wear characterisitics of UHMWPE has received considerable attention over the past decade. In particular, the wear of UHMWPE sliding against stainless steel, under dry and lubricated conditions, has been extensively researched. Table 3.2 summarises the experimental findings of other workers in this particular field.

TABLE 3.2 : A summary of the experimental findings of other workers on the wear of UHMWPE sliding against steel under dry and lubricated conditions

AUTHOR	TEST GEOMETRY	TYPE OF MOTION	LUBRICATION	PRESSURE $N.mm^{-2}$	SLIDING SPEED $m.s^{-1}$	SURFACE PREPARATION		SURFACE ROUGHNESS Ra (m)		SPECIFIC WEAR RATE $mm^3.N^{-1}m^{-1}$
						COUNTERFACE	POLYMER	COUNTERFACE	POLYMER	
Atkinson et al (1978)	Pin-on-disc	Uni-directional	Dry	2,5-15,5	0,24	AISI 316 Ground & Lapped	Turned	0,01-0,10	0,7-1,5	$0,6\text{-}2,6 \times 10^{-7}$
Challen & Dawson (1976)	Pin-on-disc	Uni-directional	Dry	13-20	0,24	AISI 316 Ground & Lapped	Turned	0,005-0,015	0,7-1,5	$1,6\text{-}5,6 \times 10^{-7}$
Mustafaev et al (1976)	Pin-on-disc	Uni-directional	Dry	10	0,24	AISI 316 Ground & Lapped	Turned	± 0,015	0,7-1,5	$5,4 \times 10^{-7}$
Anderson & Robbins (1976)	Flat-on-flat Thrust bearing configuration	Uni-directional	Dry	0,7	0,26	070M20 Abraded	Abraded	0,2-0,3	0,7-1,0	$1,15 \times 10^{-6}$
Dumbleton & Shen (1976)	Flat-on-flat Thrust-washer wear tester	110° Oscillation	Dry	3,5	0,04	AISI 316 Abraded & Polished	Abraded & Polished	0,13	-	5×10^{-7}
Brown et al (1982)	Pin-on-plate	Reciprocating	Dry	4,5-10	0,018	AISI 316 Ground & Lapped	Turned	± 0,01	0,37	$0,7\text{-}0,9 \times 10^{-7}$
Dowson et al (1976)	Pin-on-plate	Reciprocating	Dry	10	0,30	AISI 316 Cross-ground	Turned	0,27-1,25	0,7-1,5	$5,5 \times 10^{-8}$ - $4,2 \times 10^{-5}$
Furber et al (1976)	Pin-on-plate	Reciprocating	Dry	2,5-6,5	0,018	AISI 316 Ground & Lapped	Turned	± 0,015	0,7-1,5	$1,3\text{-}2,5 \times 10^{-6}$
Dowson et al (1974)	Pin-on-plate	Uni-directional	Water	15	0,24	AISI 316 Polished	Turned	± 0,05	0,7-1,5	8×10^{-9}
Dumbleton & Shen (1976)*	Plate-on-plate Thrust-washer Wear tester	110° Oscillation	Water	3,5	0,04	AISI 316 Abraded & Polished	Abraded & Polished	0,13	-	$1,6 \times 10^{-7}$
Rostoker & Galante (1976)*	Disc-on-plate	Oscillatory	Water	6,2	0,1	AISI 316	-	-	-	$2,9 \times 10^{-7}$
Dowson et al (1984)	Pin-on-plate	Reciprocating	Water	4,5-10	0,25	AISI 316 Ground & Lapped	Turned	0,005-0,5	0,7-1,5	5×10^{-8} - 3×10^{-5}
Mustafaev et al (1976)	Pin-on-disc	Unidirectional	Mineral Oil	10	0,24	AISI 316 Lapped	Turned	± 0,015	0,7-1,5	$1,4 \times 10^{-7}$

* Converted from Imperial Units

Atkinson et al (1978), has shown that during unidirectional sliding of UHMWPE against relatively smooth, dry stainless steel counterfaces the wear graph can be divided into three regions as illustrated in Figure 3.31. Initially, the wear is erratic and during this "running-in" period the machined polymer surface is removed and general bedding-down of the experimental equipment takes place. This is followed by two distinct steady-state regimes, designated sections A and B wear respectively. In the first section, adhesion is the predominant wear mechanism and a transfer film of polymer builds up on the steel counterface. After a certain sliding distance, determined by the load, the adhesive mechanism is augmented by fatigue wear and the wear rate increases sharply and remains constant at the new value.

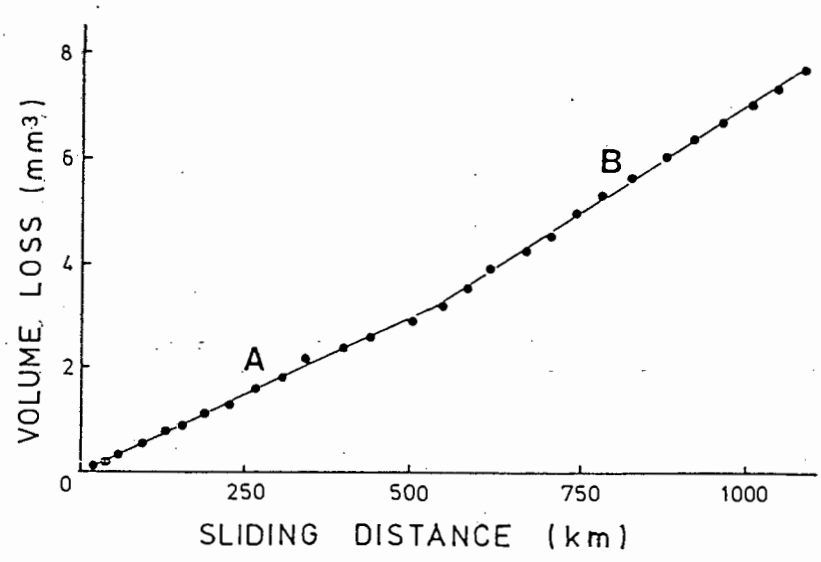

FIGURE 3.31 : A wear curve from a dry test showing the two steady-state wear regions. Applied pressure : 2,5 $N.mm^{-2}$; sliding speed : 0,25 $m.s^{-1}$; surface roughness : 0,018 micrometers Ra (after Atkinson et al, (1978))

Atkinson et al (1978) and Furber et al (1976) showed that the sliding distance to the onset of type B wear varied between 100 and 500 km. During section A wear the primary adhesive wear mechanism involved the extrusion of streamer debris due to surface melting of the polymer whilst the onset of section B wear is marked by the occurrence of cracks in the polymer surface and the

formation of fine, powdery and brittle wear debris. The transfer film exhibited a brown coloration which is indicative of oxidative degradation caused by the continual exposure of the film to high temperatures. A transition in the steady-state wear rate was also reported by Anderson and Robbins (1976) who observed an increase in the wear rate occurring after only 23 km of dry, unidirectional sliding on mild steel in a thrust-washer wear tester. Initially a brown film of iron oxide was formed on the polymer surface which became disrupted after this sliding distance, resulting in the wear rate increasing by almost a factor of three.

However, Dowson et al (1976) and (1984) did not observe any transition from type A to type B wear after several hundred km of reciprocating sliding against stainless steel counterfaces with a wide range of roughnesses, under dry and lubricated conditions.

Dowson et al (1974) also investigated the wear of UHMWPE against stainless steel in unidirectional sliding under water lubrication. As in the dry tests, the graph of volume loss against sliding distance showed two distinct steady-state wear regimes after an initial period of running-in. However, during lubricated sliding the wear rates were considerably lower and the transition from type A to type B wear only occurred after 1100 km of sliding. The transition was attributed to the appearance on the pin ends of fatigue cracks, transverse to the wear direction. Polymer transfer also occurred during these tests and the commencement of steady-state section A wear coincided with the appearance of a polymer transfer film on the counterface.

3.6.3.1 The effect of load/pressure

Simple theories of wear based on adhesion predict a direct proportionality between wear rate and load. However, this proportionality will be observed only when changes in load do not induce changes in any other variable affecting wear. Evans and Lancaster (1979) reported that above a critical load, the wear rate of

UHMWPE increased rapidly and it was attributable to thermal softening of the polymer. For UHMWPE this critical load increases following γ-radiation, which introduces cross linking and inhibits melting (Matsubara and Wanatabe, (1966)). Below this critical load, which is typically one-third of the compressive strength of the polymer, the wear of UHMWPE is generally independant of load as illustrated in Figure 3.32 (Anderson, (1982)).

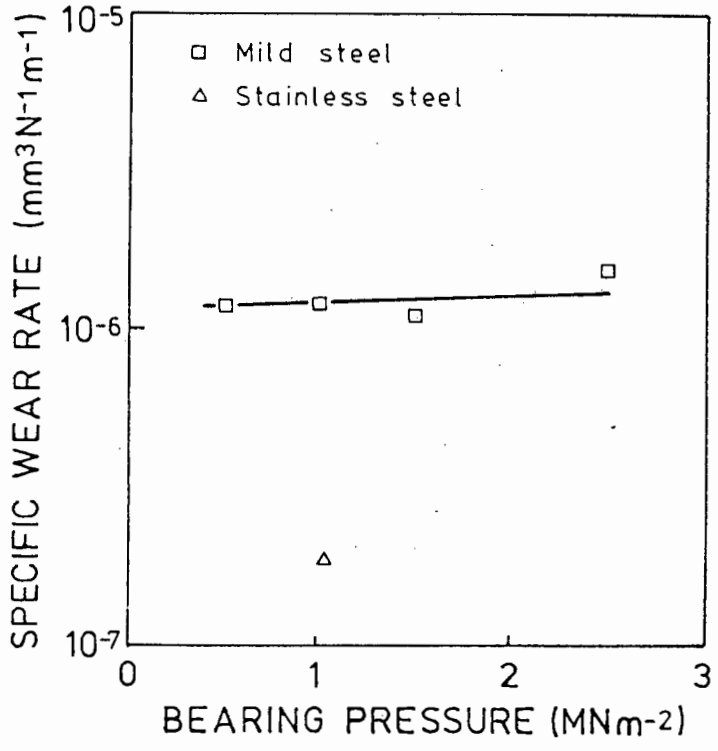

FIGURE 3.32 : The variation of the specific wear rate of UHMWPE with bearing pressure (after Anderson, (1982))

Anderson (1982), Challen and Dowson (1976) and Furber et al (1982) have shown that the sliding distance to the point of transition in the wear rate of UHMWPE sliding against dry stainless steel is strongly dependent on applied load, a characteristic which is usual in fatigue effects. This is illustrated in Figure 3.33.

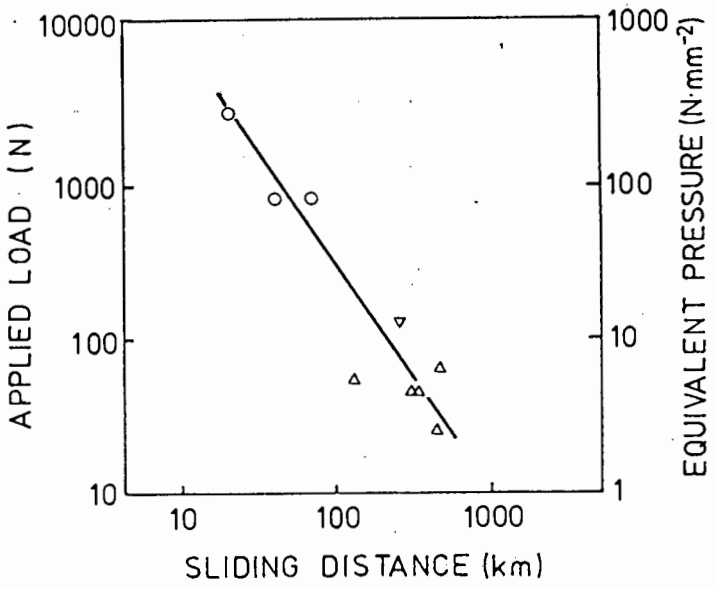

FIGURE 3.33 : Load vs. sliding distance to the onset of the transition from type A to type B wear. ○ Anderson : thrust bearing; ▽ Challen and Dowson : pin-on-disc; △ Furber et al : pin-on-flat (after Anderson, (1982))

Dumbleton and Shen (1976) showed that for UHMWPE sliding in water, the initial wear rate generally increases with increasing pressure before the linear part of the curve is reached. Thereafter, the steady-state wear rates were independant of pressure as illustrated in Figure 3.34.

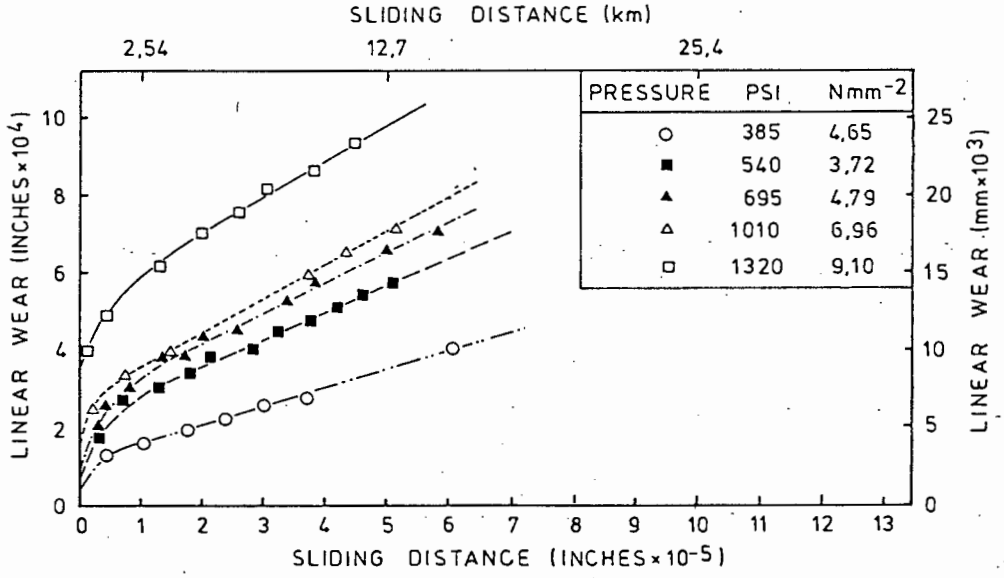

FIGURE 3.34 : The effect of pressure on the wear of UHMWPE tested in water (after Dumbleton and Shen, (1976))

3.6.3.2 The effect of sliding speed

The principal effect of sliding velocity on the wear rate of a polymer occurs through its influence on the temperature at the sliding surface. Anderson (1982) observed a critical sliding speed above which the wear of UHMWPE pins sliding against dry mild steel discs increased dramatically. This speed corresponds to the point where the calculated flash temperatures (the instantaneous temperatures at the asperities) reached the melting/softening point of the polymer, leading to thermal softening, extrusion and gross flow of material (Evans and Lancaster, (1979)). Similar tests were carried out using water and a 5:95 oil/water emulsion as lubricants and the results indicated the absence of a definite critical speed under lubricated conditions as shown in Figure 3.35.

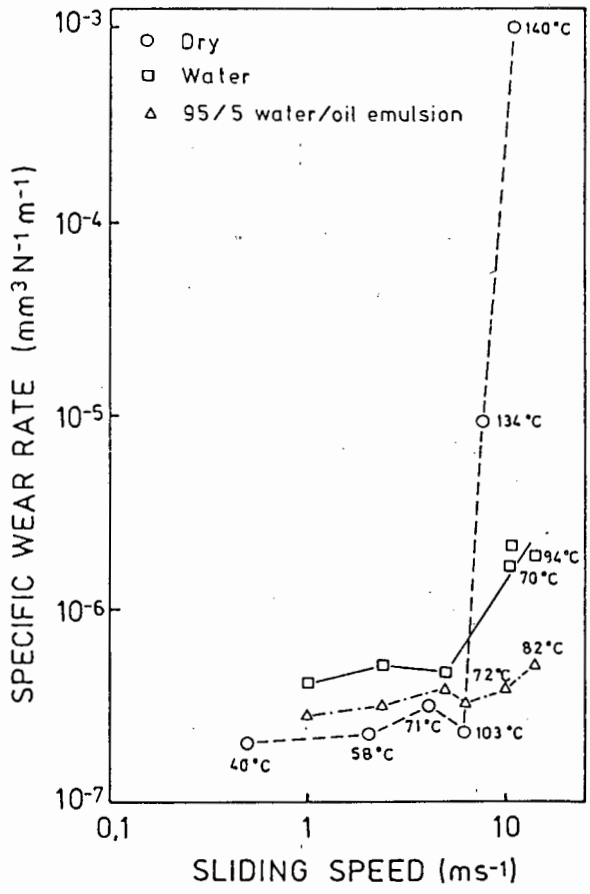

FIGURE 3.35 : The variation of specific wear rate of a UHMWPE pin on a steel disc with sliding speed. The temperatures plotted are the sum of the measured surface temperature and the calculated flash temperature at each velocity (after Anderson, (1982))

Lancaster (1971) showed that for polymers the flash temperatures are more sensitive to sliding speed than applied load and are also critically dependant on the thermal conductivity of the counterface. However, the main difficulty in determining the critical speed at which melting occurs is that there is no reliable way of either calculating or measuring the localised temperatures at contacting asperities.

It is important for design purposes to specify the limiting conditions of operation of dry bearing polymer materials. The usual criterion is a PV factor, the product of the nominal pressure and the linear velocity. This is commonly quoted in two ways and is illustrated in Figure 3.36 (Lancaster, (1973)).

a) The "limiting PV" above which wear increases rapidly either as a consequence of thermal effects or of stresses approaching the elastic limit. The limiting PV values are those at which the total temperature rise at the surface - the flash temperature superimposed on the mean surface temperature resulting from the dissipation of frictional heat - reaches a value near to the melting/softening point of the polymer.
b) The "maximum PV" for continuous operation at some arbitrarily specified wear rate.

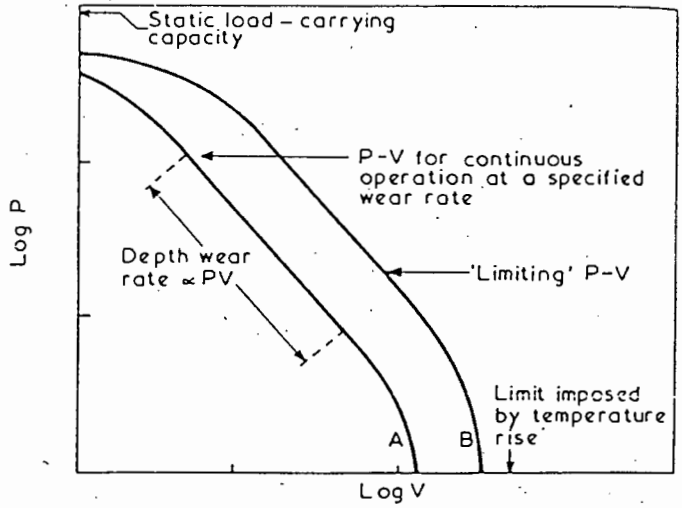

FIGURE 3.36 : Relationships between P and V for dry bearings. A-"Maximum" PV curve; B-"Limiting" PV curve (after Lancaster, (1973))

The main difficulty with both of these approaches is that no account is taken of the variation in the strength of the material, and its wear rate, with temperature (Lancaster, (1971) (1973); Anderson, (1982)). To incorporate this aspect, a modified design procedure for dry bearings has recently been introduced. The surface temperature of the bearing is first calculated by approximate methods and suitable materials are then selected from the known relationships between allowable pressure and temperature (Crease, (1973)) as illustrated in Figure 3.37. Figure 3.37 indicates that at low pressures and surface temperatures, the specific wear rate is essentially independant of these parameters and the specific wear rate under these conditions is designated K_o.

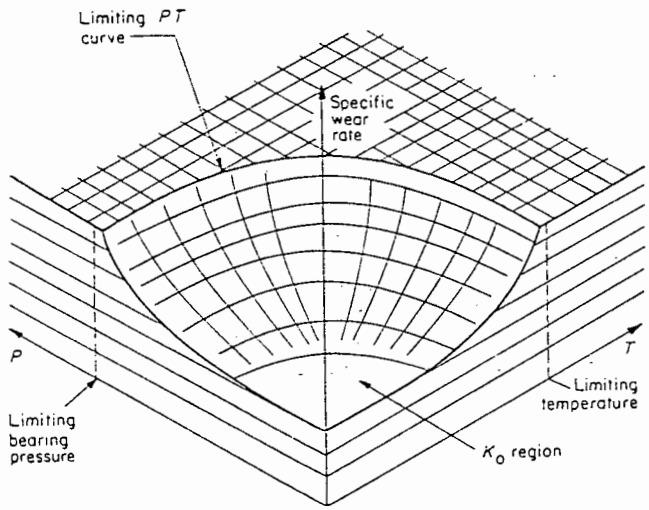

FIGURE 3.37 : The variation of specific wear rate with bearing pressure and temperature for polymer materials (after Crease, (1973))

3.6.3.3 The effect of temperature

Temperature is particularly important in thermoplastics, whose softening or melting points are, in general, relatively low. For a given bearing pressure and friction coefficient, the frictional heat generated at the surface will increase in proportion to the sliding velocity. The steady-state mean surface temperature

attained will then depend upon the heat transfer properties of the bearing assembly.

Thus : $\varphi = R \mu PV$

where μ is the friction coefficient, P is the pressure, V the sliding velocity, φ the mean surface temperature and R the thermal resistance of the bearing assembly. Thus, on this argument the influence of sliding velocity on the wear rate can be converted to that of temperature (Anderson, (1982)). Equivalent surface temperature in a rubbing bearing can be generated either by frictional heating at low ambient temperature or by high ambient temperature where frictional heating is low. Anderson and Robbins (1976) showed that the method of temperature generation has only a small effect on the wear rate of polymers sliding against stainless steel.

Lancaster (1979) showed a rapid increase in the wear rate of thermoplastics above a critical temperature and again attributed this to overall thermal softening. The heat generated at the sliding interface depended more on speed than on load.

Kar and Bahadur (1982) used a pin-on-disk wear machine to observe the effect of temperature rise on the wear failure of thermoplastics, under varying sliding speed and load conditions. For high density polyethylene there was a transition from steady to unsteady state temperature conditions in the sliding speed range 1,5 - 2,5 $m.s^{-1}$ and that the transition was governed more by the sliding speed than the load. Failure occurred at about 114°C and this occurred due to thermal softening at the interface and excessive deflection of the pin which created unstable sliding conditions.

3.6.3.4 The effect of surface roughness

It has been often suggested that there is an optimum roughness for minimum wear of polymers, but the

experimental evidence for this is conflicting. Buckley (1974) showed that the optimum surface finish which gives a minimum wear rate for the dry sliding of UHMWPE against stainless steel in a disc and shoe apparatus is 0,37 microns r.m.s. (approximately 0,4 microns Ra).

Dowson et al (1976) have shown that in dry reciprocating sliding of UHMWPE against stainless steel, the wear rate decreases as the surface roughness decreases and passes through a minimum at a Ra value of 0,03 microns (for parallel ground and lapped surfaces) as illustrated in Figure 3.38.

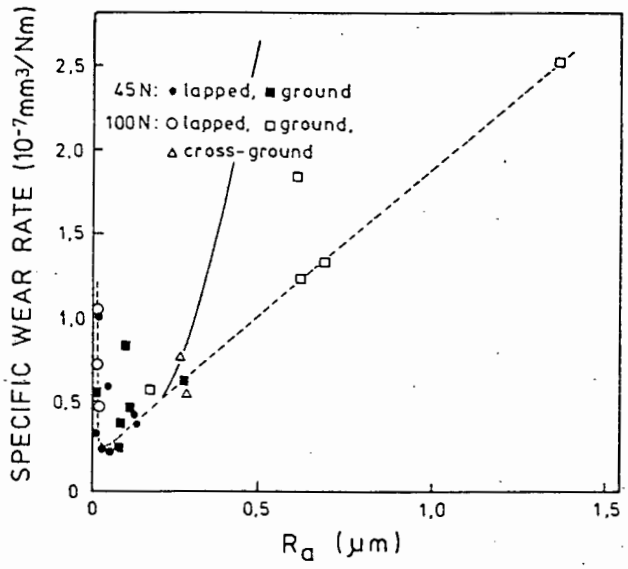

FIGURE 3.38 : The effect of surface roughness on the dry wear rate of UHMWPE (sliding speed 0,3 $m.s^{-1}$) (after Dowson et al, (1976))

During sliding against rough surfaces the transfer of polymer fills up the valleys and decreases the effective roughness. However, with very smooth surfaces, "lumpy" polymer transfer was observed. Thus, the high wear rates observed for the very smooth surfaces are due to highly adhered polymer "lumps" whilst abrasive effects dominate the wear processes for the rougher surfaces. At the optimum roughness, the lumpy transfer due to adhesion and the ploughing effect due to abrasion are both low. This optimum coincided, approximately, with a transition from grinding to lapping during counterface

preparation. Cross-ground surfaces were much more sensitive to changes in roughness than the parallel ground specimens. It was suggested that the magnitude rather than the nature of the asperities is important in the wear of polymers. Dowson et al (1984) further monitored the effect of surface roughness in reciprocating sliding on stainless steel under dry and water lubricated conditions. Statistical analysis of the counterfaces revealed meaningful relationships between Ra and other significant features of the topography, namely profile height, valley depth, peak height, profile mean absolute slope and radius of curvature of asperity peaks. Under dry conditions, the optimum Ra for minimum wear was in the range 0,05 to 0,1 micrometers. The wear rates were steady over a wide range of roughnesses extending over about two orders of magnitude. The polymer transfer film, and particularly its thickness relative to the counterface roughness, is responsible for the observed minimum wear rate under dry conditions.

The presence of distilled water largely inhibits transfer film formation and this resulted in a much more pronounced effect of counterface roughness on the wear rate as illustrated in Figure 3.39.

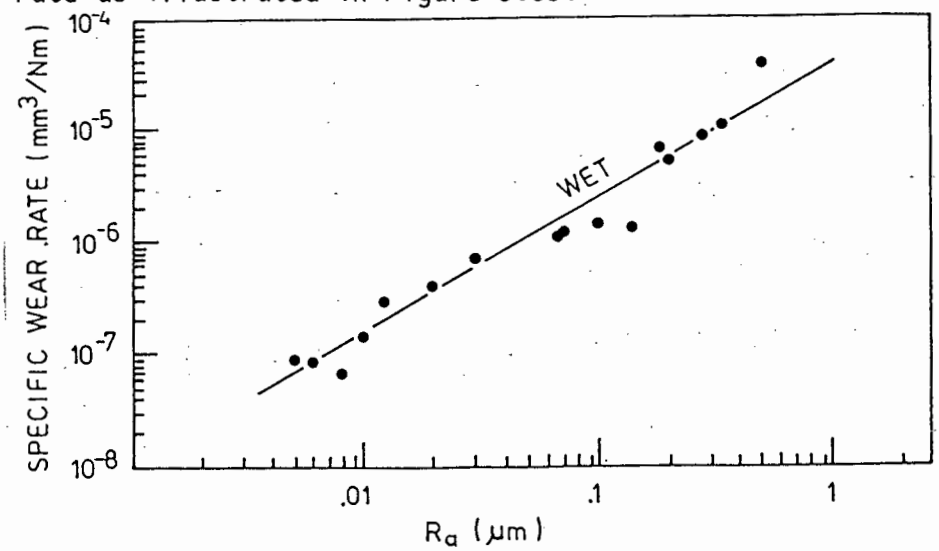

FIGURE 3.39 : Wear rate as a function of counterface roughness (Ra) under water lubrication. Sliding speed 0,25 $m.s^{-1}$; normal load 4,25 - 10 $N.mm^{-2}$ (after Dowson et al, (1984))

By superimposing the two curves, it can be seen in Figure 3.40 that for roughnesses in excess of about 0,01 microns Ra the 'wet' wear rates exceed the dry ones.

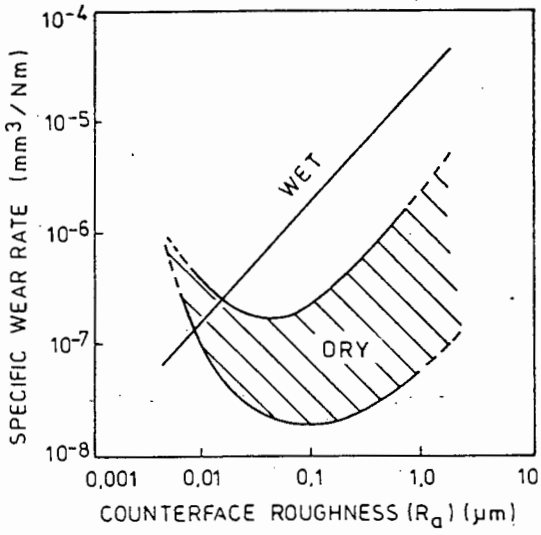

FIGURE 3.40 : Wear rates for both dry and wet conditions as a function of counterface roughness (Ra). Sliding speed 0,25 $m.s^{-1}$; normal load 4,25 - 10 $N.mm^{-2}$ (after Dowson et al, (1984))

3.6.3.5 The effect of type of motion

Brown et al (1982) observed that the wear of UHMWPE takes place by the same basic wear mechanisms whether unidirectional or reciprocating motion is used, but the latter produces slightly less wear overall.

CHAPTER 4

THE DESIGN OF A LABORATORY WEAR TESTING MACHINE

4.1 GENERAL DESIGN CRITERIA

The objective of wear testing is to obtain data on the performance and reliability of specific components in service conditions. The use of simple test apparatus operating in more clearly and defined conditions than those likely to be encountered in service, satisfy two objectives:

1. To rank materials for wear resistance in conditions that simulate the essential features of the application.

2. To obtain basic information about wear mechanisms to aid failure diagnosis and the development of new materials.

Thus, versatile laboratory equipment is needed with which the major parameters influencing wear such as load, speed, temperature, etc can be defined accurately and varied over a wide range. To this end, a linear reciprocating pin-on-plate wear machine was designed and assembled in the Department of Materials Engineering, U.C.T. which has the facilities for measuring the wear rates, frictional forces and surface temperatures resulting during sliding of various material couples under a wide range of operating conditions. A reciprocating system was chosen, primarily, in order to simulate the action of a steel piston sliding against a polymer seal in a hydraulic cylinder. The subsequent testing of components from other sliding applications within the mining industry is also possible using this apparatus.

Apart from the type of sliding motion, a number of operating variables are known to affect the wear of materials in sliding contact. These include:

i) The normal load/pressure exerted at the sliding interface.
ii) The relative sliding velocity of the two components in contact.
iii) The surface roughness of the sliding couple.
iv) The presence of a lubricant between the sliding surfaces.

v) The presence of foreign abrasive particles at the interface.

vi) The stroke or distance over which sliding occurs.

The final selection of the operating variables was a compromise between the physical capabilities of the test rig and the conditions prevailing during normal operation of hydraulic stoping machines, such as the impact hammer and hand-held rockdrill, whose sliding mechanisms are being simulated.

4.2 SELECTING THE VARIABLES

4.2.1 Materials Selection

The material couple chosen for this study is ultra-high molecular weight polyethylene (UHMWPE) sliding against heat treated AISI 431 martensitic stainless steel. UHMWPE is used extensively for the seals in the high speed actuator assemblies of the hydraulic stoping machines operating on 5:95 and the intention is to use the same material when the transition is made to mine service water. AISI 431 was an initial choice for numerous components in the water-powered rockdrills and impact hammers.

4.2.2 Load/Pressure

Fluid pressures of approximately 18 MPa are seen by the polymer seals of the impact hammer whilst the piston seals of the rockdrill are required to seal against pressures ranging from 0-35 MPa. A pressure of 35 MPa was considered to be too large for the laboratory test rig. However, pressures of up to 15 MPa were considered to be feasible and a compromise between the specimen size and load had to be reached. Thus, a maximum normal load of 150 kg on a specimen with a contact area of approximately 100 mm^2 was selected for technical reasons.

4.2.3 Sliding Velocity

The sliding components of the hydraulic stoping machines are exposed to a wide range of sliding velocities during a single impact cycle. In the rock-breaking hammer the impact head reaches

a maximum sliding velocity of 10 $m.s^{-1}$ on the firing stroke but decreases to approximately 0,9 $m.s^{-1}$ on the return stroke. The piston of the rockdrill, on the other hand, reaches the same firing velocity and then decreases to 3 $m.s^{-1}$ during the return stroke. The high sliding velocities reached during firing and the geometry of the seal ensure that hydrodynamic lubrication conditions prevail for almost the entire length of the firing stroke. Wear is only likely to occur, if at all, at the beginning of the stroke where the low sliding velocities allow contact to occur between the rubbing surfaces. For the remainder of the firing stroke a hydrodynamic fluid film completely separates the sliding surfaces, resulting in practically no wear at all. On the return strokes, however, the velocities are such that boundary or mixed lubrication processes probably occur along an appreciable length of the stroke as illustrated in Figure 4.1 which estimates the time and distance over which boundary contact occurs during a single cycle of the impact hammer. This data is based on the assumption that boundary lubrication conditions prevail at relative velocities below $\pm$ 0,75 $m.s^{-1}$.

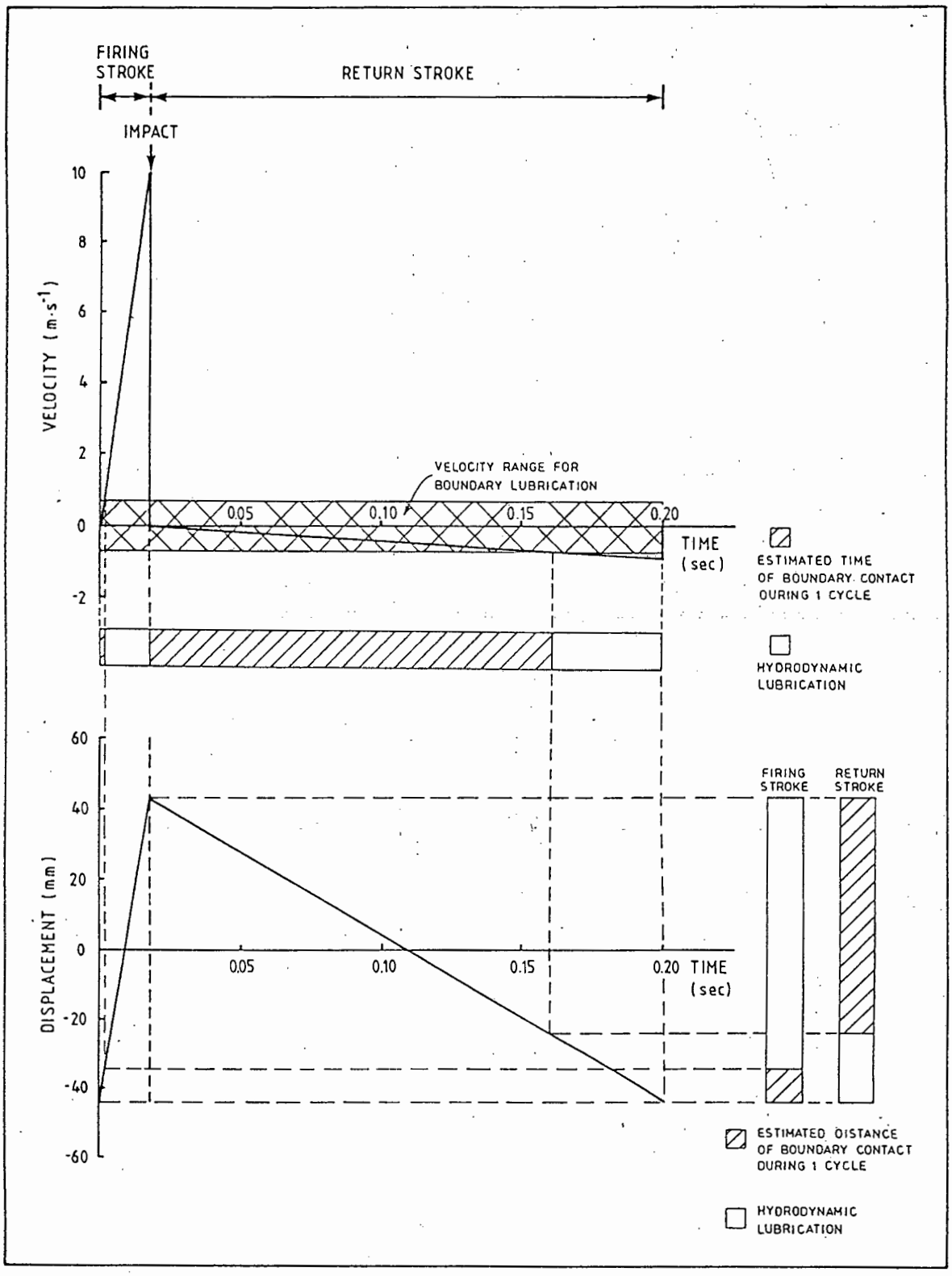

FIGURE 4.1 : An estimation of the boundary contact occurring during a full cycle of the hydraulic impact hammer

Figure 4.1 shows that boundary contact is estimated to occur for approximatley 50% of the length of a cycle whilst a hydrodynamic fluid film forms at the higher velocities. Hence, because wear is only likely to occur during boundary contact, the laboratory wear test rig was designed to run at velocities in the boundary lubrication region. A sinusoidal motion with an average velocity of the order of 1 $m.s^{-1}$ was therefore selected for the test rig. Thus, although the velocities occurring in the stoping machines are considerably higher, the actual velocity over which wear is taking place is comparable.

4.2.4 Surface Roughness

The surface roughnesses of the steel sliding components in the hydraulic stoping machines varied considerably. The impact head of the hammer is machined to a roughness of 0,8 micrometers c.l.a. whilst the chrome plated and liquid honed piston of the rockdrill is finished to a roughness of approximately 0,2 micrometers c.l.a. It was decided that the laboratory tests should be able to accommodate steel counterfaces having roughnesses between 0,1 and 1,0 micrometers c.l.a. Furthermore, the surface roughness of the polymeric seals of the stoping machines is approximately 1,8 micrometers c.l.a. and to comply with this condition the polymer pins in the laboratory tests were machined to an equivalent surface roughness.

4.2.5 Lubricant

The stoping machines under investigation were designed to operate on the high water-based hydraulic fluid named 5:95 which contains 5% of an oil additive in water. It was subsequently determined from detailed SEM examinations of failed seals and bearings taken from impact hammers and hand-held rockdrills that quartzite particles, entrained in the hydraulic fluid, were partially responsible for the wear of these components underground. In addition, the proposed transition from the use of 5:95 hydraulic fluid to pure water is likely to introduce changes in the tribological performance of the polymeric sliding components which

need to be investigated. It is therefore important that the test rig be designed with the facility of being able to test in different lubricants, with or without the addition of abrasive particles. It should be noted, however, that although this study was not intended to cover the addition of abrasive particles to the lubricant the rig was designed with the above in mind.

4.2.6 Stroke

The strokes of the impact hammer and rockdrill are 85 mm and 23 mm, respectively. A stroke of 50 mm was selected for the laboratory wear tester which is a compromise between the above two strokes.

4.2.7 Summary

The test rig is usually a scaled-down version of the real machine, capable of reproducing, at the specimen interface, the operating conditions experienced in service. However, this is not always possible and some compromises have to be made. Table 4.1 compares the operating variables prevailing in the impact hammer and rockdrill with those used during the laboratory tests.

TABLE 4.1 : A comparison of operating variables prevailing in the experimental rig, rockdrill and impact hammer

VARIABLE	EXPERIMENTAL RIG	ROCKDRILL	IMPACT HAMMER
Stroke (mm)	50	23	85
Sliding velocity ($m.s^{-1}$) - firing stroke - return stroke	1,0 (ave.)	10 (max) 3 (max)	10 (max) 0,9 (max)
Pressure (N/mm^{-2})	15	35	18
Surface roughness (micrometers c.l.a.)	0,1 - 1,0	0,2 - 0,4	0,3 - 0,8

Figure 4.2 highlights the differences in the velocity/time and displacement/time curves of the impact hammer and experimental rig, respectively.

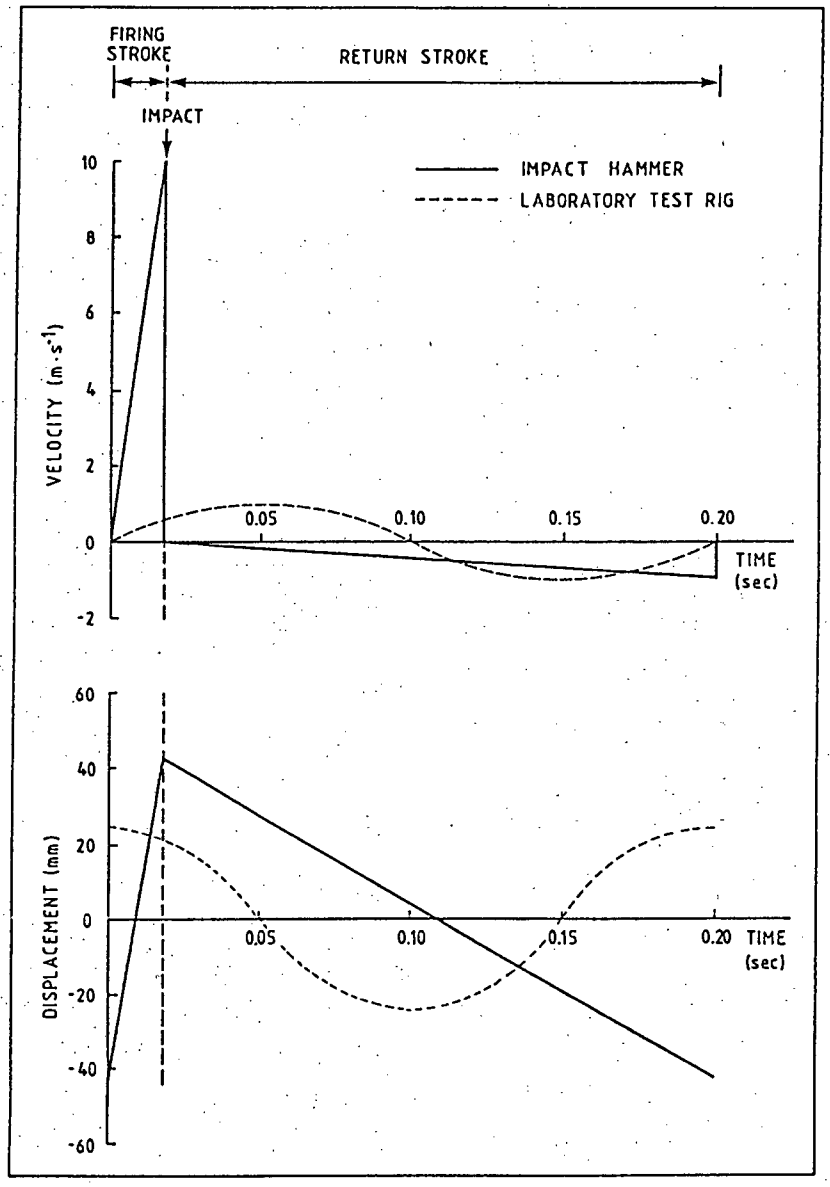

FIGURE 4.2 : Velocity/time and displacement/time curves of the laboratory rig compared with those of the impact hammer

4.3 THE LABORATORY WEAR TESTING MACHINE

Figure 4.3 shows the test rig and peripheral instrumentation.

FIGURE 4.3 : The laboratory wear tester and peripheral instrumentation. The letters refer to the components listed below

The test apparatus consists of the following components:

a) A 0,72 kW D.C. electric motor which supplies mechanical power to the system.

b) A 4:1 ratio gear box which steps down the speed of the motor from 2000 to approximately 500 r.p.m.

c) A thyristor controller which regulates the speed of the motor.

d) A spherical roller bearing which reduces the lateral movement of the gearbox output shaft, caused by the reciprocating motion of the rig.

e) An aluminium housing in which the sliding UHMWPE pin (the seal) is clamped. The whole assembly is rigidly supported between four bearings and is coupled to the gearbox via a system of shafts, cranks and bearings.

f) A friction transducer which measures the friction forces generated at the interface during sliding.

g) An instrumentation amplifier which amplifies the friction force signal from the friction transducer.

h) A polaroid camera for photographing the friction force vs time curve.

i) Thermocouples and a chart recorder used to monitor the sub-surface and lubricant temperatures during sliding.

j) A Linear Variable Differential Transformer (LVDT) which is mounted above the upper sliding specimen and is used to continuously monitor the length-loss of the specimen during a test.

k) A safety shut-off mechanism which operates on a feed-back signal from the LVDT.

l) A stainless steel bath which enables tests to be conducted in various lubricating media.

m) A copper heat exchanger which is used to regulate the lubricant temperature.

n) A lubricant reservoir to supplement lubricant lost from the bath.

o) A float-valve and float which regulates the level of the lubricant in the bath.

4.3.1 The Aluminium Housing

Figure 4.3 shows a detailed drawing of the aluminium housing (component (e) in Figure 4.2).

The whole assembly is supported between four bearings, by two steel rods (C), one on either side. The upper sliding specimen (A) is clamped in the housing by an aluminium T-section (D). Load is transmitted to the specimens by a pre-calibrated steel spring (E), via a screw (F). The spring was calibrated and found to exert a force of 4,75 kg per millimeter of compression. The whole housing then reciprocates against a stationary specimen (B).

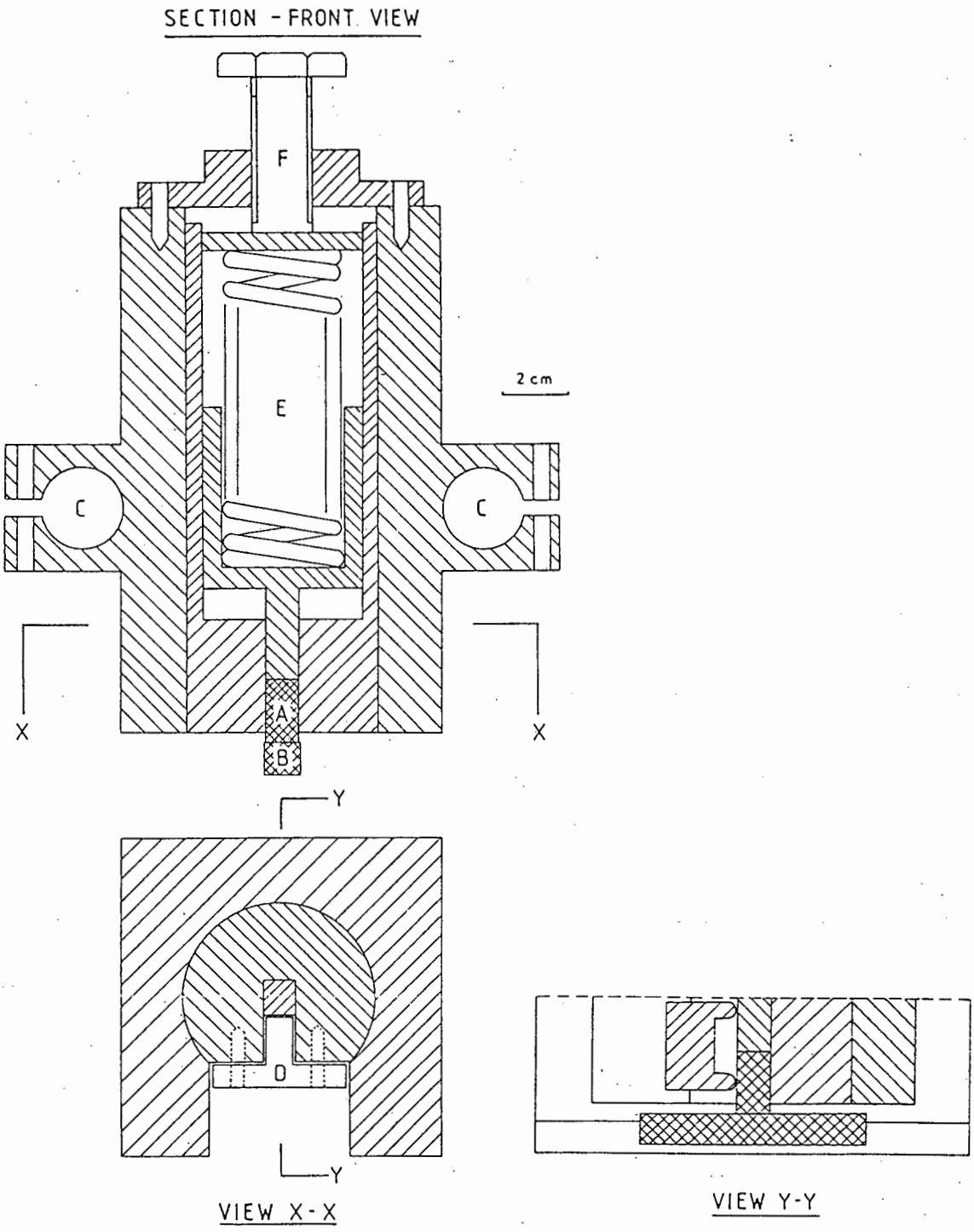

FIGURE 4.4 : A detailed drawing of the aluminium housing

4.3.2 The Stationary Specimen

Figure 4.5 shows the clamping system used to locate the stationary steel plate (the piston) below the sliding polymer pin. The center of the plate coincides exactly with the mid-stroke of the reciprocating housing.

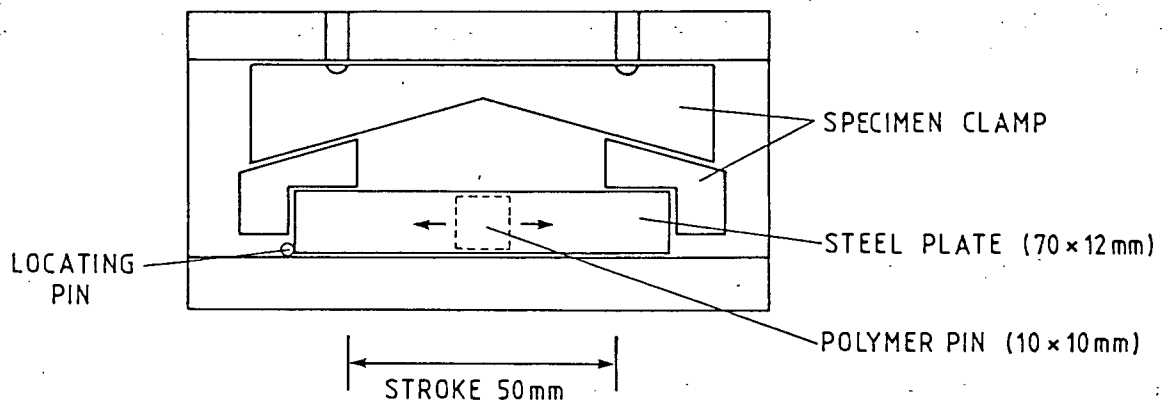

FIGURE 4.5 : The clamping system used to secure the lower specimen. The arrows indicate the reciprocating type of motion

4.3.3 The Lubricant Temperature and Lubricant Level Regulating Systems

The frictional heat generated by the rubbing process, both at the specimen interface and in the rig itself, caused the temperature of the lubricant in the bath to increase appreciably during a test. In order to maintain a constant lubricant temperature during sliding, a system was devised in which water, cooled by a radiator and fan unit, was continuously pumped through a copper heat exchanger coil immersed in the lubricant.

In order that a constant level of lubricant be maintained above the sliding surfaces, a system was designed to continuously replenish any lubricant lost from the bath as a result of splashing or evaporation. The system consists of a simple float-valve and float mechanism which is fed, from a reservoir, with the particular lubricant being used in the test. Figure 4.6 is a schematic representation of the regulating system.

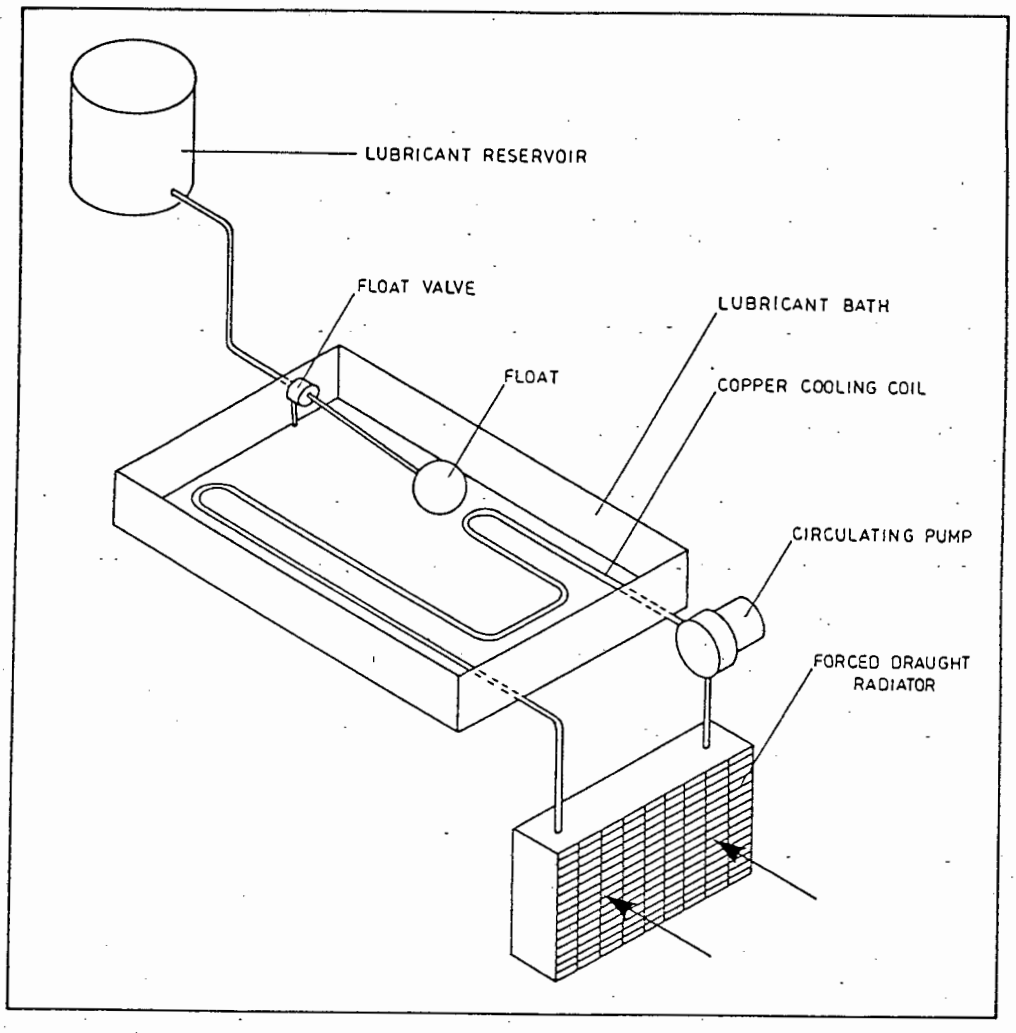

FIGURE 4.6 : A schematic representation of the system used to maintain a constant temperature and level of lubricant in the bath

4.4 METHODS OF MEASURING WEAR RATE, FRICTIONAL FORCE AND SURFACE TEMPERATURE

4.4.1 Wear Rate Calculated from Weight Loss Measurements

The specimens were weighed on a Mettler balance to an accuracy of 0.1 milligrams and the wear rates were calculated from the weight losses recorded after pre-determined sliding distances.

4.4.2 Wear Rate Calculated from Length Loss Measurements

4.4.2.1 Measurement of Length Loss Using a Micrometer

During the interrupted tests a micrometer was used to record the length of the specimen, to an accuracy of

0,01 mm, after each successive sliding interval. However, these values had to be corrected for viscoelastic creep in order to isolate the wear component from the creep component in the total recorded length loss. The corrected length-loss values (due to wear only) were converted to equivalent volumes by multiplying by the nominal surface area of the pin and the wear rates computed.

4.4.2.2 Measurement of Length Loss Using a LVDT

A system was also devised for continuous monitoring of the polymer wear rate. The system consisted of an LVDT located above the polymer specimen holder in such a way that it could measure the progressive reduction in the length of the pin during a test. The measuring system is illustrated in Figure 4.7.

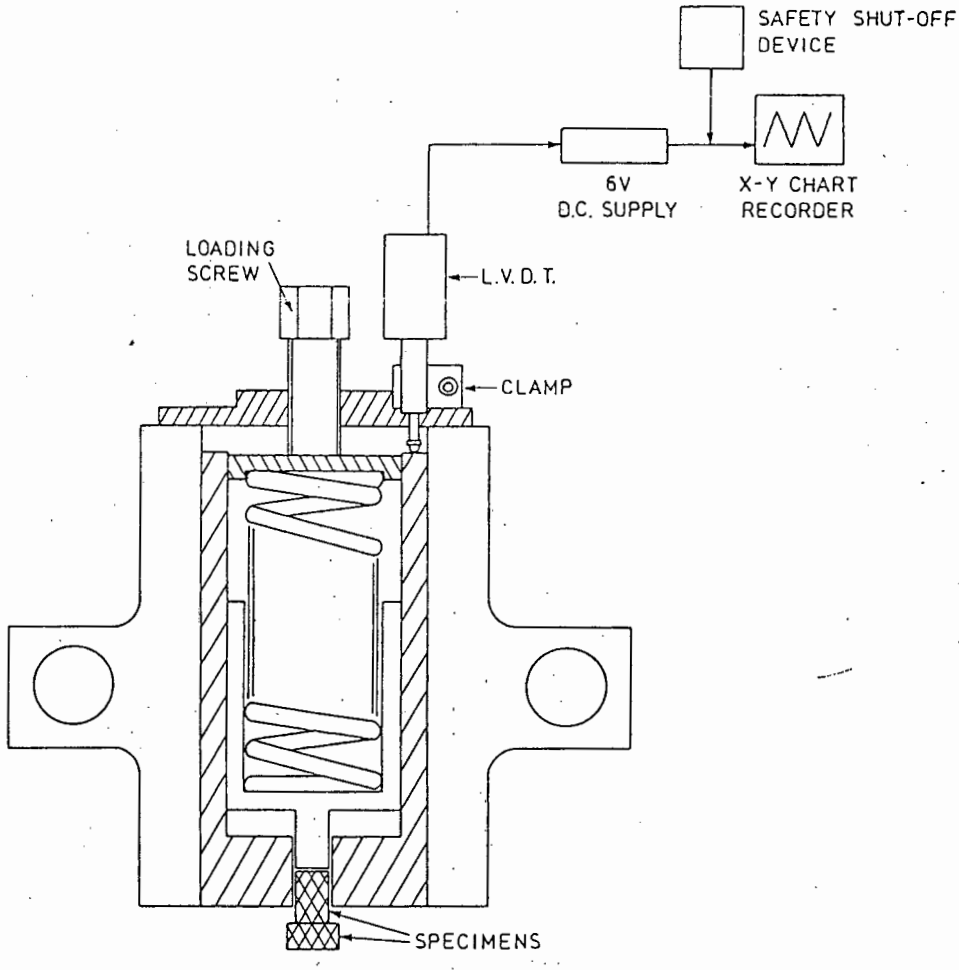

FIGURE 4.7 : The system used for continuous measurement of the polymer wear rate

As the pin creeps and wears down, the specimen holder, to which it is clamped, is lowered by an equivalent distance and this displacement is monitored by the spring-loaded LVDT. The signal is amplified and recorded on a chart.

As a preventative measure, a safety shut-off system was designed which operates on a simple feed-back signal from the LVDT. When the wear of the polymer pin, determined by the extension of the LVDT, exceeded a pre-set limit the rig was automatically switched off.

4.4.3 Measurement of the Frictional Force

Figure 4.8 shows, schematically, the transducer used to measure the friction force at the sliding interface.

The lower specimen holder is mounted on several rows of stainless steel ball bearings which are constrained to move, in the direction of sliding, within parallel machined grooves. Thus, the entire specimen holder can be considered as a nominally "frictionless" trolley. The trolley is connected, via a rigid steel beam, to a vertically mounted bending beam load cell. Frictional forces generated at the sliding interface produce corresponding horizontal displacements of the trolley which are transmitted directly to the load cell. The signal is amplified using an instrumentation amplifier and the friction force is displayed on the screen of a cathode ray oscilloscope. The friction wave-form was then photographed using a polaroid camera modified to fit the oscilloscope. The coefficient of friction was calculated by dividing the horizontal friction force by the applied normal load.

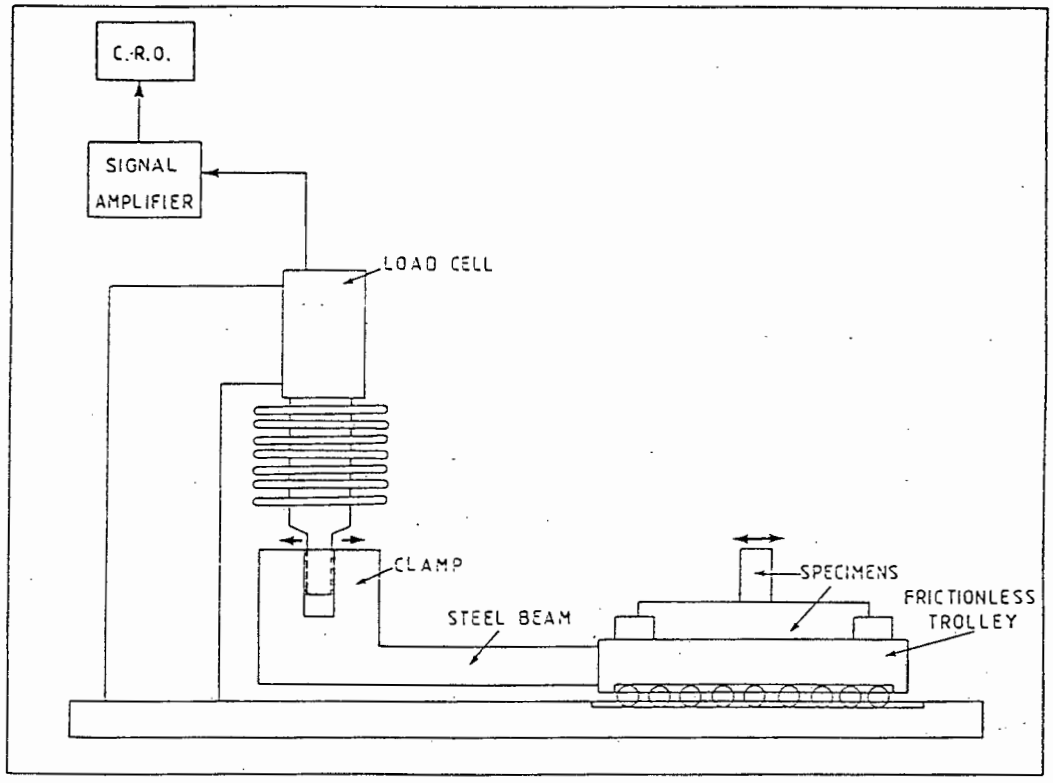

FIGURE 4.8 : A schematic representation of the friction-force transducer

Figure 4.9 is a trace of a typical friction-force curve generated during a lubricated test. At the start of the stroke the sliding velocity is zero and the force required to overcome the static friction is high, i.e., the surfaces "stick" until the static friction force is overcome. The moving specimen then begins to slide with increasing velocity, i.e., "slip" occurs and the friction force decreases to a kinetic value. However, the friction force curve was modified by additional damped vibrations resulting from the motion of the force-measuring system. It is important to note that these vibrations are not artefacts of the actual sliding process and that only one stick-slip cycle occurs at the interface during each cycle.

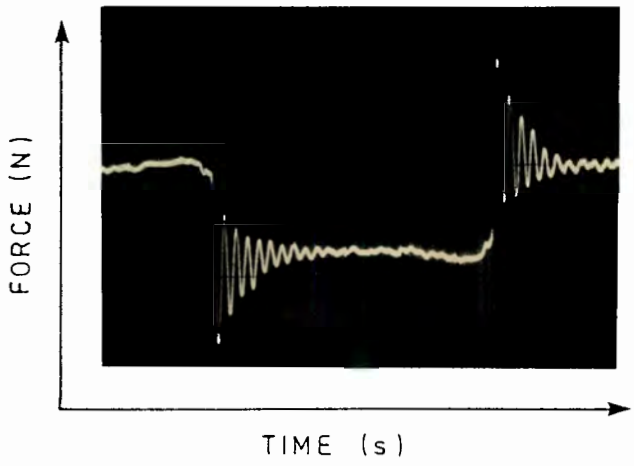

FIGURE 4.9 : A typical friction-force curve recorded during a test in water at a sliding speed of 0,5 $m.s^{-1}$

4.4.3 Measurement of the Surface Temperature

No attempt was made to compute the actual temperatures at the sliding interface. The different thermal properties of the materials of the couple, the complex geometry of the specimens and the fact that sliding was occurring under lubrication required that complex calculations, involving thermal conductivities and heat transfer, be carried out in order to determine the actual temperatures occurring at the contacting asperities. Instead, an estimation of the mean surface temperature-rise resulting from frictional heating at the interface was obtained by locating iron-constantan thermocouples in drilled holes between 0,1 and 0,3 millimeters below the surfaces of the steel plates. With reference to Figure 4.10, one thermocouple was located at the end of the stroke to measure the temperature generated by the high static friction peak and the other was located at mid-stroke to record the temperature generated at the point of maximum sliding velocity.

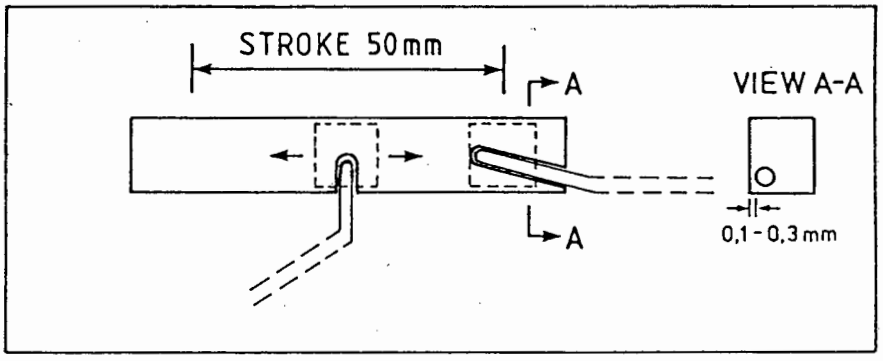

FIGURE 4.10 : The location of the thermocouples for measuring the temperature rise at the surface of the steel specimen

The thermocouples, which have a sensitivity of 0,05 millivolts per degree Celcius at room temperature, were used simply to compare the temperatures generated under the various sliding conditions. An identical thermocouple was used to monitor the temperature of the lubricant throughout the test and both the subsurface and lubricant temperatures were recorded on a chart. The difference between the two temperatures at any point gives the mean temperature-rise at the interface.

CHAPTER 5

EXPERIMENTAL TECHNIQUES

5.1 SPECIMEN PREPARATION

5.1.1 The AISI 431 Stainless Steel Plates

The plates were machined from round bar stock, obtained from a single supplier, to dimension of 70 mm x 12 mm x 10 mm. The holes for locating the subsurface thermocouples were drilled using a 3 mm diameter drill. The plates were then subjected to the following heat treatment; soaked at 1010°C for 45 minutes, oil quenched and double tempered at 260°C for one hour. This treatment, which is used for AISI 431 machine components, improves the fatigue strength and impact toughness, as well as the corrosion and wear resistance of the steel. The resulting hardness, measured on a universal hardness tester, was 395-420 HV30 (40-42 HRC) which is in good agreement with specifications of 40-46 HRC. The final surface finish was obtained using a mechanical surface grinder. Where possible, all the specimens from a test series were ground at the same time as great difficulty was experienced in reproducing a particular surface finish. The specimens were always ground perpendicular to the sliding direction and by carefully controlling the feed rate, depth of cut and the dressing of the grinding wheel roughnesses of between 0,1 and 1,0 micrometers c.l.a. were possible. Figure 5.1 is a SEM micrograph of the surface of a ground steel plate.

Machining chips similar to the one circled in Figure 5.1 were randomly distributed on the ground steel sufaces. It is thought that these sharp fragments, which are fatigued from the surface during sliding, become embedded in the reciprocating polymer pin and cause severe damage to both surfaces of the couple by a three body abrasive wear mechanism. Evidence supporting this mechanism is presented in Chapter 6.

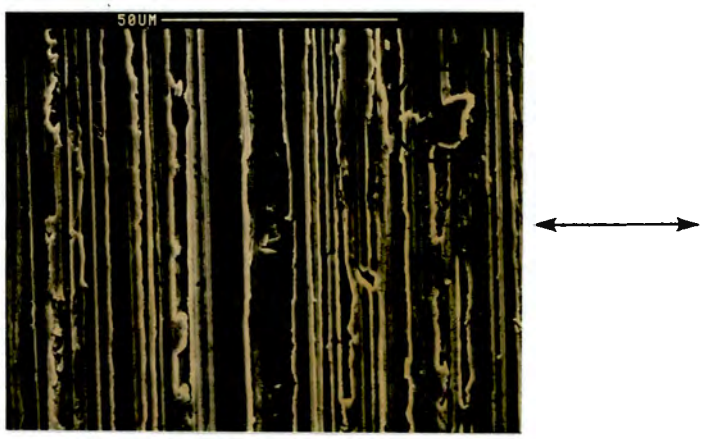

FIGURE 5.1 : The ground surface of an AISI 431 specimen before a test (c.l.a. surface roughness : 0,404 ± 0,032 micrometers). The arrow indicates the sliding direction

The surface roughness was measured using a Taylor-Hobson Talysurf profilometer. The readings were taken perpendicular to the grinding direction, i.e., in the direction of sliding. The centre-line-average (c.l.a.) roughness values quoted are the mean values of ten traversals at arbitrarily chosen positions on the specimen surface. A pen-recorder trace of each surface was also obtained. Figure 5.2 shows the magnified profile of the surface of the specimen shown in Figure 5.1.

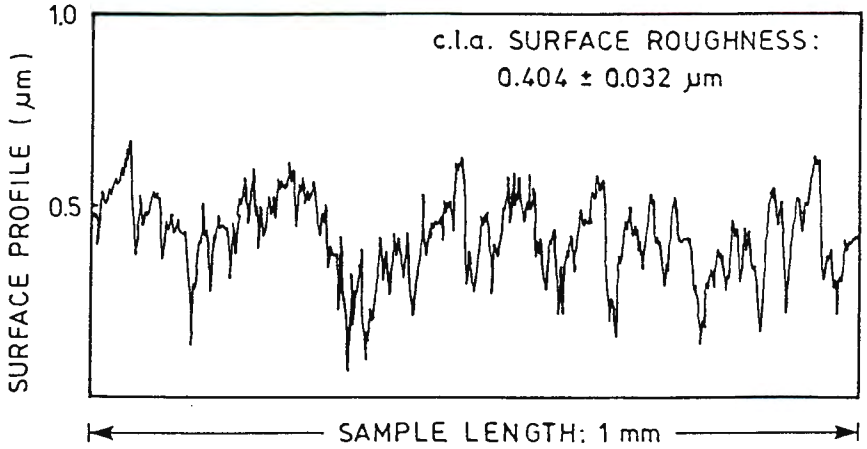

FIGURE 5.2 : The surface profile of the specimen shown in Figure 5.1

After machining the plates were ultra-sonically cleaned in alcohol and then passivated by immersing them in dilute (20%) aqueous nitric acid for 30 minutes. This process, which results in the formation of an impervious, passive oxide film on the surface, is used to improve the corrosion resistance of the steel.

5.1.2 The UHMWPE Pins

The UHMWPE used in this study was Hostalen GUR which was supplied in the form of an extruded round bar. Table 5.1 gives some of the physical and mechanical properties of UHMWPE.

TABLE 5.1 : Physical and mechanical properties of UHMWPE (taken from the Fulmer Materials Optimiser)

PROPERTY	UNITS	VALUE
Specific gravity at 23°C	$g.cm^{-3}$	0,937-0,960
Tensile stress; at yield at break	$MN.m^{-2}$	17-27 38-48
Elongation at break	%	300-500
Elastic modulus in tension	$MN.m^{-2}$	140-170
Notched impact strength	$J.m^{-1}$	No break
Hardness	Shore D	60-70
Flexural Creep Modulus, 1 minute value	MPa	680-890
Maximum continuous service temperature, no load	°C	90
Heat deflection temperature 1,85 MPa 0,45 MPa	°C	68-82 95
Molecular weight		$2\text{-}10 \times 10^6$
Water absorption, 24 hours	%	<0,01

Figure 5.3 illustrates how specimens, with dimensions 25 mm x 10 mm x 10 mm, were machined from the bar with their lengths parallel to the extrusion direction. This means that, at the interface, sliding takes place perpendicular to the extrusion direction. All specimens were taken from the central core of the rod in order to minimise possible anisotropy effects across the diameter of the bar, i.e., as a result of the extruding operation, density and molecular orientation at the outer circumference of the rod are likely to differ from those at the centre. As an added precaution the machined specimens were marked to ensure that the direction of the final machining marks were identical on all specimens.

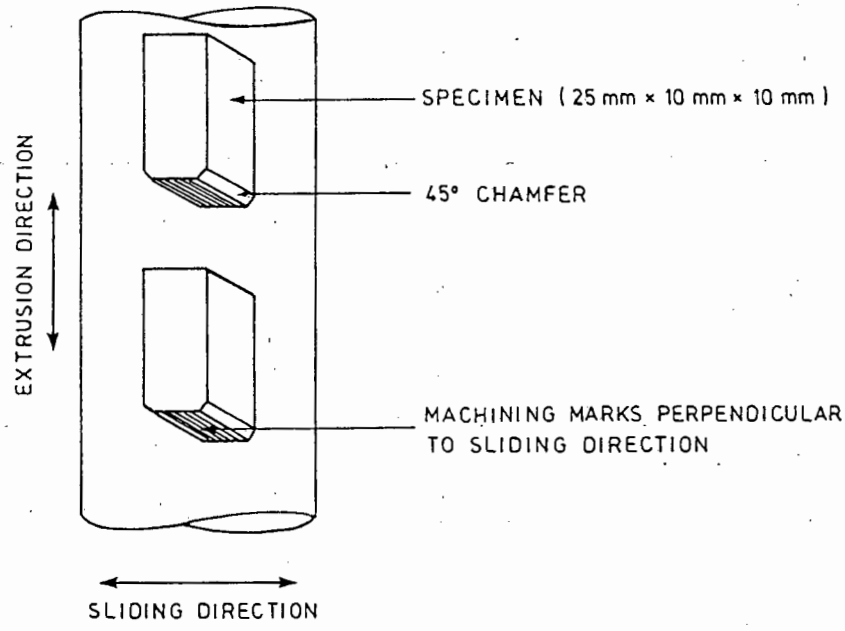

FIGURE 5.3 : A schematic representation showing the method in which the polymer specimens were machined from the extruded rod

To minimise distortion of the specimen under load, a 45˚ chamfer was cut along the leading and trailing edges of the specimen. This is illustrated in Figure 5.3 above. The chamfer also ensured that the polymer wear debris was totally removed from the specimen surface during sliding. The nominal surface area was reduced to approximately 90 mm^2 by the chamfer. The final machined surface

was reproduced on a milling machine using a 20 mm diameter side-cutter. By controlling the feed-rate and spindle speed, a roughness value of approximately 2,0 ± 0,3 micrometers c.l.a. was obtained. As on the steel plates, the machining marks run perpendicularly to the sliding direction. Figure 5.4 is a SEM micrograph of the machined polymer surface prior to testing.

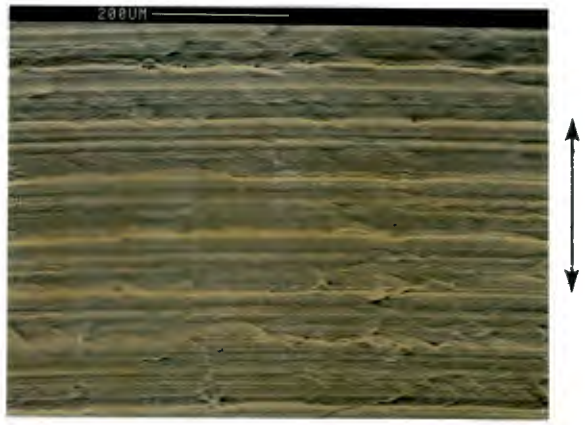

FIGURE 5.4 : The machined polymer surface prior to testing (c.l.a. surface roughness : 2,04 ± 0,031 micrometers). The arrow indicates the sliding direction

Finally, the specimens were ultra-sonically cleaned to remove any dirt resulting from the machining process.

5.2 TEST PROCEDURE

Wear is affected by many different factors and in order to eliminate unwanted variables a standard practice was developed and rigorously adhered to.

(i) The steel plate with the thermocouples in place, was loosely clamped in the lower specimen vice.

(ii) The aluminium housing was centred at mid-stroke.

(iii) A 1,5 mm spacer was used to ensure that a constant length of polymer pin protruded from beneath the upper specimen holder and the pin was lightly secured with the T-clamp.

(iv) The load spring was placed in position and the load screw secured such that no load was being exerted.

(v) The LVDT was clamped in its vice above the polymer specimen and the load applied (1 revolution = 1,5 mm of compression = 7,125 kg force).

(vi) For extended tests a safety limit was set on the LVDT system.

(vii) Both specimens were fully tightened.

(viii) The lubricant was added and, if necessary, the level was adjusted with the float and float-valve mechanism.

(ix) The chart recorders were switched on.

(x) The sliding speed was set on the thyristor controller.

(xi) The thermocouple temperatures were zeroed and the temperature regulating system switched on.

(xii) The C.R.O. was switched on and the polaroid camera attached.

5.2.1 Measurement of the Specific Wear Rate

5.2.1.1 The Weight-Loss Method

Weight-losses were recorded to an accuracy of 0,1 milligrams after each test period. For the lubricated tests the weight losses were corrected for absorbtion of lubricant by the polymer pin. Initially, absorbtion was determined by immersing an identical specimen in the lubricant for the duration of the test and measuring the resultant weight gain. The absorption of lubricant by the UHMWPE pins under these static conditions was, however, inconsistent and difficult to measure. It is also likely that dynamic absorption of lubricant at the sliding interface is different from that under the static

conditions mentioned above. Alternatively, the specimens were stored in a dessicator and reweighed after 12 hours in order to monitor any fluctuations in the weight of the specimen resulting from absorption. The final weight loss measurements were then taken as the differences between successive "acclimatised" values. The weight losses were converted into equivalent volumes by dividing by the density of the polymer and a cumulative volume loss versus sliding distance graph was plotted from this data as illustrated in Figure 5.5.

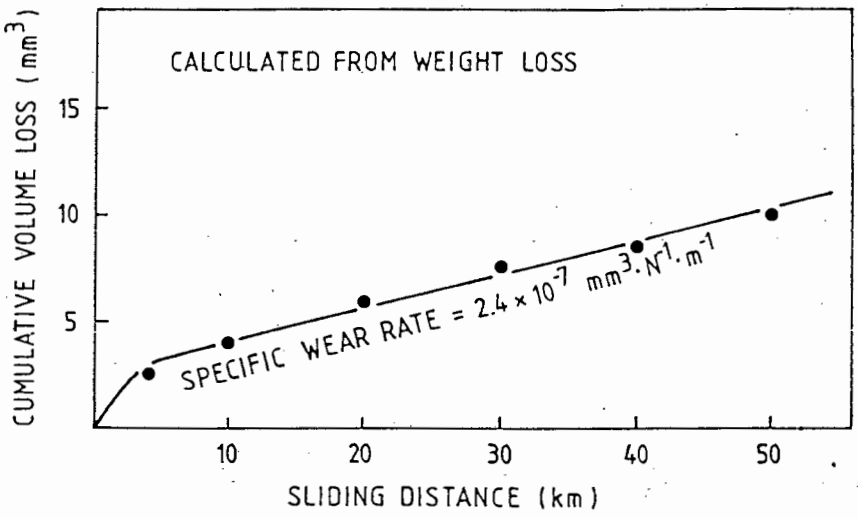

FIGURE 5.5 : A cumulative volume loss vs sliding distance curve calculated from weight loss measurements (sliding speed : 0,5 $m.s^{-1}$; normal load : 100 kg; counterface roughness : 0,419 ± 0,042 microns c.l.a.; lubricant : water)

The curve is characterised by a high initial wear rate or "running-in" period, followed by a steady-state period in which the relationship between volume loss and sliding distance is linear. The specific wear rate for the test was finally calculated by dividing the slope of the linear portion of the graph by the applied normal load.

5.2.1.2 The Length Loss Method Using a LVDT

An LVDT was used to record the reduction in the length of the specimen whilst sliding was actually taking place. However, accurate measurement of length loss was considerably impaired by the superimposed effects of viscoelastic creep. As a result of the viscoelastic behaviour of the polymer the length loss values recorded during the wear tests were comprised of a wear component and a creep component. In order to calculate the wear rate the two components had to be separated. This is illustrated schematically in Figure 5.6.

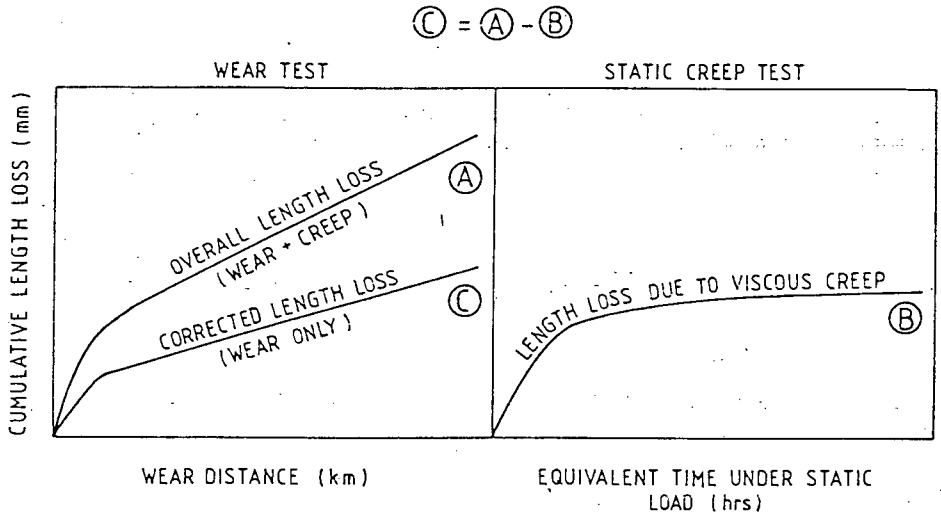

FIGURE 5.6 : Separation of the creep component from the wear component in the total length loss value recorded during a wear test

To determine the creep component of the length-loss a series of static loading tests were performed. Identical polymer pins were subjected to the same loading/unloading sequence as that used during a normal wear test and the resulting change in the length of the specimen was monitored as a function of time using the LVDT. Figure 5.7 shows the static creep response of a polymer specimen recorded by the LVDT. The specimen was placed under a

100 kg load for 20 hours, unloaded and then allowed to recover viscoelastically for 20 hours. The elastic, viscoelastic and non-recovered viscous creep components can be easily distinguished.

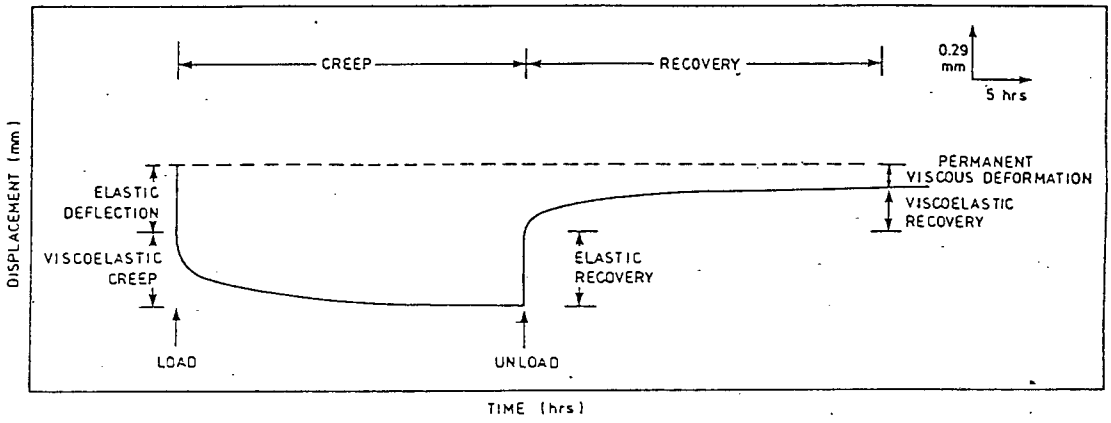

FIGURE 5.7 : The static creep response of a polymer specimen under load and during viscoelastic recovery

Figure 5.8 shows a static creep curve and the curve obtained from a 20 hour wear test in water.

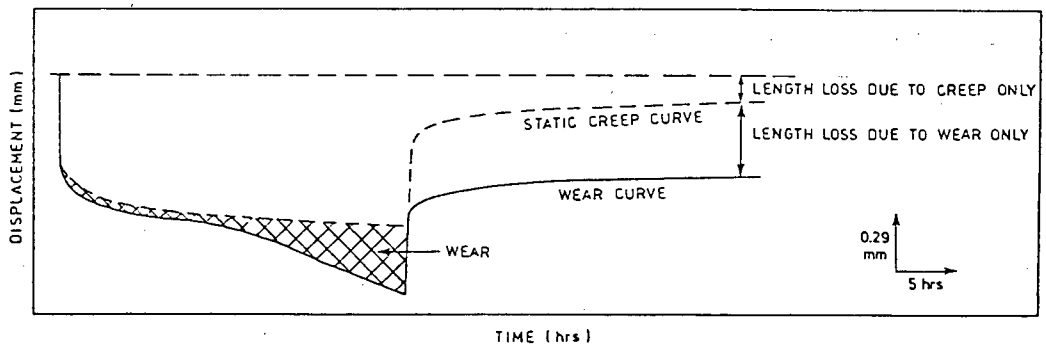

FIGURE 5.8 : A static creep curve and a wear curve measured by the LVDT during a 20 hour test in water (sliding velocity : 0,5 $m.s^{-1}$; normal load : 100 kg; counterface roughness : 0,410 ± 0,031 micrometers c.l.a.)

In order to determine the length loss due to wear alone the static creep curve was subtracted from the wear curve which is composed of both wear and creep components. The resulting length loss curve is shown in Figure 5.9.

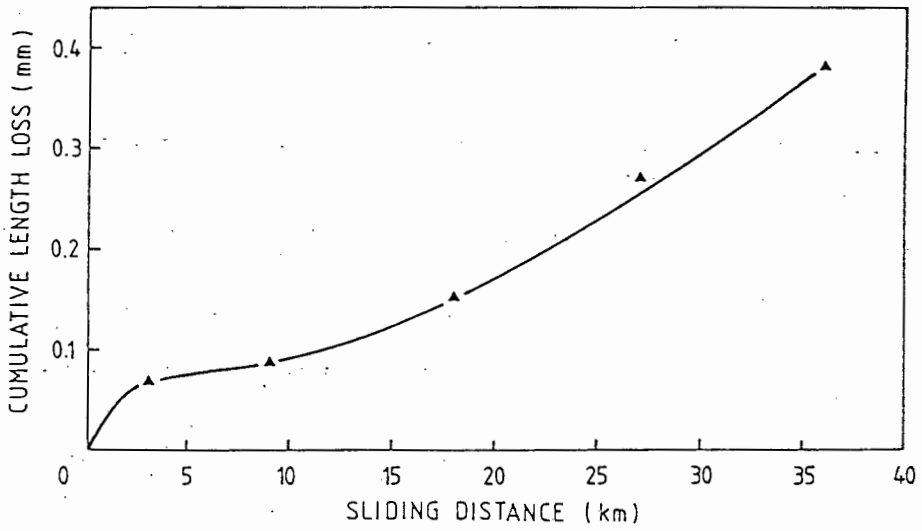

FIGURE 5.9 : Length loss vs sliding distance curve calculated from the wear and creep curves plotted in Figure 5.8

Figure 5.9 shows that a steady-state wear rate was not attained during these continuous tests. Instead, there was an exponential increase in the length loss with sliding distance which made the calulation of the specific wear rate extremely difficult. The viscoelastic properties of the polymer ultimately resulted in poor reproducibility of both the wear and creep data measured with this system and it was subsequently discontinued.

5.2.1.3 The Length Loss Method Using a Micrometer

During the interrupted tests a micrometer was used to

record the length loss of the polymer after each sliding interval. The length was recorded to an accuracy of 0,01 mm and each measurement was the average of five readings. However, the length losses recorded in this way also had to be corrected for viscoelastic creep in order to isolate the wear component in the total recorded length loss. A creep curve was thus established during a series of static loading tests. The specimen length was measured prior to loading and, after a pre-determined time under load, the pin was unloaded and allowed to recover for 12 hours before the length was re-measured. The non-recoverable viscous deformation for each successive load/unloading cycle was then plotted on a cumulative length loss versus time graph. Figure 5.10 shows the length loss due to viscous deformation of three polymer pins subjected to a loading sequence of 2, 3, 5, 5, 5, 5 hours under a load of 100 kg.

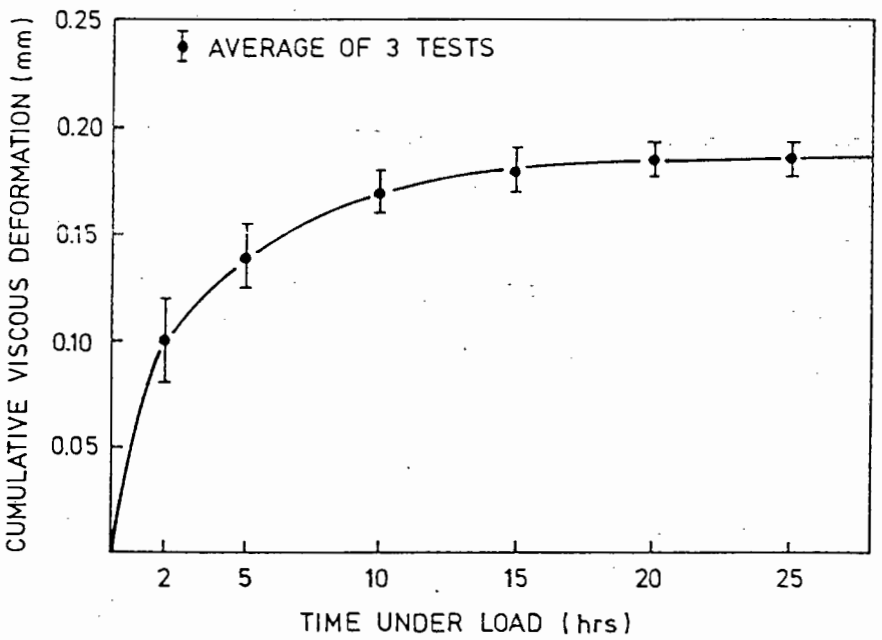

FIGURE 5.10 : Static creep tests : The cumulative length loss due to permanent viscous deformation. The loading sequence was 2, 3, 5, 5, 5, 5 hours under a load of 100 kg

The graph shows that the viscous deformation was considerable during the first 10 hours under load and then levelled off. In fact, there was no measurable viscous deformation after 25 hours, i.e., the specimens recovered fully after the removal of the load. This data was then used to isolate the wear component in the total length-loss recorded during a test, i.e., the value of permanent viscous deformation measured for a particular time under static load was subtracted from the overall length-loss measured for the equivalent time during the actual wear test. Figure 5.11 shows the overall length-loss recorded during a wear test and the corrected length-loss obtained by subtraction of the viscous creep curve shown in Figure 5.10.

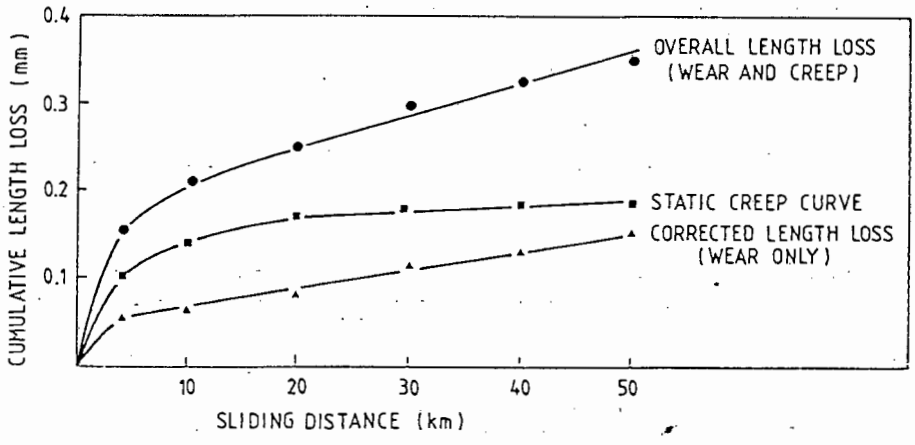

FIGURE 5.11 : The overall length loss and corrected length loss curve measured during a wear test (sliding velocity : 0,5 $m.s^{-1}$; normal load : 100 kg; counterface roughness : 0,419 ± 0,042 micrometers c.l.a.; lubricant : water)

The corrected length losses were converted to equivalent volumes by multiplying by the nominal surface area of the pin. These areas, which were calculated after each

sliding interval, were accurately measured with a vernier mounted on an optical microscope.

5.2.1.4 A Comparison of the Weight Loss and Length Loss Measuring Methods

Figure 5.12 compares the cumulative volume loss versus sliding distance curves calculated from weight loss with those resulting from the two length loss measuring methods.

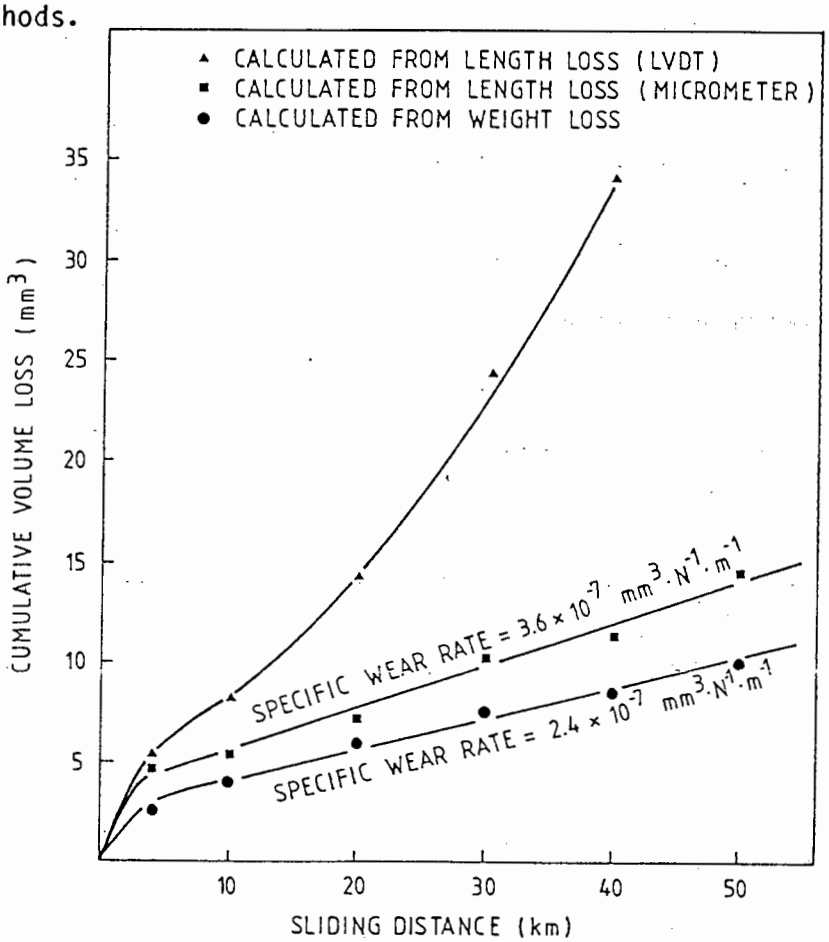

FIGURE 5.12 : Cumulative volume loss vs sliding distance curves calculated via the three measuring methods

The figure shows that the shapes of the wear curves and the resulting specific wear rates varied from one measuring system to the next. The specific wear rates calculated via weight loss and length loss (with a micrometer) for the same test were 2,4 x 10^{-7} and 3,6 x 10^{-7} $mm^3.N^{-1}.m^{-1}$, respectively whilst the calculation of

the specific wear rate from the length loss measured with the LVDT was not possible. The discrepancy in the wear rates calculated via the weight loss and length loss (micrometer) methods can be ascribed to the fact that the creep component of the length loss could only be determined under static loading conditions which are likely to differ from the conditions prevailing during sliding. The accelerating wear rates observed during the continuous tests are probably due to increased thermal degradation of the polymer surface layers.

It became apparent during the course of this study that the calculation of the polymer wear rate from length-loss measurements was not practical due to the viscoelastic nature of the material which required that separate static creep tests be performed in order to isolate the wear component from the creep component in the total measured length loss. However, the length-measuring system could easily be adapted to measure the wear rates of other materials, such as metals and ceramics, which do not creep at room temperature. Consequently, the wear rate data quoted in this study were all calculated from weight losses.

5.2.2 Measurement of the Coefficient of Friction

The friction-force tranducer in the experimental rig allows the coefficient of friction to be calculated at any time during a test. It also distinguishes between the static friction peak occurring at the start of the stroke and the steady-state friction which prevails for the remainder of the cycle. These will be referred to as the "static" and "kinetic" friction coefficients, respectively. During the tests friction measurements were taken hourly during the running-in wear period and then less frequently once steady-state sliding was established. The friction force was calculated from the magnitude of the amplified friction-force signal generated by the transducer and displayed on the C.R.O. The friction coefficients are calculated by dividing the frictional force, in Newtons, by the applied normal force in

Newtons. In order to observe the effect of the various operating conditions on the shape of the friction force vs time curve, polaroid photographs were taken when required. Figure 5.13 illustrates how the friction coefficients (static and kinetic) were calculated from the friction force vs time curves.

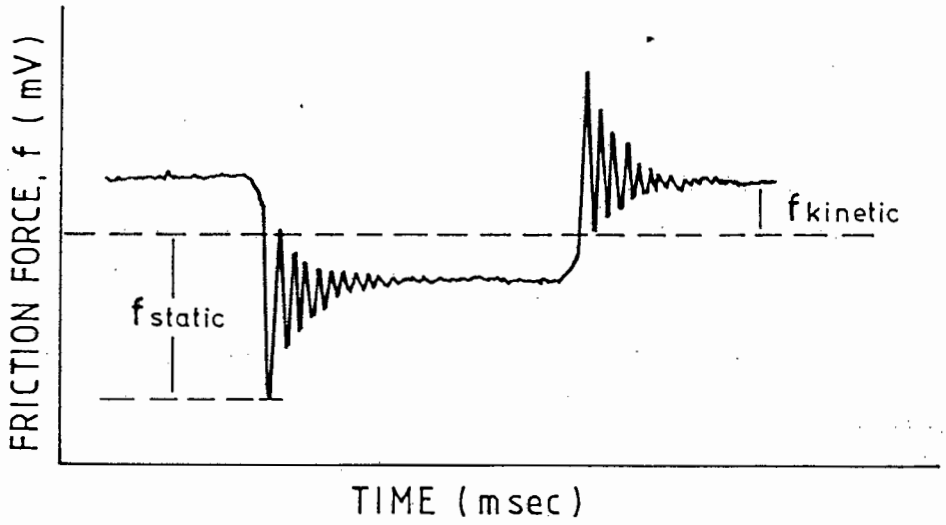

FIGURE 5.13 : The calculation of the friction coefficients from the friction force curve

The friction coefficients plotted in the subsequent chapters are those calculated at the end of each test period, i.e., prior to the test being stopped for weighing of the polymer pin.

5.2.3 Measurement of the Surface Temperature

The temperature measured by the subsurface thermocouples in the steel plates and the one in the lubricant were monitored on a x-t chart recorder throughout the test. Figure 5.14 shows the surface and lubricant temperatures recorded during a test in water. The temperature usually rose rapidly at the start of the test and then levelled out at a steady-state value whilst the temperature regulating system maintained a constant lubricant temperature. The temperature-rise at the specimen surface was calculated by subtracting the lubricant temperature from the steady-state surface temperature.

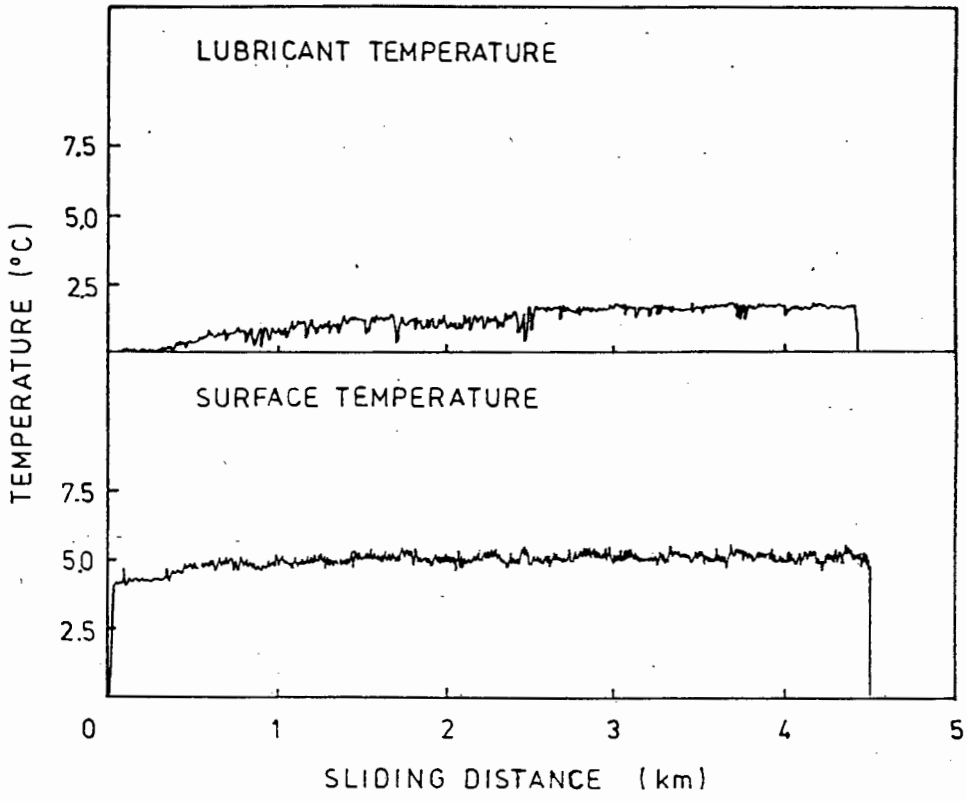

FIGURE 5.14 : The surface temperature and lubricant temperature recorded during a test in water (sliding velocity : 0,25 $m.s^{-1}$; normal load : 100 kg; counterface roughness : 0,376 ± 0,029 micrometers c.l.a.)

5.2.4 The Test Duration

Each test was divided into intervals, the length of which was determined by the sliding distance required for a measurable weight loss. In order to monitor running-in wear the sliding intervals were shorter during the initial stages of the test. Once a steady-state wear regime was attained the intervals were lengthened. The standard test lasted for 25 hours and was usually divided into a sequence of 2, 3, 5, 5, 5, 5 hour intervals. Depending on the sliding velocity, this meant that the total sliding distance covered during the laboratory tests varied between 20 and 50 km. This distance is shorter than the total length of sliding endured by the polymer seals in the stoping machines, where the average life of a piston seal from a rockdrill is estimated to be approximately 100 km of boundary contact.

However, the distance over which steady-state sliding occurred was approximately 40 km of a 50 km test which is considered to be long enough to extrapolate to the real situation. The possibility of a wear transition occurring during the laboratory tests was considered to be extremely unlikely as the transition was shown to occur only after many hundred kilometers of lubricated sliding.

5.2.5 Scanning Electron Microscopy (SEM)

The worn surfaces of both the polymer pin and the steel counterface were examined in a Cambridge Stereoscan 200 SEM in order to identify the wear mechanisms occurring under the different operating conditions and to compare the features with those observed on the worn polymer components from the hydraulic stoping machines. Representative polymer specimens, selected from each series of tests, were cleaned in Arklone and Au/Pd coated. The steel counterfaces were coated in order to protect, if any, the sensitive polymer transfer film. Polymer wear debris, which was recovered from the lubricant after each test, was also examined. The micrographs appearing in subsequent sections were taken in such a way that the sliding direction was from left to right in each case.

5.3 THE REPRODUCIBILITY OF THE TEST

It is of paramount importance that laboratory wear tests should yield reproducible results. By careful control of the operating variables and the use of a standard testing procedure, it was possible to maintain the reproducibility of the test at an acceptable level. The reproducibility of the test was determined during a series of three tests conducted under the following operating conditions:

TABLE 5.2 : Operating conditions applied during the reproducibility tests. (The key refers to the curves shown in Figure 5.15)

TEST	KEY	SLIDING SPEED $m.s^{-1}$ (ave.)	NORMAL LOAD (kg)	c.l.a. SURFACE ROUGHNESS (m)	LUBRICANT
1	▲	0,25	100	0,374 ± 0,033	Water
2	●	0,25	100	0,362 ± 0,018	Water
3	■	0,25	100	0,334 ± 0,015	Water

Each test was divided into intervals of 2, 3, 5, 5, 5, 5 hours to allow the weight-loss measurments to be carried out. The weight losses were converted into equivalent volumes and the cumulative volume losses plotted against sliding distance. The results of the three tests are shown in Figure 5.15 and in Table 5.3. All the tests followed the same general trend of an initial running-in period, where the wear rate was higher, followed by a steady-state wear regime in which the relationship between volume loss and sliding distance was linear. (The linear correlation coefficients in the steady-state region were all better than 0,99). However, due to small variations in the operating parameters, particularly the counterface roughness, the slopes of the graphs in the steady-state regions varied accordingly.

The reproducibility of the test was determined by accumulating the results of the three tests and plotting them on a single graph, i.e., the mean cumulative volume-losses and corresponding standard deviations were calculated after each sliding interval. Linear regression was used to plot a line of best fit through these points and the mean specific wear rate for the series of tests was calculated by dividing the slope of the line by the applied normal load. This is illustrated in Figure 5.15.

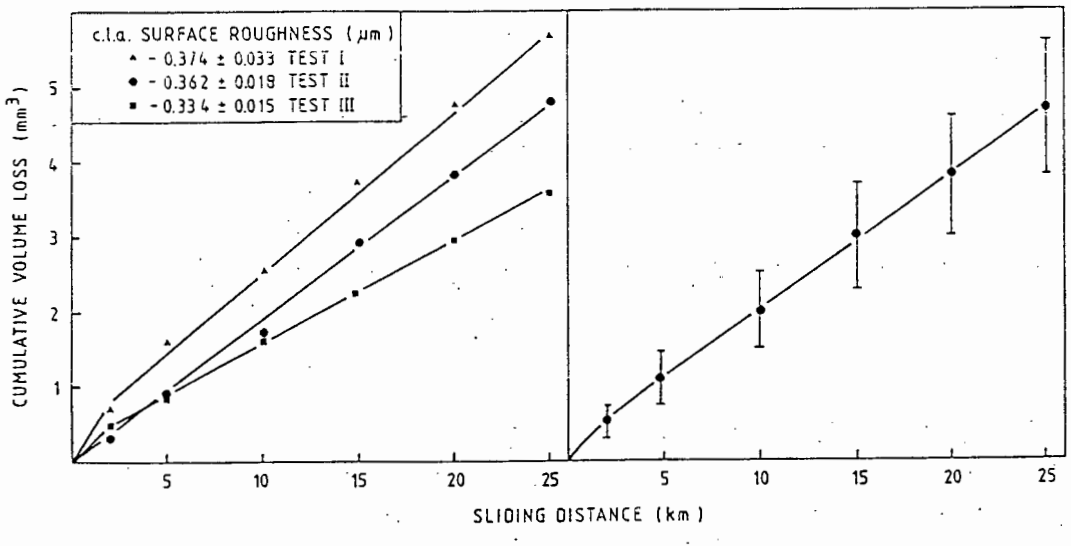

FIGURE 5.15 : The reproducibility of the volume loss measurements (sliding speed : 0,25 $m.s^{-1}$; normal load : 100 kg; lubricant : water)

TABLE 5.3 : Results of the reproducibility tests. (The key refers to the curves in Figure 5.15)

TEST	KEY	c.l.a. SURFACE ROUGHNESS (μm)	STEADY-STATE WEAR RATE (mm^3/km)	LINEAR CORRELATION COEFFICIENT	SPECIFIC WEAR RATE ($mm^3.N^{-1}.m^{-1}$)
1	▲	0,374 ± 0,033	0,2426	0,9981	$2,43 \times 10^{-7}$
2	●	0,362 ± 0,018	0,2173	0,9970	$2,17 \times 10^{-7}$
3	■	0,334 ± 0,015	0,1566	0,9981	$1,57 \times 10^{-7}$
Average		0,357	0,2055	-	$2,06 \times 10^{-7}$
Standard Deviation %		± 5,7%	± 21,5%	-	± 21,5%

Considering the viscoelastic nature of the material and the interrupted test procedure used, the reproducibility of the test was considered to be of an acceptable level. The reproducibility of each individual test, however, was very good, as indicated by the high linear correlation coefficients. The difference in the wear rates of the three tests is ascribed to the variation in counterface roughness.

The friction coefficients (static and kinetic) and surface temperature-rise data from the three tests were also measured in order to determine their reproducibility. Figure 5.16 shows the friction coefficients measured during the separate tests, as well as the mean and standard deviations calculated at each point. The reproducibility of the friction values was good, especially during steady-state wear. The gradual decrease in the friction coefficients with sliding distance during the water lubricated tests should be noted.

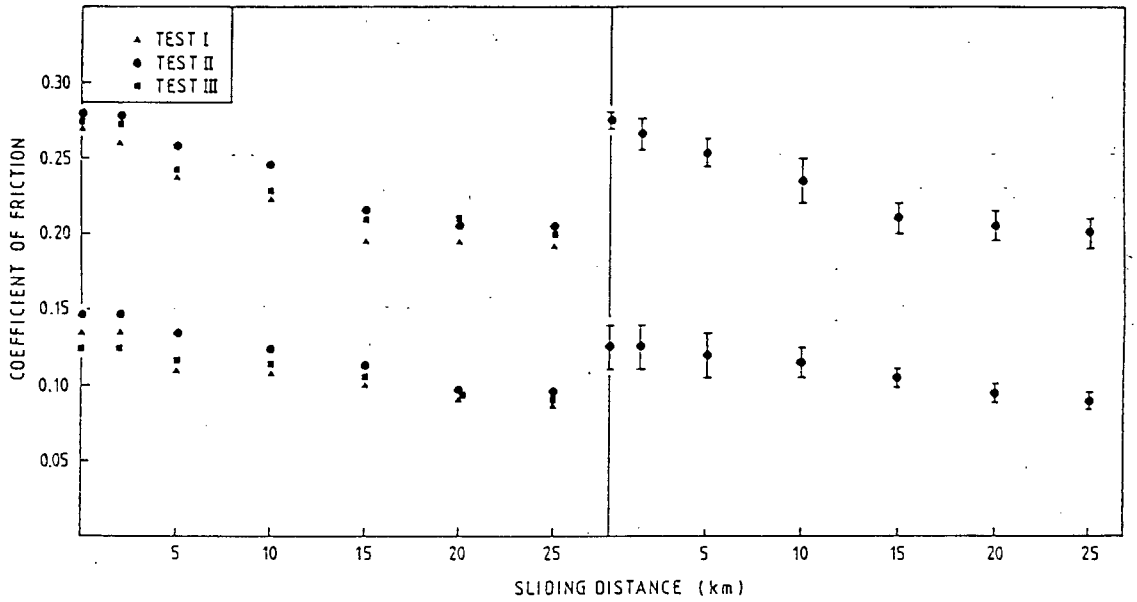

FIGURE 5.16 : The reproducibility of the friction coefficient data. (The key is the same as in Figure 5.15)

The reproducibility of the temperature rise values is given in Figure 5.17. The standard deviations, on a mean value of approximatley 3°C, was less than 1°C.

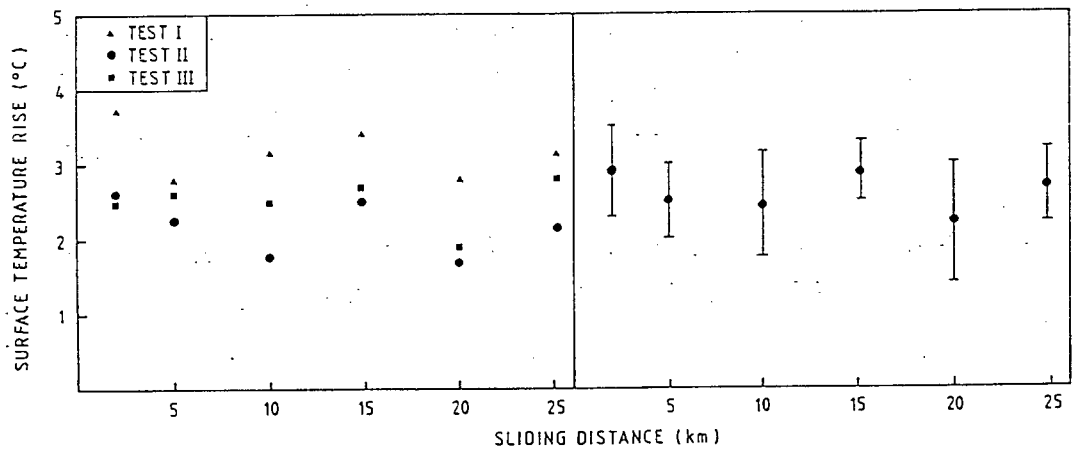

FIGURE 5.17 : The reproducibility of the surface temperature-rise measurements. (The key is the same as in Figure 5.15)

The tests showed that the major parameters of the test, namely wear rate, friction and temperature could be reproduced to within acceptable limits by careful control of the test conditions. The laboratory wear rig can, therefore, be considered as satisfactory for evaluating the wear performance of polymers sliding against stainless steel under a range of operating conditions.

CHAPTER 6

RESULTS AND DISCUSSION

The primary objective of this project was to compare the wear performance of UHMWPE sliding against AISI 431 stainless steel in water and 5:95, respectively. Secondly, the effects, if any, of the various operating parameters on the wear of the polymer, in both lubricating media, needed to be established. To this end, a number of reciprocating sliding wear tests were conducted in which the sliding velocity, normal load, counterface roughness and lubricant was varied systematically over a wide range and the resulting wear rates, friction coefficients, surface temperatures and microscopic surface morphologies monitored.

In order to establish the effect of sliding velocity, tests were run in 5:95 and water at two different speeds, under conditions of constant normal load and counterface roughness.

To monitor the effect of counterface roughness, in both 5:95 and water, the roughness of the metal plate was varied over a wide range of values whilst maintaining a constant sliding velocity and normal load.

The effect of normal load was investigated during tests run in water and 5:95 under a range of normal loads but at a constant sliding speed and counterface roughness.

A series of dry tests was also conducted, under conditions similar to those used in the lubricated tests, in order to establish the effect of boundary lubrication on the overall wear process.

6.1 THE EFFECT OF SLIDING VELOCITY

6.1.1 Velocity Tests Conducted Under Water Lubrication

In order to determine the effect of sliding velocity on the friction and wear characteristics of UHMWPE sliding against

stainless steel under water lubrication tests were performed at average velocities of 0,25 $m.s^{-1}$ and 0,5 $m.s^{-1}$, respectively and under the following conditions:

Normal Load : 100 kg (equivalent to a pressure of approximately 10 MPa)

Counterface Roughness : 0,38 ± 0,03 micrometers c.l.a. (average of six specimens)

Test Duration : 25 hours (divided into a sequence of 2,3,5,5,5,5 hour intervals)

Note:- Since the test duration was the same at both velocities, the sliding distance covered in the 0,25 $m.s^{-1}$ tests was half that covered during the 0,5 $m.s^{-1}$ tests.

Figures 6.1(a) & (b) are the cumulative volume loss vs. sliding distance curves of the test series run at 0,25 $m.s^{-1}$ and 0,5 $m.s^{-1}$, respectively. Each curve represents the mean of three separate test runs.

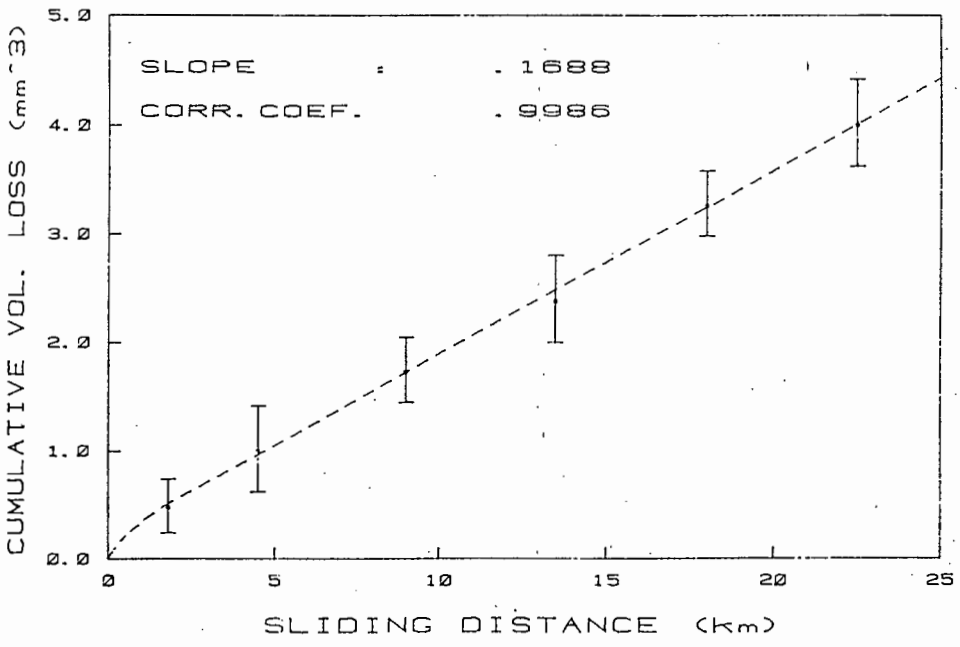

FIGURE 6.1(a) :

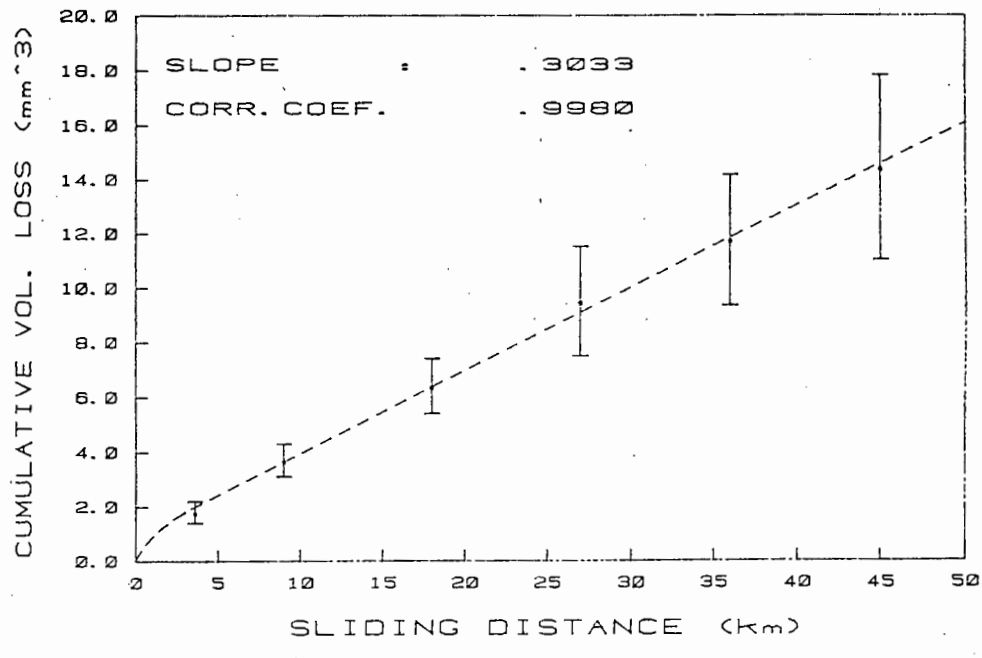

FIGURES 6.1(a) & (b) : Cumulative volume loss versus sliding distance curves of the tests run in water at 0,25 and 0,5 $m.s^{-1}$, respectively

Both curves show a high initial rate of wear or "running-in". During this period, the initial machined polymer surface is readily removed and general bedding down of the specimens occurs. The sliding distance necessary for running-in varied from approximately 2 km at the lower speed to 5 km at 0,5 $m.s^{-1}$. This is in agreement with Dumbleton and Shen (1976) who showed that UHMWPE displayed a high running-in period, lasting between 1 and 3 km, during sliding against AISI 316 stainless steel under water lubrication in a thrust-washer tester (sliding speed : 0,04 $m.s^{-1}$; pressure : 3,4 $N.mm^{-2}$; counterface roughness : 0,13 micrometers c.l.a.).

During running-in the wear rate was strongly dependant on the initial surface roughness of the counterface, i.e., the wear rate increased with counterface roughness even though the variation in roughness was small. Similar behaviour was observed during the reproducibility tests, as illustrated in Figure 5.15. This may suggest that the primary wear mechanism operating during the initial stages of the test was abrasion by the sharp asperities of the ground counterface.

The running-in period was followed by a steady state wear regime which lasted for the duration of the tests, i.e. no transition in the wear rate was observed at either velocity. The commencement of steady-state wear coincided closely with the appearance of a brown film on the steel counterface. A similar occurrence was reported by Dowson et al (1974) who observed the formation of a polymer transfer film during the initial stages of steady-state wear of UHMWPE sliding under water lubrication against AISI 316 in a pin-on-disc wear tester (sliding speed 0,24 $m.s^{-1}$; pressure 17 $N.mm^{-2}$; counterface roughness : 0,05 micrometers c.l.a.). They suggest that the brown colouration is a result of oxidative degradation caused by the continual exposure of the film to high temperatures. Thus, during water lubricated sliding of polymers against steel, adhesion also plays an important role in the overall wear process, leading to the formation of a transfer film on the counterface.

Transfer does not occur as a uniform layer of material. Instead, the rupture of adhesively bonded interfacial junctions results in the deposition of discrete lumps of polymer on the counterface. During repeated contacts polymer is deposited preferentially at these sites and the film builds up in this manner until a steady-state or equilibrium condition is reached. At this point, the rate at which polymer is being deposited on the surface is equivalent to the rate at which material is being removed from contact and, consequently, the film has little tendency to grow in thickness. It is likely that the film is built up during the running-in period and steady-state wear commences once an equilibrium transfer film has been formed on the surface. The effective surface roughness of the counterface is reduced and sliding now occurs between oriented polymer chains on both surfaces, resulting in a reduction in the wear rate of the polymer.

Figures 6.1(a) and (b) show that by doubling the sliding velocity, the specific wear rate of the UHMWPE pin increased from $1,7 \times 10^{-7}$ to $3,0 \times 10^{-7}$ $mm^3.N^{-1}.m^{-1}$. Anderson (1982) showed that the specific wear rate of UHMWPE sliding against mild steel under water lubrication in a pin-on-disc wear tester increased from 4×10^{-7} to 2×10^{-6} $mm^3.N^{-1}.m^{-1}$ in the velocity range 1 - 10 $m.s^{-1}$.

He suggested that the principal effect of sliding velocity on the wear rate occurs through its influence on the temperature at the sliding surface. However, during reciprocating sliding, an increase in velocity increases the number of stop/start cycles occurring over a given sliding distance and this is also considered to have an effect on the wear rate.

It is doubtful that the change in sliding velocity brought about any changes in the lubrication processes occurring at the sliding interface, i.e., both velocities lie within the boundary lubrication region of the Stribeck curve. The formation of a hydrodynamic fluid film under these conditions is, therefore, highly unlikely.

Figures 6.2(a) and (b) show the friction coefficients measured during the tests at the different velocities. Both the initial or "static", and the "kinetic" coefficients are plotted.

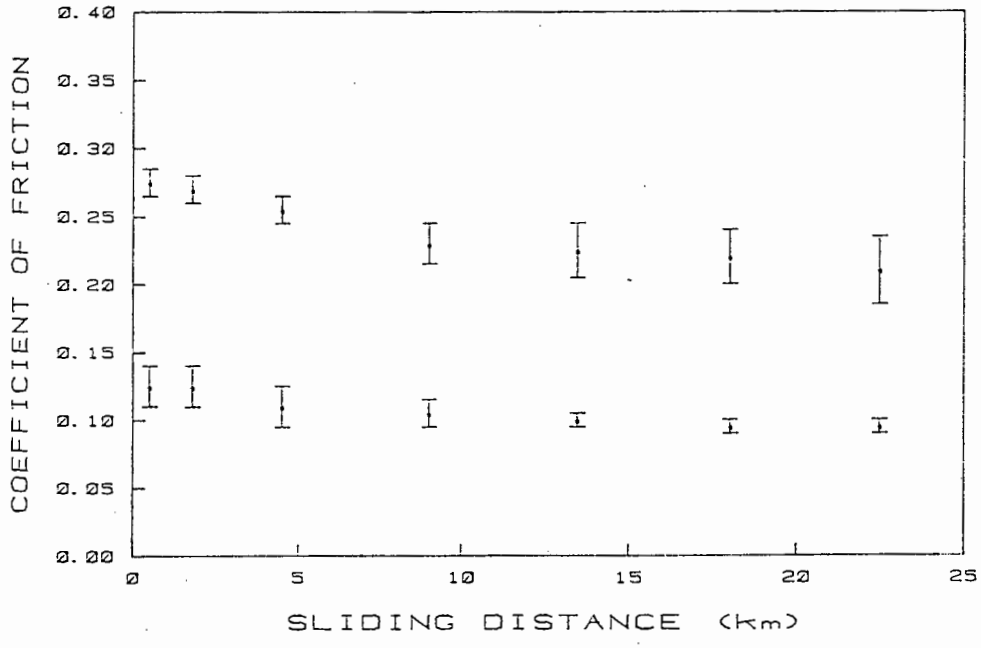

FIGURE 6.2 (a) :

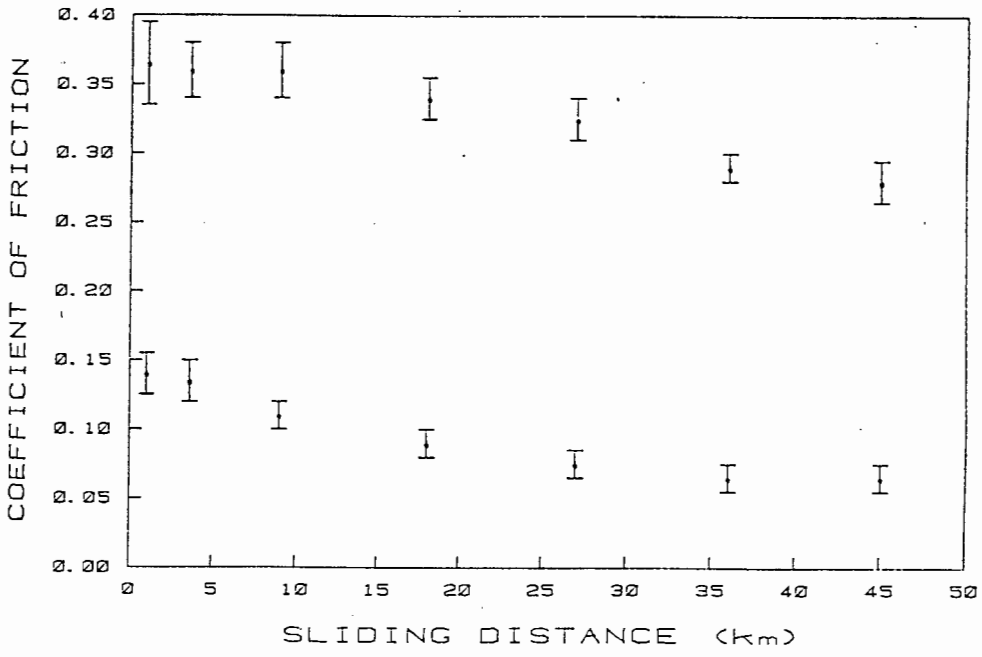

FIGURES 6.2(a) & (b): Friction coefficients (static and kinetic) recorded during the tests run in water at 0,25 and 0,5 $m.s^{-1}$ tests, respectively

The graphs show that the static coefficient of friction is approximately twice the kinetic value at the lower speed and almost three times higher at the higher sliding velocity. Furthermore, the increase in velocity resulted in a noticeable increase in the static coefficients whilst the kinetic coefficients remained unaffected by the velocity change.

The friction force resulting from the sliding of a polymer against a hard counterface may be divided into two components, namely, the adhesion component resulting from the shearing of adhesive bonds in the regions of real contact and the deformation component resulting from the dragging of asperities of the counterface through the polymer surface. When the surfaces are at rest, adhesive junctions are formed between the asperities of the couple and the force required to rupture these bonds when sliding commences is high. During sliding, however, the probability of forming a junction is reduced, resulting in a lowering of the adhesive component of friction. Moore (1972) has shown that sliding also induces stiffening of the polymer surface which leads to a reduction in the real area of contact and, consequently, a lower contribution of deformation to the total friction force.

The above two processes may account for the higher static friction coefficients measured during the tests.

The increase in the static friction coefficient with velocity is a consequence of the processes occurring at the interface. At the higher velocity there is a higher energy input into the system and some of this energy is dissipated at the interface in the form of heat. An increase in the mean surface temperature causes softening of the polymer surface layers, resulting in the material becoming more viscoelastic in nature. Consequently, the real area of contact increases which, in turn, increases the number and size of the adhesive junctions formed between the contacting asperities. The deformation contribution of the friction force also increases because lesser asperities, which were not in contact at the lower velocity, now play a part in the wear process.

The increase in the static peak with velocity is well illustrated in Figures 6.3(a) and (b) which are characteristic friction force curves recorded on the C.R.O. during the 0,25 and 0,5 $m.s^{-1}$ tests, respectively. The magnitude of the initial stick-slip cycle is greater at the higher velocity.

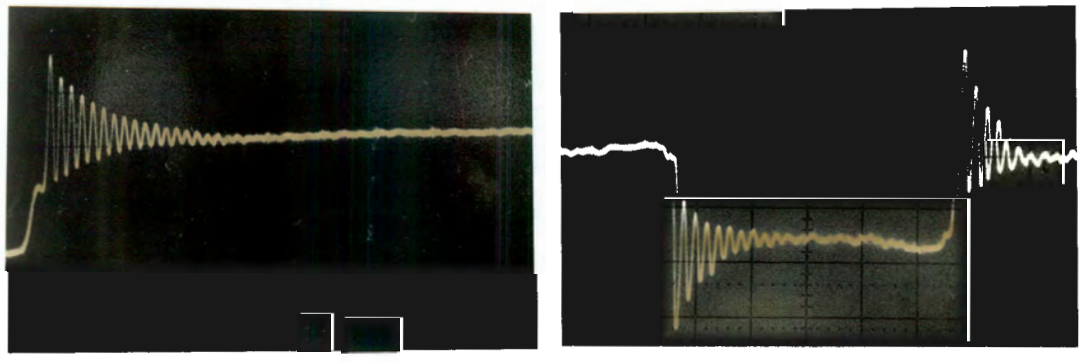

FIGURES 6.3(a) & (b) : Friction force curves recorded during the 0.25 and 0,5 $m.s^{-1}$ tests, respectively

It is difficult to quote a value of friction for the above tests because the coefficients, both static and kinetic, decreased continuously throughout the tests. (The kinetic friction coefficient decreased to almost 0,05 after 45 km sliding at 0,5 $m.s^{-1}$). The decline in friction with sliding distance was less rapid for the kinetic coefficients which illustrates the greater sensitivity of the static values to the processes occurring at the interface. A possible explanation for this decrease is that the counterfaces were being constantly modified by the various wear processes and by polymer transfer to the counterface. Furthermore, Pooley and Tabor (1972) showed that, with HDPE, sliding induces preferred orientation of the molecular chains in the surface of the sliding polymer and in the transfered layer. They attribute this behaviour to the smooth molecular profile of the polymer. Thus, subsequent sliding of the polymer over the transfered film is easier, resulting in a steady drop in friction. In addition, degradation of the transfer film probably reduces its adhesive nature and further contributes to the lowering of the friction coefficients. Reports of similar behaviour could not be found in the literature.

Figures 6.4(a) and (b) show the surface temperature rise data recorded during the 0,25 and 0,5 $m.s^{-1}$ tests. The values quoted are corrected for the temperature of the lubricant in the bath.

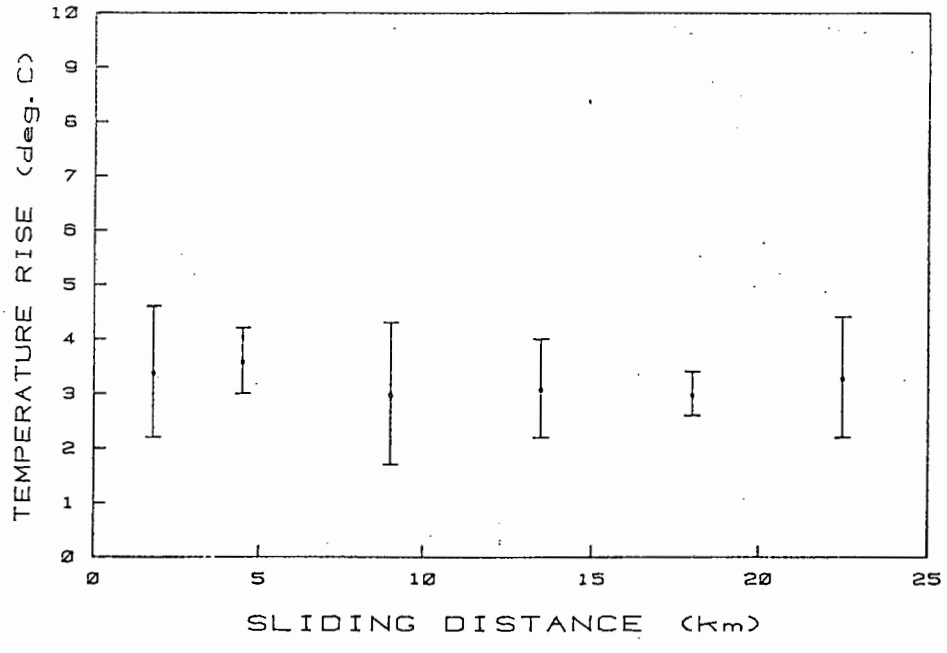

FIGURE 6.4(a) :

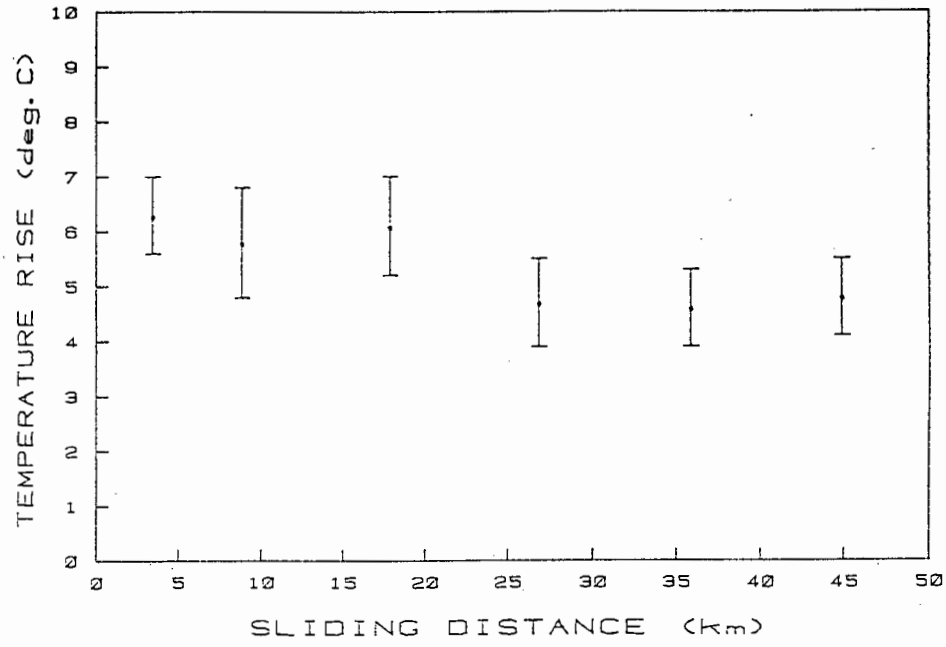

FIGURES 6.4(a) & (b) : Surface temperature rise data recorded during the 0,25 and 0,5 $m.s^{-1}$ tests in water, respectively

The slight decrease in temperature with sliding distance during the 0,5 $m.s^{-1}$ tests is consistent with the decrease in friction resulting from the modification of the couple during sliding.

There was no detectable difference between the temperature recorded by the thermocouples located at mid-stroke and at the stroke end (refer to Figure 4.10). This indicates that the temperature-rise resulting from frictional heating is uniformly distributed over the steel counterfaces. The temperature-rise values recorded during both tests were less than 10°C. However, the increase in velocity resulted in a significant increase in temperature which supports the theory that, as the velocity increases, the temperature at the surface increases, resulting in a higher static friction coefficient and, consequently, a higher wear rate.

Anderson (1982) reported that the mechanical properties of all polymers decrease as the temperature increases, resulting in an

increase in the wear rates with temperature. Also, for a given pressure and friction coefficient, the frictional heat generated at the interface increases in proportion to the sliding velocity, as shown by the equation $\varphi = R\mu Wv$ where φ is the mean surface temperature, R the thermal conductivity of the counterface, μ the coefficient of friction, W the normal load and v the sliding velocity. He suggested that because of the poor thermal conductivity of polymers, the instantaneous temperatures at the contacting asperities (flash temperatures) can be significantly above the mean surface temperature. Lancaster (1971) showed that the flash temperatures are more sensitive to sliding speed than applied load and are also critically dependant on the conductivity of the counterface.

The experimental data shown above suggests that the influence of sliding velocity on the wear rate can be converted to that of temperature, i.e., an increase in velocity increases the mean surface temperature. Consequently, the elastic modulus of the polymer decreases, resulting in an increase in the true contact area. There is a greater amount of deformation of the polymer surface by the asperities of the counterface and the adhesion contribution to the friction force is also increased by the larger contact area. The static friction coefficient increases and the overall effect is an increase in the wear rate.

An extensive scanning electron microscope examination of the worn surfaces (polymer and steel) was carried out in order to identify and isolate the various wear mechanisms occurring during lubricated polymer/metal sliding. Furthermore, SEM also assisted in explaining the increase in the wear rate resulting from the increase in sliding velocity. Abrasion was identified as the primary material removal process operating at the polymer/steel interface. Wear of the polymer surface generally took the form of parallel grooves of varying depth, width and spacing, which ran the length of the specimen in the direction of sliding. Both microcutting and ploughing/shearing processes, which are the principal components of abrasive wear, were observed in one form or another. However, these wear processes were more severe at the higher sliding velocity which is consistent with the greater

volume loss measured during the 0,5 $m.s^{-1}$ tests. Figures 6.5(a) and (b) are scanning electron micrographs of worn polymer surfaces of representative specimens taken from the 0,25 and 0,5 $m.s^{-1}$ tests, respectively.

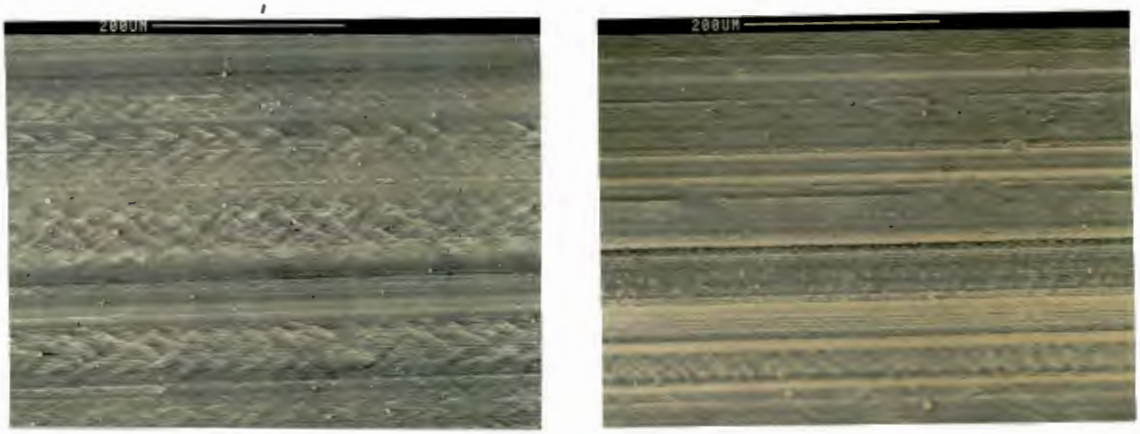

FIGURES 6.5(a) & (b) : Worn surfaces of polymer specimens tested in water at 0,25 and 0,5 $m.s^{-1}$. The arrow indicates the sliding direction

The relative magnitude of the degradation of the surfaces from the tests at the different velocities is immediately obvious. The surfaces of the specimens from the 0,25 $m.s^{-1}$ tests were characterised by a few widely spaced abrasive grooves, which were generally less than 100 micrometers in width. The surfaces of the specimens from the 0,5 $m.s^{-1}$ tests, however, displayed numerous, closely spaced wear tracks which were deeper and wider (up to 200 micrometers) than those observed at the lower velocity. This supports the argument of a larger contact area prevailing during the tests at the higher speed.

Two different abrasive type mechanisms were thought to be responsible for the formation of the wear grooves. Firstly, the asperities of the machined counterface caused uniform abrasion of the polymer surface by a simple two-body wear process in which the metal asperities acted as plough shares, forming wear grooves by plastic deformation. It is possible that the interfacial adhesive forces operating at the tips of the asperities cause the surfaces to "stick" on a micro-scale, allowing the asperities to plough into the polymer surface.

The second material removal process was identified as a three-body microcutting wear mechanism in which metal fragments, fatigued from the counterface, became embedded in the polymer surface. This leads to the removal of long, thin streamers of polymer by a cutting/shearing mechanism and, at the same time, caused wear to the counterface. A similar mechanism was described by Evans and Lancaster (1979) who suggested that adhesive processes can initiate abrasive wear of the surfaces by the transfer of metal to the polymer during polymer/metal sliding. This occurs when the sub-surface strength of the metal falls below that of the adhesive or mechanical interactions at the interface. They also reported that conventional surface finishing treatments may generate locally weakened asperities even before sliding begins. Figures 6.6(a) and (b) show abrasive wear grooves on the surfaces of specimens from the low and high speed tests.

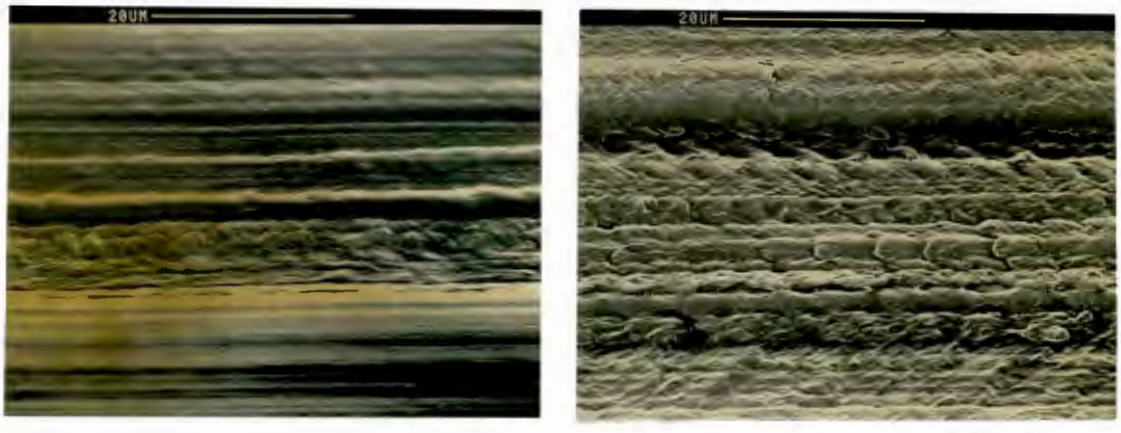

FIGURES 6.6(a) & (b) : Detailed views of wear grooves formed by abrasion at the surfaces of polymer specimens run at 0,25 and 0,5 $m.s^{-1}$ in water. The arrow indicates the sliding direction

SEM examination of the polymer wear debris recovered from the chamfered edges of the polymer specimens provided further support to the three-body mechanism. The surfaces of the polymer streamers, which were often longer than 5 mm, displayed a characteristic chatter-like feature which might indicate that

removal of the streamer did not occur in a single traversal of the embedded fragment through the polymer surface, but rather via a step-wise process involving many cycles. This is illustrated in Figures 6.7(a) and (b) which show polymer wear debris recovered from the low and high speed tests. The debris from the 0,5 $m.s^{-1}$ tests was generally thicker which is consistent with the deeper abrasive grooves observed on the polymer surfaces from these tests.

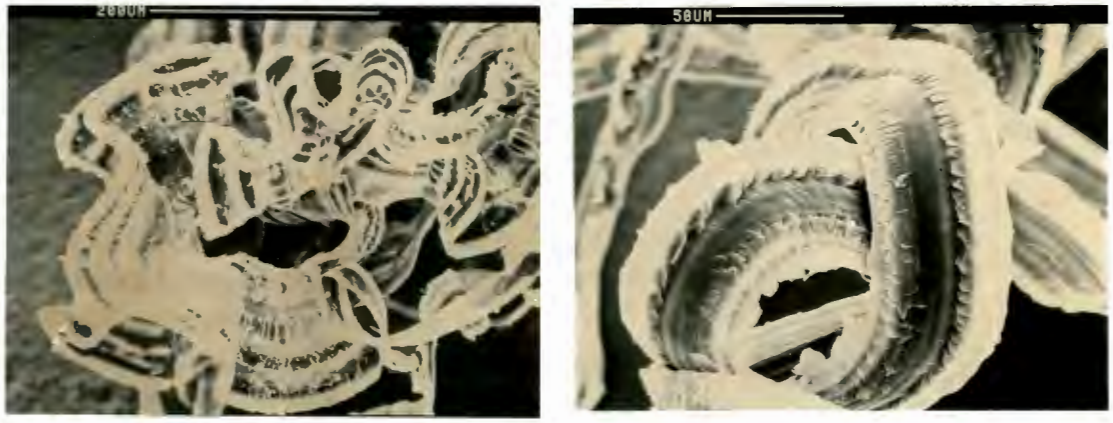

FIGURES 6.7(a) & (b) : Polymer wear debris from the 0,25 and 0,5 $m.s^{-1}$ tests in water

The presence of a third body between the sliding surfaces caused severe damage to the steel counterfaces whose surfaces were scarred by numerous wear tracks of varying widths running the full length of the stroke in the direction of sliding. These tracks usually conformed with the positions of the wear grooves occurring on the polymer surface against which sliding had taken place. This indicates that they were formed by the sliding of work-hardened steel fragments, such as the one shown in Figure 5.1, which were fatigued from the counterface and embedded in the surface of the reciprocating polymer. Gross plastic deformation of the steel surface occurred, resulting in the total removal of the machining marks. Secondary wear scars were often observed on the already-worn areas. It is likely that a similar wear mechanism operates during sliding of polymers in the presence of abrasive particles, the only difference being that the abrasive particles form the "third-body", as opposed to the steel fragments which caused wear during the laboratory tests. Figures 6.8(a) and (b) show worn steel counterfaces from the low and high speed tests.

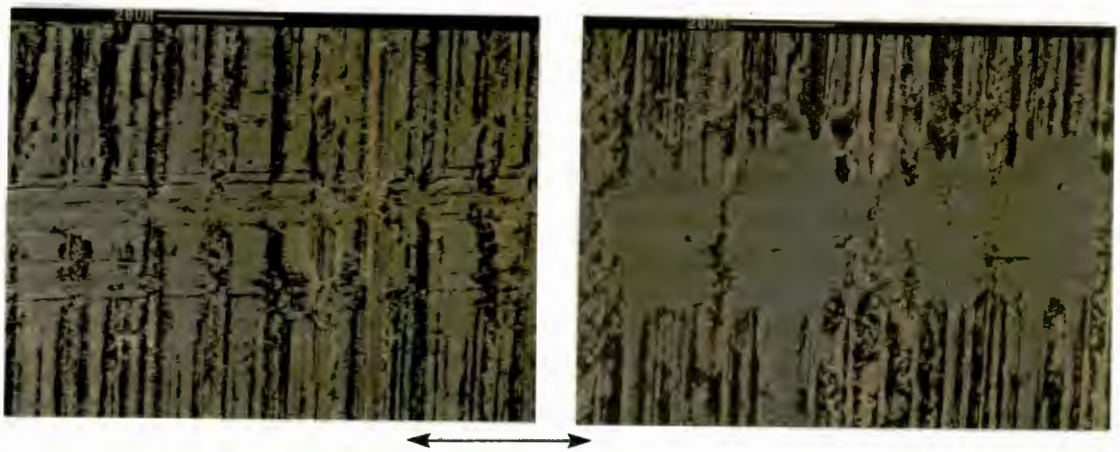

FIGURES 6.8(a) & (b) : Wear scars on the surfaces of steel specimens from the 0,25 and 0,5 $m.s^{-1}$ tests. The arrow indicates the sliding direction

Note:- The surfaces shown in Figures 6.8(a) and (b) were not Au/Pd coated. Consequently, the polymer film was destroyed by the electron beam and shows up as the dark material between the machining marks.

Adhesive wear was less prominent on the polymer surfaces. It occurred on the flat areas between the abrasive grooves and generally took the form of broad bands (up to 200 micrometers wide) of cresents or ridges lying at right angles to the sliding direction and occurring at a constant wave-length. These ridges are considered to be the result of an adhesive stick-slip process occurring on a micro-scale at the specimen interface. Similar structures were observed by Atkinson et al (1978) who also regard them as artefacts of adhesive wear. Figure 6.9 shows a typical adhesive wear artifact on the surface of a specimen from a test run in water at 0,5 $m.s^{-1}$.

FIGURE 6.9 : Adhesive wear of the polymer surface from a test in water at 0,5 $m.s^{-1}$. The arrow indicates the sliding direction

Transfer of polymer to the counterface occurred during both series of tests. Transfer did not occur as a uniform coherent film but rather in the form of irregular lumps of material deposited in the valleys formed by the machining marks. Subsequent sliding over these deposits caused smearing of polymer in the sliding direction. Figure 6.10 shows the nature of the polymer transfer from a water lubricated test. There was no apparent difference in the transfer characteristics resulting from the tests at the different velocities.

FIGURE 6.10 : Polymer transfer on the counterface of a specimen from a 0,25 $m.s^{-1}$ test in water. The arrow indicates the sliding direction

It would appear, from the SEM examination, that wear of the couple occurred mainly by two and three body abrasive mechanisms which were initiated by the high adhesive forces occurring at the polymer/steel interface. It is interesting to note that the decrease in the friction coefficients did not cause a lowering of the wear rate as sliding progressed. This is because, even though sliding was being made easier by chain orientation effects and degradation of the transfer film, the mode of material removal remained unchanged during steady-state wear.

6.1.2 Velocity Tests Conducted Under 5:95 Lubrication

In order to compare the lubricating capabilities of a 5:95 oil/water emulsion with those of water, two test series, each comprising three separate runs, were conducted at average sliding velocities of 0,25 and 0,5 $m.s^{-1}$, respectively. The tests were

run under identical conditions to those applied during the water lubricated tests except the counterface roughnesses were slightly lower. The average roughness of the six specimens was 0,32 ± 0,015 micrometers c.l.a. as opposed to the 0,38 ± 0,03 micrometers c.l.a. prepared for the water tests. Also, because of the extremely low wear rates encountered during the 0,25 $m.s^{-1}$ tests, the sliding intervals were increased in order that measurable weight losses could be recorded. Hence, the test was divided into a sequence of 5, 10, 10 hour intervals. Figures 6.11(a) and (b) are the cumulative volume loss versus sliding distance curves of the tests conducted in 5:95 at the different velocities.

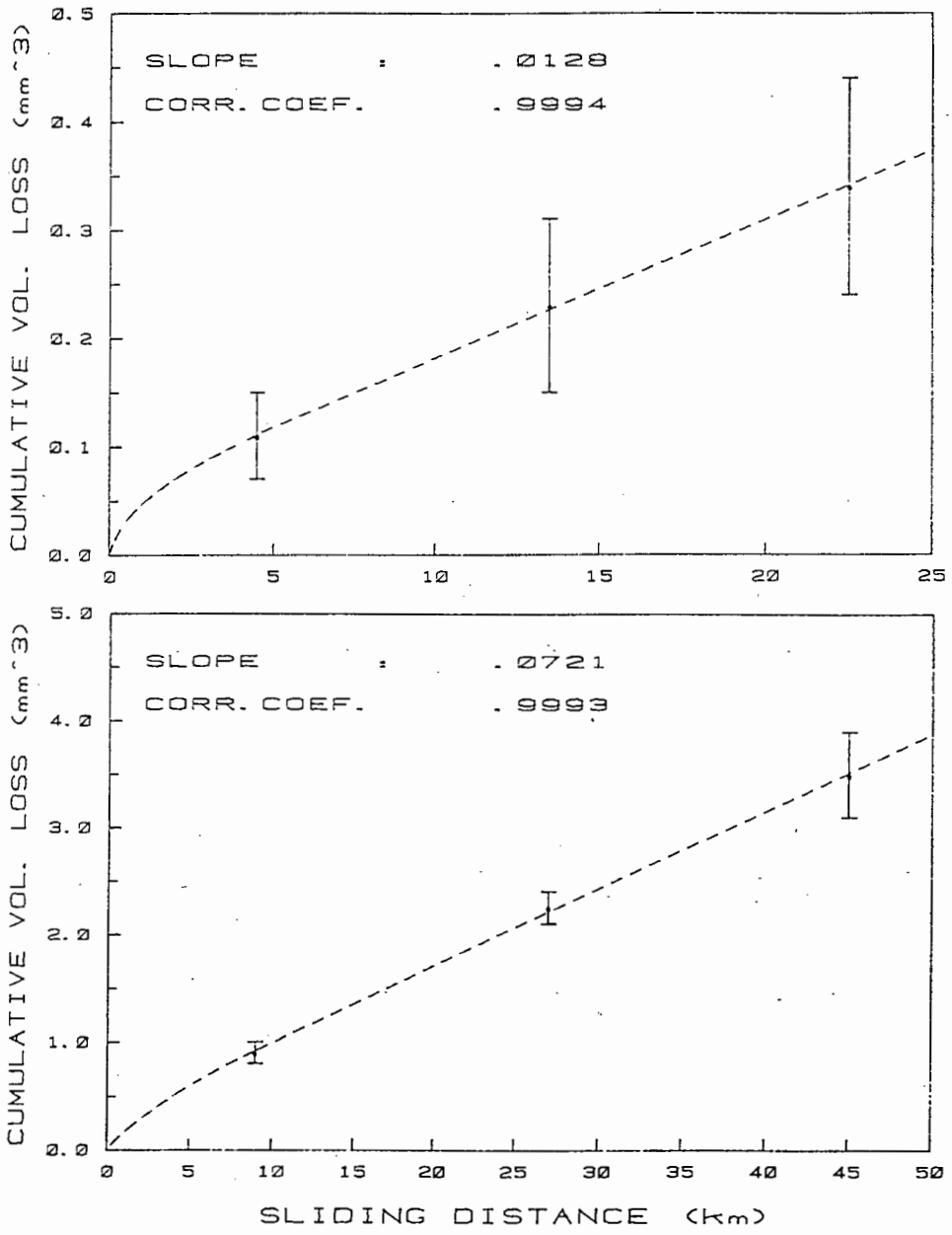

FIGURES 6.11(a) & (b) : Cumulative volume loss vs sliding distance curves of the tests conducted in 5:95 at 0,25 and 0,5 $m.s^{-1}$, respectively

The shapes of the curves were similar to those resulting from the water tests, i.e., a high initial running-in period was followed by a linear steady-state wear regime which lasted for the duration of the test. A similar trend was observed by Mustafaev et al (1976) during unidirectional sliding of UHMWPE against AISI 316 with mineral oil as the lubricant (applied pressure, 10 $N.mm^{-2}$; sliding speed, 0,24 $m.s^{-1}$; counterface roughness, 0,015 micrometers Ra).

Although the running-in wear rates were high, relative to the steady-state wear rates, they were considerably lower than the running-in wear rates recorded during the tests in water. At the lower speed the running-in wear (after 5 km) was ten times less than in the corresponding water tests whilst at 0,5 $m.s^{-1}$ it was four times lower. This suggests that the interfacial contact processes occurring during sliding under 5:95 are very different from those in water.

As was observed in the water tests, there was a marked dependence of the polymer wear rate on the sliding velocity. Increasing the sliding velocity from 0,25 to 0,5 $m.s^{-1}$ caused the specific wear rate to increase from $1,2 \times 10^{-8}$ to $7,2 \times 10^{-8}$ $mm^3.N^{-1}.m^{-1}$. This increase was less than half that resulting from the same velocity increase during the water tests. Of particular interest, however, was the dramatic overall reduction in the wear rates, at both velocities, brought about by the change in the lubricating medium from water to 5:95. Figure 6.12 summarises the variations in the specific wear rates with velocity in both lubricants.

The change from water to 5:95 caused a considerable lowering of the wear rates at both velocities although the difference was greater at the higher sliding speed. Figure 6.12 also illustrates the greater sensitivity of the water lubricated tests to the increase in velocity.

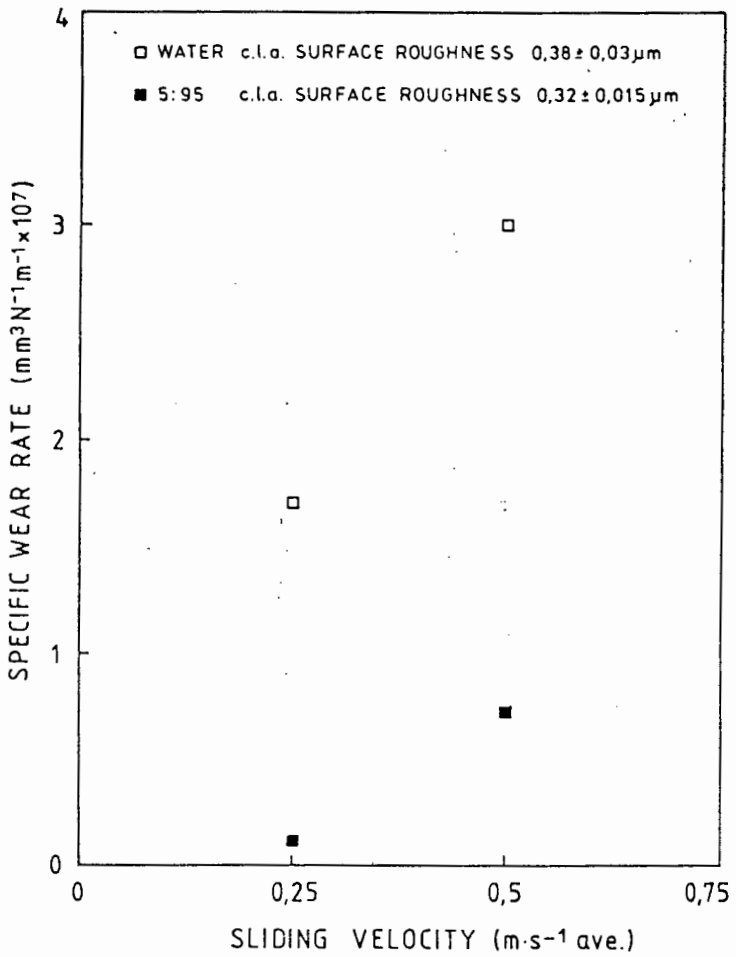

FIGURE 6.12 : The effect of velocity on the wear rates of the tests conducted in water and 5:95

Since both velocities lie in the boundary lubrication range hydrodynamic separation effects are unlikely to have occurred and it is simply the improved boundary lubricating properties of the emulsion which accounted for the lowering of the wear rates. The emulsion has a higher viscosity than water, is more easily sheared and exhibits lower surface tension and wettability. Thus, in the presence of 5:95 the forming of interfacial adhesive junctions is prevented and almost the total frictional force is provided by the deformation or ploughing component as illustrated in Figure 3.22.

Figures 6.13(a) and (b) show the friction coefficients recorded during the tests in 5:95 at the different velocities.

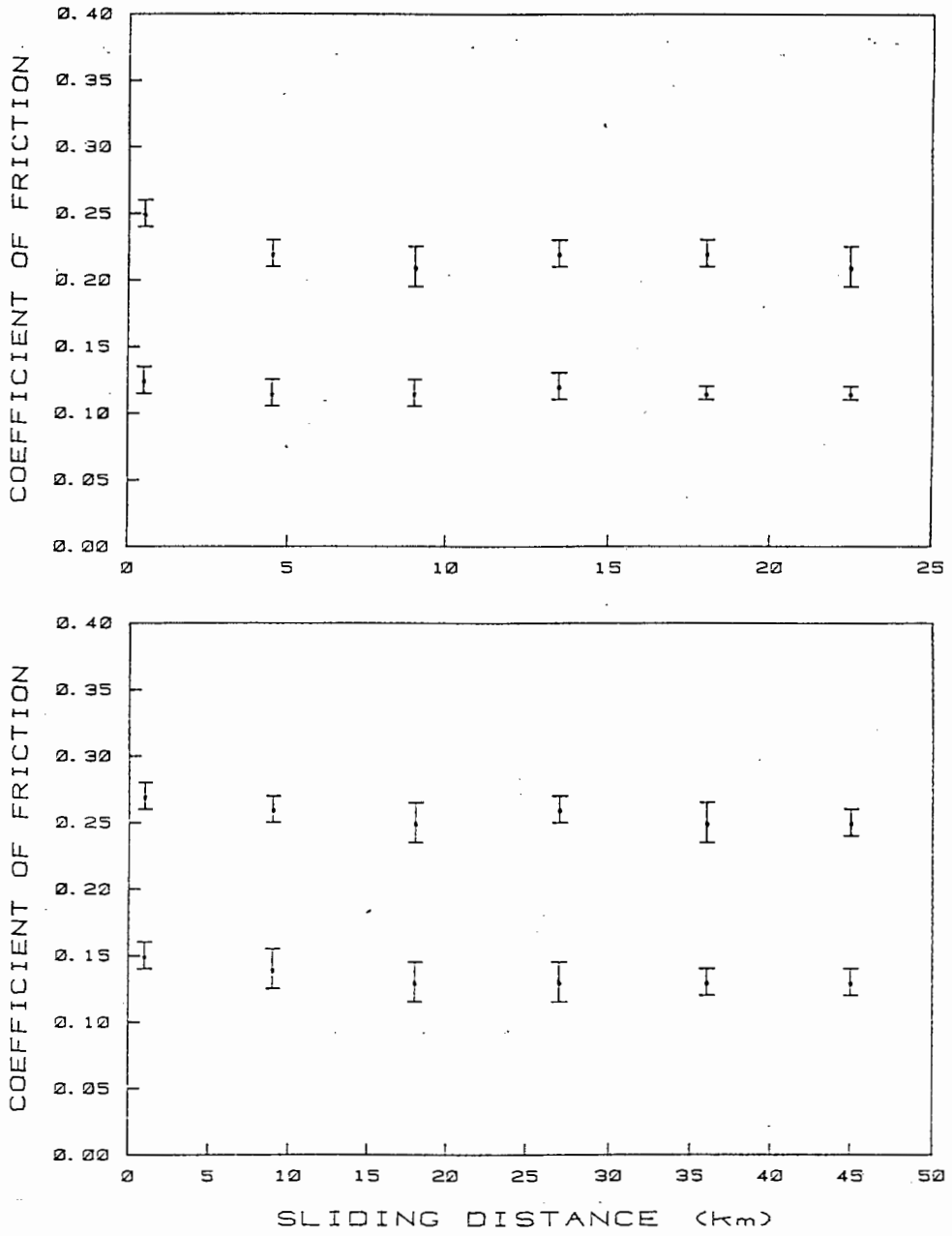

FIGURES 6.13(a) & (b) : Friction coefficients recorded during the 0,25 and 0,5 $m.s^{-1}$ tests in 5:95, respectively

Except for the running-in period, where the friction coefficients (static and kinetic) were marginally higher, the friction coefficients at both velocities remained constant for the duration of the tests. This contrasts with the behaviour observed in the water tests where the friction coefficients decreased with sliding distance. The low adhesive forces occurring between the polymer

and the counterface in the presence of 5:95 prevented the formation of a transfer film. Thus, the equilibrium between the sliding specimens was not disturbed by modification of the counterface, resulting in a constant frictional force during sliding.

Increasing the sliding velocity resulted in a noticeable increase in the static friction coefficients and, contrary to the behaviour in the water tests, the increase in speed brought about a slight increase in the kinetic values. This is illustrated in Figure 6.14(a) and (b) which are characteristic friction force curves recorded during the 0,25 and 0,5 $m.s^{-1}$ tests in 5:95. The shapes of the curves at both velocities were essentially the same as those recorded during the water tests (refer to Figure 6.3(a) and (b)) except that the magnitude of the static peaks were noticeably smaller in 5:95 at both velocities.

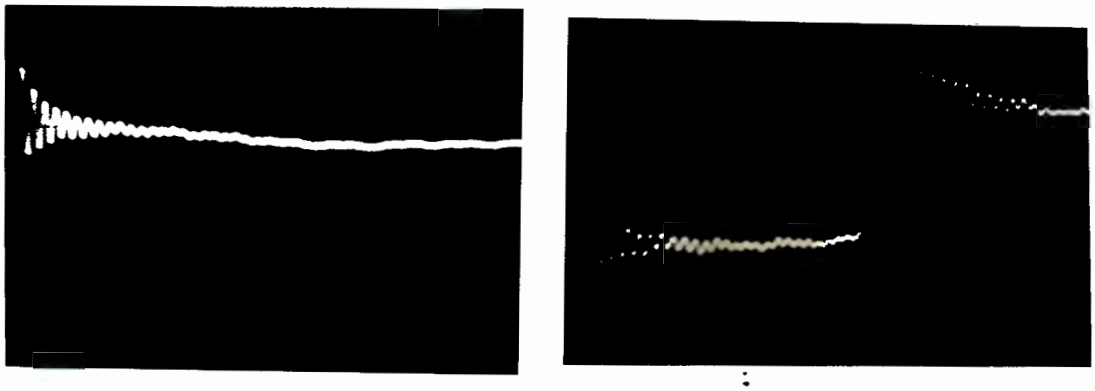

FIGURES 6.14(a) & (b) : Friction force curves from the 0,25 and 0,5 $m.s^{-1}$ tests in 5:95

Figure 6.15 compares the static and kinetic friction coefficients measured in water and 5:95 at the two velocities. The values plotted were those recorded after 9 km of sliding in each test, i.e., at the start of steady-state sliding.

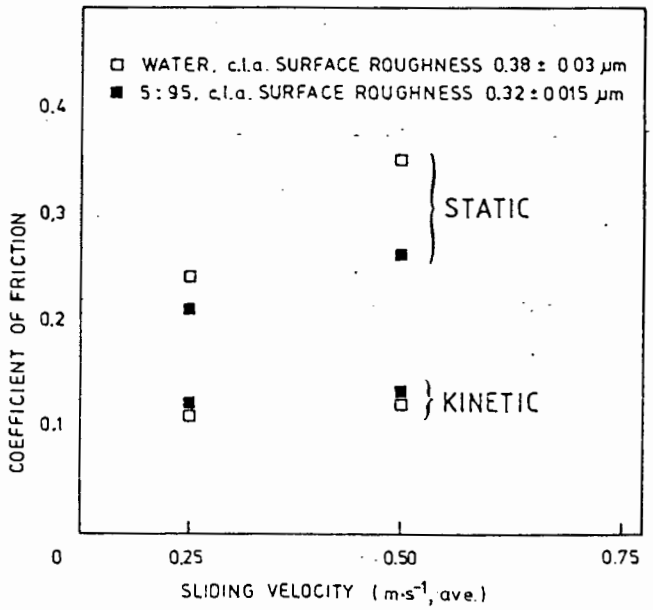

FIGURE 6.15 : The effect of sliding velocity on the static and kinetic friction coefficients of the tests run in water and 5:95

Figure 6.15 shows that the static coefficients of the water tests were higher at both velocities. However, this behaviour was reversed for the kinetic coefficients where the 5:95 values were marginally higher. The lower static coefficients recorded during the 5:95 tests are due to the absence of an adhesion contribution to the total friction force, i.e., the static friction force is provided purely by the deformation of the polymer surface. The lack of adhesion between the polymer and the counterface asperties means that the polymer can simply "ride over" the counterface asperities under conditions which might lead to ploughing of an abrasive groove in water. Thus, the lower friction in 5:95 can also be ascribed to a reduction in the ploughing component of the friction which is consistent with the lower wear rates observed during these tests. The higher kinetic friction measured at both velocities in 5:95 is due, primarily, to the absence of a polymer transfer film under these conditions. In the water tests the presence of the film reduced the deformation component of the friction, leading to a lower kinetic friction coefficient.

One might expect that the absence of adhesion in 5:95 would eliminate the static peak occurring at the start of each stroke, resulting in the static and kinetic coefficients being equal in

magnitude. The fact that the kinetic coefficients were lower than the static values can be ascribed to the lowering of the deformation term during sliding. This occurs through the effects of stiffening of the polymer surface, relative to the static condition, which reduces the real area of contact and, consequently, the friction force, as illustrated in Figure 3.22.

Figures 6.16(a) and (b) are the temperature values recorded during the 0,25 and 0,5 $m.s^{-1}$ tests in 5:95

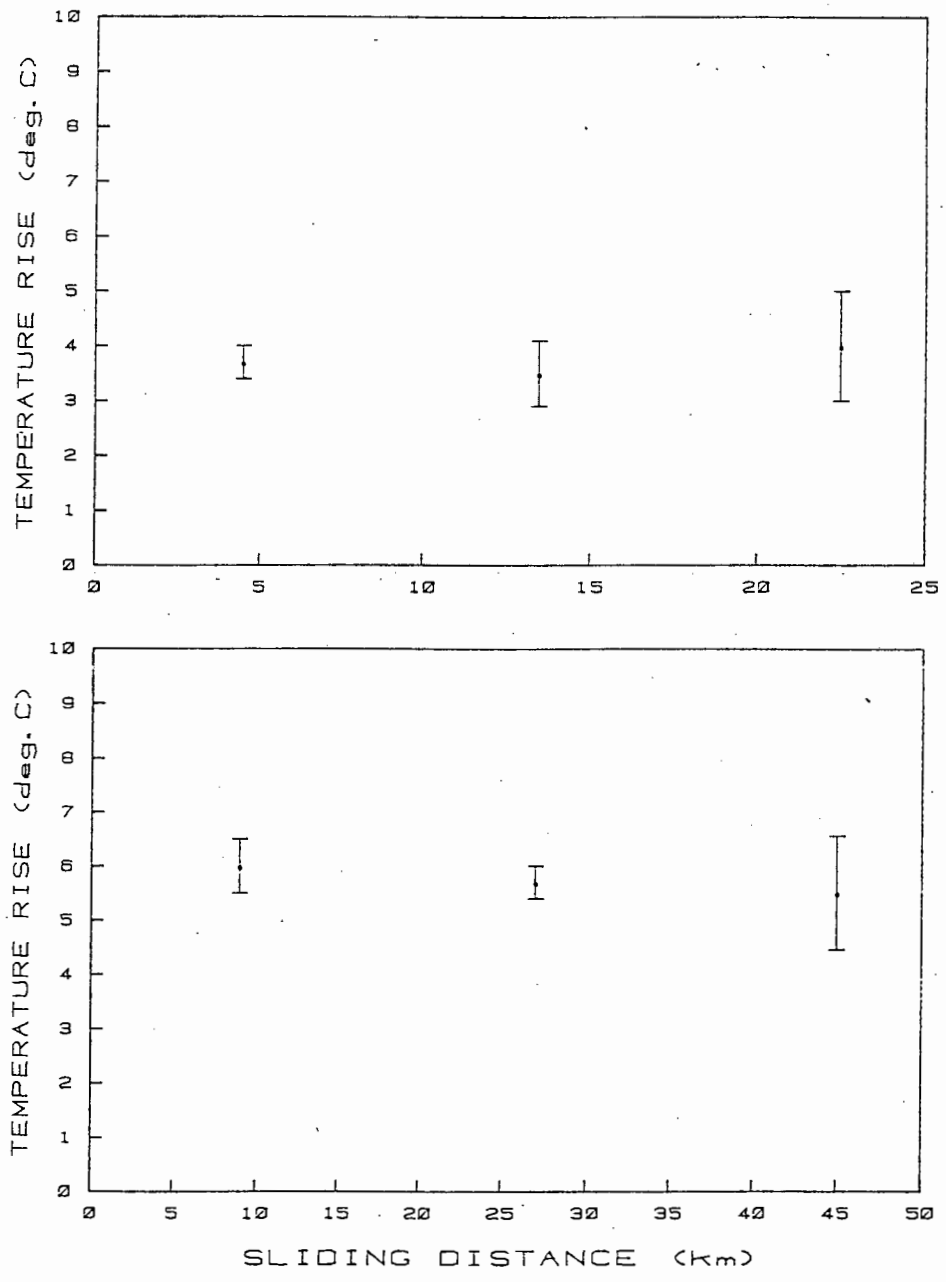

FIGURES 6.16(a) & (b) : Surface temperature-rise data recorded in 5:95 at the two velocities

The temperatures recorded during these tests were similar, at both velocities, to the temperatures resulting from the tests run under water lubrication (refer to Figures 6.4(a) and (b)). Thus, the emulsion had no apparent effect on the temperature rise at the interface. The increase in velocity did, however, cause the temperature values to increase significantly (by approximately 50%). This is consistent with the increase in wear rate which accompanied the increase in sliding velocity. The higher sliding velocity causes the mean surface temperature to rise. The elastic modulus of the polymer decreases, leading to a larger contact area. The deformation and ploughing components of friction are increased, the static friction coefficient rises and so too does the wear rate. The greater number of stop/start cycles at the higher velocity is also considered to have an effect on the wear rate.

In summary, the absence of an adhesive contribution to the friction process was thought to be responsible for the low wear rates occurring during the 5:95 tests. No transfer film is formed during sliding and the friction and wear behaviour is determined soley by deformation and ploughing of the polymer surface by the asperities of the counterface. The absence of adhesion might also explain the lower sensitivity of the friction and wear data to the increase in sliding velocity.

A scanning electron microscope examination of the worn surfaces revealed that, compared to water, sliding under 5:95 lubrication considerably reduced the severity of the wear to the polymer surfaces, which is in good agreement with the wear rate data presented above. As in the water tests the major material removal process was abrasion by the sharp asperities of the ground counterface. However, the abrasive grooves were much narrower and not as deep, as illustrated in Figures 6.17(a) and (b) which are general views of worn polymer surfaces from tests in 5:95 at 0,25 and 0,5 $m.s^{-1}$. The widths of the abrasive grooves ranged from 20 to 50 micrometers whereas abrasive tracks as wide as 200 micrometers were common in the water tests. The most striking

difference between the morphologies resulting from the tests in the different lubricants was that abrasion occurred more or less uniformly over the entire surface in the water tests whereas in 5:95 the wear grooves occurred in isolated regions, separated by wide, relatively unworn areas.

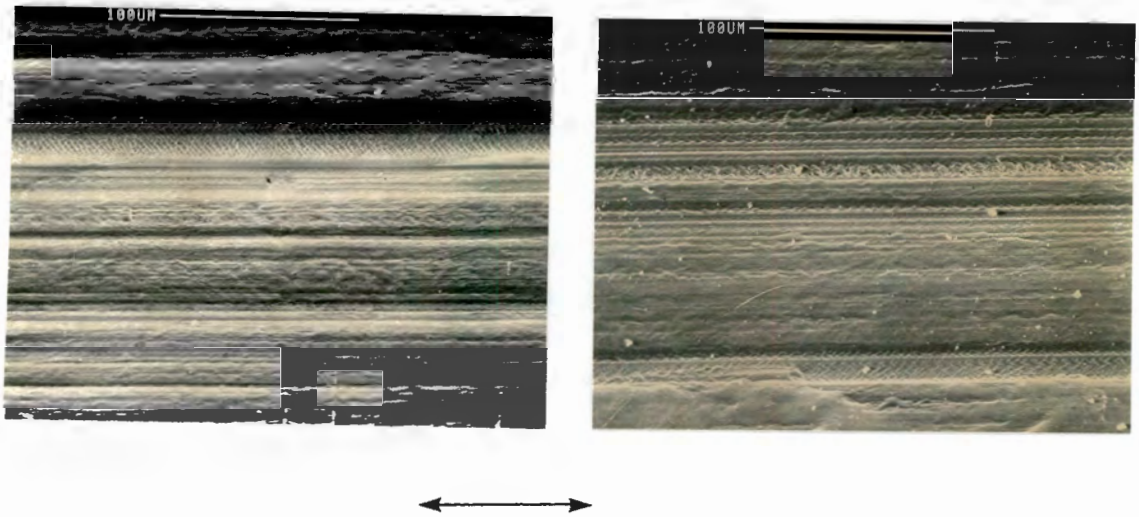

FIGURES 6.17(a) & (b) : The worn surfaces of polymer specimens from 0,25 and 0,5 $m.s^{-1}$ tests in 5:95. The arrow indicates the sliding direction

A feature peculiar to the surfaces of the polymer specimens from the 5:95 tests was a characteristic chevron-type pattern which generally occurred in broad bands up to 100 micrometers wide. The markings were equidistantly spaced and were oriented in one particular direction (the orientation differed from one location to the next). The wavelength of these markings was estimated to be between 2 and 3 micrometers which suggests that it could be due to a stick-slip process occurring on a micro-scale between the polymer surface and a counterface asperity. It is conceivable that, under water lubrication, the adhesion between the surfaces would have led to ploughing of the asperitiy through the polymer. In 5:95, however, adhesive forces are absent and the polymer is able to "ride over" the asperity with a stick-slip type of motion. Figure 6.18 shows chevron markings on the surface of a polymer specimen from a test in 5:95 at 0,5 $m.s^{-1}$.

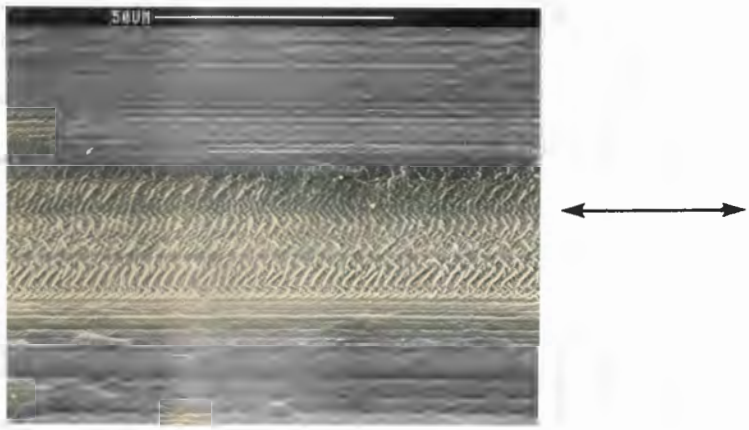

FIGURE 6.18 : Chevron-markings on the surface of a polymer specimen tested in 5:95 at 0,5 $m.s^{-1}$. The arrow indicates the sliding direction

The wear debris formed during the 5:95 tests was thin and ribbon-like in appearance, as shown in Figure 6.19. The ribbons were usually less than 2 mm in length and 50 micrometers wide. It was generally thinner than the wear debris recovered from the water tests and was not affected by the change in velocity. Abrasive wear processes are thought to have been responsible for the removal of the debris from the polymer surfaces.

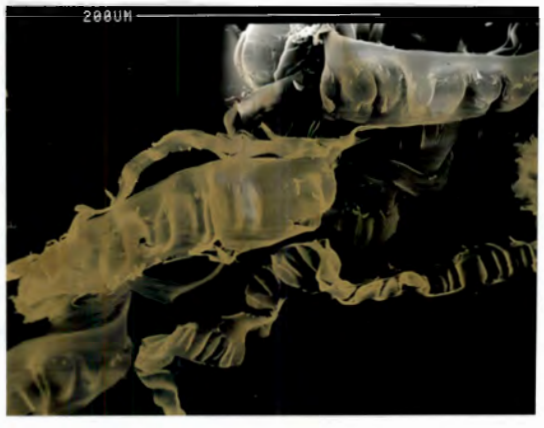

FIGURE 6.19 : Wear debris from a test in 5:95 at 0,5 $m.s^{-1}$

The steel counterfaces from the 5:95 tests were relatively unaffected by the wear process. A few fine abrasive scars were

observed on the steel surfaces which are thought to have been formed by a three-body abrasive mechanism. In general, the steel surfaces were merely "polished" by the reciprocating polymer, as illustrated in Figure 6.20. Polymer transfer did not occur in any form during either of the 5:95 tests.

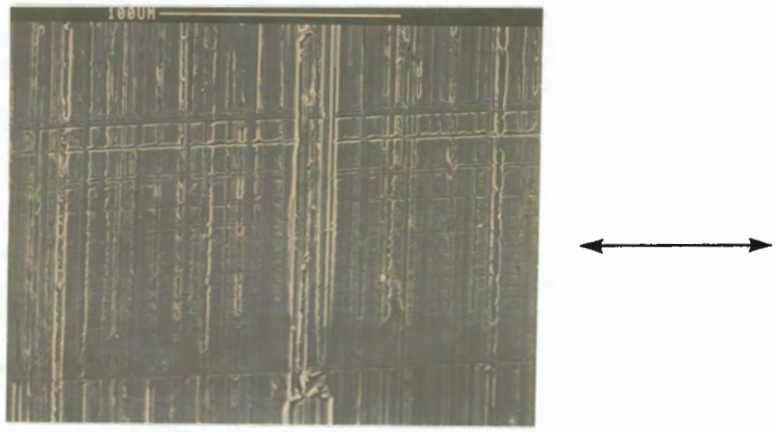

FIGURE 6.20 : The "polished" steel counterface after a test in 5:95 at 0,5 $m.s^{-1}$. The arrow indicates the sliding direction

It is possible that the low adhesive forces resulting from the presence of the lubricant between the sliding surfaces reduced the probability of forming a third-body. Thus, fewer and smaller abrasive cutting elements were introduced at the interface, leading to less wear by three-body abrasion and a consequent lowering of the wear rate compared to the tests in water.

6.2 THE EFFECT OF LUBRICATION : DRY TESTS

A series of 5 dry tests was completed in order to compare the wear performance of the polymer with that observed in the lubricated tests. Initially, tests were conducted under the identical conditions used in the lubricated tests (sliding velocity : 0,25 $m.s^{-1}$; normal load : 100 kg). However, sliding under these conditions caused gross melting of the polymer material, resulting in considerable deformation of the pin end.

Thermoplastic polymers exhibit a PV limit, where P is the mean pressure and V the sliding speed. Above this limit, temperature rises are such that surface melting occurs, resulting in excessive wear and frictional instability. The actual value of the PV limit will depend on the particular test conditions under consideration (Lancaster, (1973)). The PV limit for the above test was approximately 2500 $N/mm^2.mm/s$ which is considerably higher than the PV limit quoted for UHMWPE. Dumbleton and Shen (1974) found a limiting PV value of 190 $N/mm^2.mm/s$ under dry conditions whilst values of between 100 and 350 were reported by Atkinson et al (1978).

In order to reduce the degree of melting the applied load was reduced from 100 to 40 kg, i.e., the pressure at the polymer surface was reduced from approximately 10 to 4 $N.mm^{-2}$. This reduced the PV product to approximately 1000 $N/mm^2.mm/s$ which was, however, still considerably higher than the recommended PV limit of UHMWPE. The average surface roughness of the five counterfaces was 0,32 ± 0,02 micrometers c.l.a. Figure 6.21 is the cumulative volume loss versus sliding distance curve for the five dry tests.

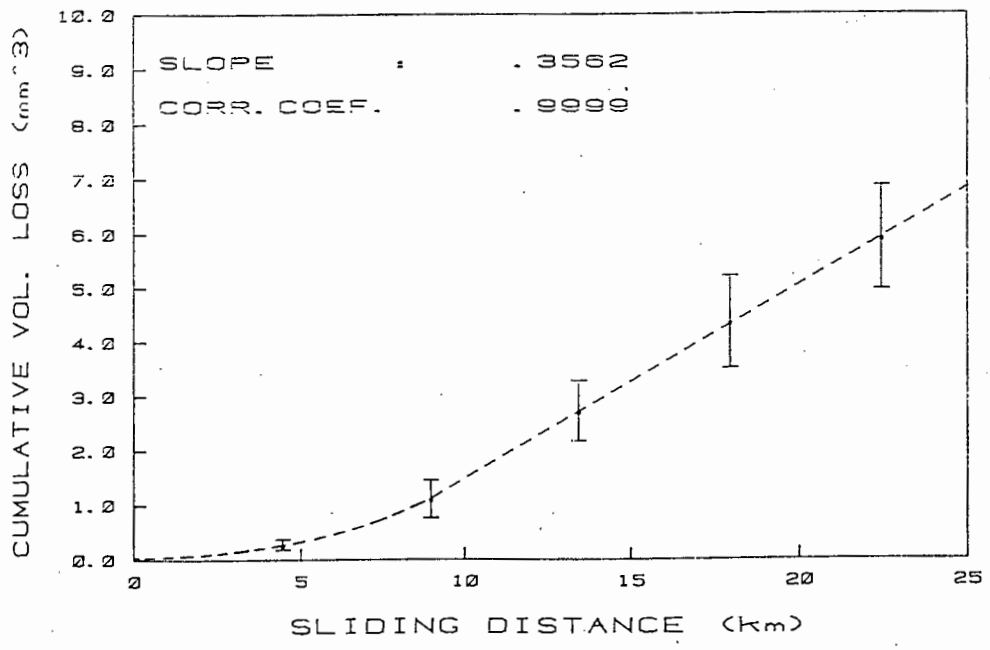

FIGURE 6.21 : The cumulative volume-loss vs sliding distance curve for the 5 dry tests

The wear behaviour of the polymer under dry conditions contrasted with the trends observed during the lubricated tests. During these tests the running-in wear rate was lower than the steady-state wear rate which followed, i.e., there was a type of incubation period in the wear process. However, the magnitude of the volume loss during this period, which lasted between 5 and 10 km, was more than half that recorded during the water tests and can, therefore, still be regarded as running-in.

A low initial wear rate was also reported by Mustafaev et al (1976) and Challen and Dowson (1976) during dry pin on disc tests with UHMWPE sliding against AISI 316 whilst Anderson and Robbins (1976) reported a low wear rate during the first 10 km for UHMWPE sliding against dry mild steel in a thrust bearing configuration. Dowson et al (1976) noted a similar trend during dry reciprocating sliding of UHMWPE against AISI 431. An explanation for the low initial wear rate is that, under dry conditions, transfer of polymer to the counterface occurs unhindered. The effective roughness of the counterface is reduced, resulting in less abrasive wear. As the test proceeds the polymer surface is degraded by the high temperatures occurring at the interface. The surface layers of the polymer, which are in a semi-molten or viscous state, are easily sheared from the surface during sliding and, consequently, the wear rate increases.

The specific wear rate in the steady-state region was $8,9 \times 10^{-7}$ $mm^3.N^{-1}.m^{-1}$ which is considerably higher than both the lubricated values recorded at the same velocity ($1,2 \times 10^{-8}$ $mm^3.N^{-1}.m^{-1}$ in 5:95 and $1,7 \times 10^{-7}$ $mm^3.N^{-1}.m^{-1}$ in water). However, the dry specific wear rate lies within the range of values recorded by other workers (refer to Table 3.2).

Figure 6.22 shows the friction coefficient data of the five dry tests. Unlike the lubricated tests, which showed higher coefficients during running-in, the dry values were slightly lower during the initial stages of the test which is consistent with the low wear rate occurring during running-in.

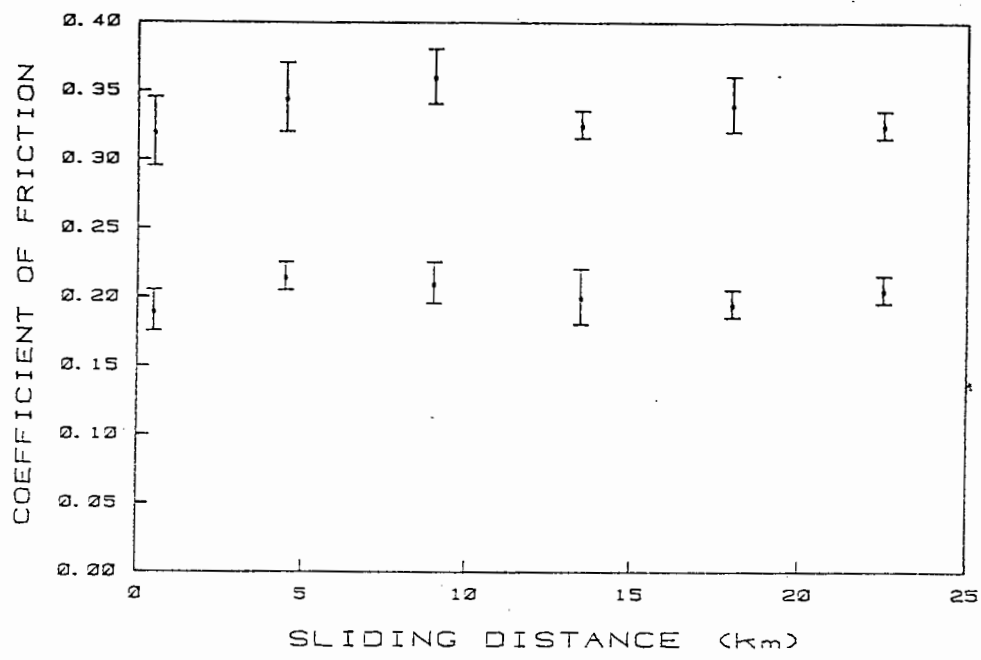

FIGURE 6.22 : The static and kinetic friction coefficients measured during the dry tests

Comparison with the 0,25 $m.s^{-1}$ lubricated tests shows that the presence of a boundary lubricant considerably reduced both the static and kinetic friction coefficients. This is because the adhesion contribution to the friction force is considerably greater under dry conditions. In the absence of a lubricant the temperatures occurring at the sliding interface are extremely high. Melting of the surface occurs, the area of real contact increases and, consequently, the adhesive forces are high.

During the water tests, the presence of the transfer film caused the friction coefficients to decrease as the test progressed. During the dry tests, however, the friction values remained constant throughout the test. It is possible that the interaction of water with the transfered film resulted in a continuous reduction in its adhesive properties. No such degradation occurred in the dry tests and, consequently, the friction remained constant.

Figure 6.23 is a friction force curve from a dry test.

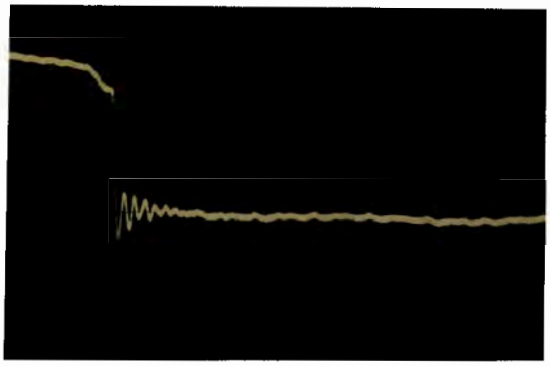

FIGURE 6.23 : A friction force curve from a dry test

The smaller static peak is probably because the material in the surface layers is no longer elastic but viscous as a result of the high temperatures generated at the interface. The surface layers can easily shear over one another and, consequently, the resistance to sliding is low.

The temperatures recorded by the subsurface thermocouples were, predictably, higher than in the lubricated tests. Temperatures of between 50 and 60°C above ambient were recorded during the series as illustrated in Figure 6.24. This indicates that, during sliding, the temperatures reached at the contacting asperities may be near to, or even exceed, the melting point of the polymer (approximately 120°C).

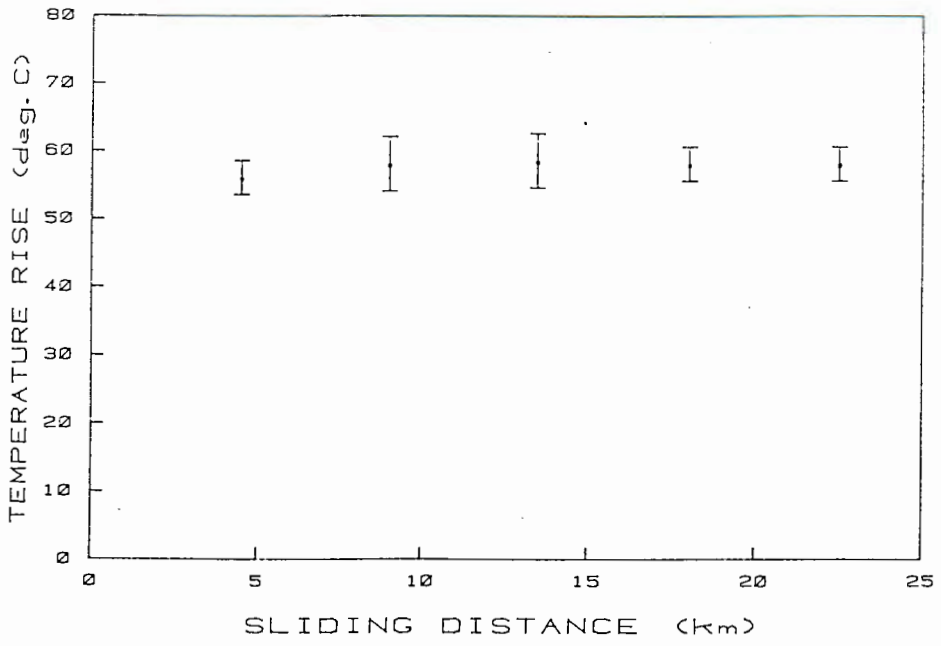

FIGURE 6.24 : Surface temperatures recorded during the dry tests

Challen and Dowson (1976) measured the surface temperature during dry pin on disc wear tests by placing a thermocouple in a hole drilled in the polymer pin. During tests with UHMWPE sliding against AISI 316 over a range of loads (8 - 20 $N.mm^{-2}$) and sliding velocities (0,23 - 0,61 $m.s^{-1}$), surface temperatures of between 70 and 130°C were recorded. They also showed that the wear of the polymer changed from a steady-state or "mild" regime to "severe" at temperatures higher than 125°C.

It was obvious that the wear processes occurring during dry sliding are totally dominated by the high surface temperatures generated at the interface which cause gross melting of the polymer. If, during a dry test, the steel specimen was cooled to temperatures within the range occurring during lubricated sliding, it is likely that a completely different wear mechanism would prevail.

SEM examination of the worn surfaces confirmed that the wear mechanism operating under dry conditions was dominated by temperature effects. Material removal did not occur by the ploughing out of long, thin streamers of polymer by two and three-body abrasion. Instead, large, flat platelets of polymer, up to 2 mm wide, were sheared or extruded from the polymer surface. The debris was also considerably thicker than that formed during the lubricated tests. Figure 6.25 shows the nature of the wear debris formed during the dry tests.

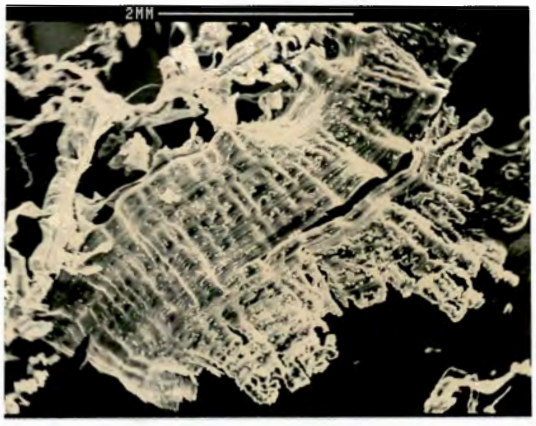

FIGURE 6.25 : Polymer wear debris from a dry test

Melting of the polymer surfaces had occurred, resulting in considerable modification of the surface topography. The surfaces were generally flat

and almost featureless with very little evidence of abrasion. The surfaces were extremely sensitive to the electron beam which suggests that thermal degradation had occurred. Figure 6.26 shows the molten polymer surface after a dry test.

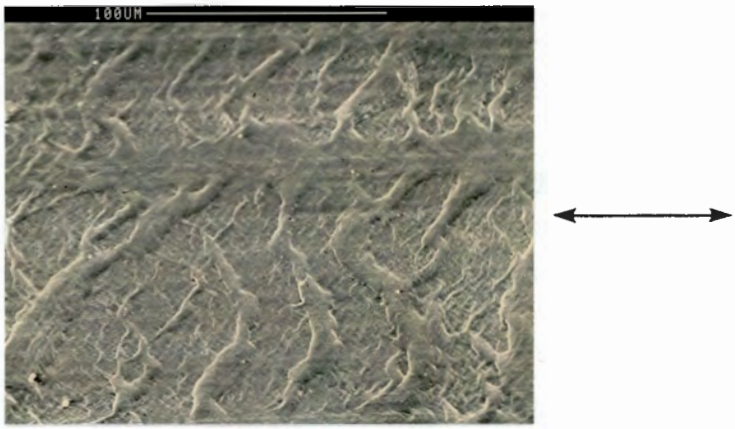

FIGURE 6.26 : The polymer surface from a dry test showing evidence of localised melting. The arrow indicates the sliding direction

A considerable amount of polymer transfer to the counterface occurred during the dry tests. Material was either deposited in the valleys between the machining marks or lumps of polymer were simply smeared across the counterface in the sliding direction as shown in Figure 6.27.

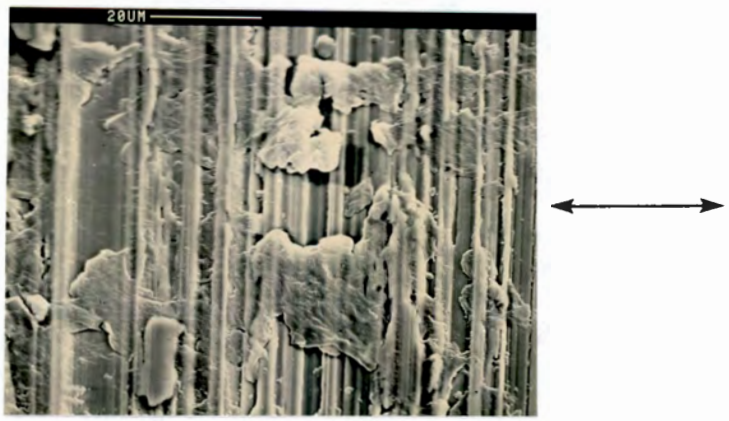

FIGURE 6.27 : Polymer transfer to the counterface during a dry test. The arrow indicates the sliding direction

6.3 THE EFFECT OF COUNTERFACE ROUGHNESS

6.3.1 Tests in Water

A series of four tests was completed under water lubrication in which the steel counterface roughness was varied between 0,1 and 1,0 micrometers c.l.a. Each test was run at an average sliding speed of 0,25 $m.s^{-1}$ and under a normal load of 100 kg. The length of each test, however, varied according to the wear rate prevailing at the respective roughnesses, i.e., the test was discontinued when the chamfered tip of the polymer pin was worn away.

Table 6.1 gives the results of the tests conducted at the different counterface roughnesses. Appendices A1, 2, 3 and 4 are the cumulative volume loss versus sliding distance curves of the four tests. The reproducibility of the separate tests was very good, as shown by the high linear correlation coefficients during steady-state wear. The curves also show that, as the roughness increased, running-in wear became less and less prominent.

TABLE 6.1 : Results of the tests conducted in water at different surface roughnesses

TEST	SLIDING SPEED ($m.s^{-1}$)	NORMAL LOAD (kg)	c.l.a. SURFACE ROUGHNESS (μm)	LUBRICANT	TEST DURATION (hours)	LINEAR CORRELATION COEFFICIENT	SPECIFIC -WEAR RATE $mm^3.N^{-1}.m^{-2}$
1	0,25	100	0,136 ± 0,013	Water	25	0,9941	$3,43 \times 10^{-8}$
2	0,25	100	0,557 ± 0,029	Water	20	0,9910	$8,80 \times 10^{-7}$
3	0,25	100	0,794 ± 0,021	Water	10	0,9999	$3,46 \times 10^{-6}$
4	0,25	100	1,06 ± 0,031	Water	0,3	-	$3,91 \times 10^{-5}$

The specific wear rates calculated at each roughness were then plotted as a function of surface roughness on a log-linear graph as illustrated in Figure 6.28. The wear rates calculated from the tests completed during the velocity tests in water were also included (surface roughnesses ± 0,38 micrometers c.l.a.).

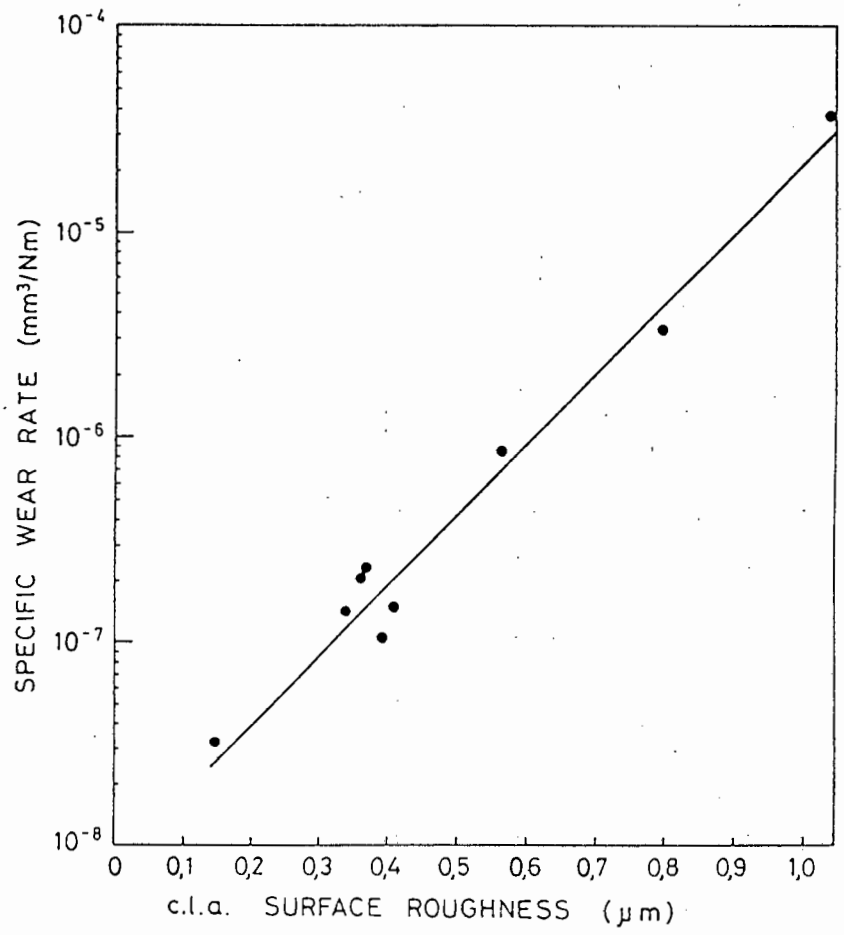

FIGURE 6.28 : The effect of counterface roughness on the wear of UHMWPE in water

Figure 6.28 shows that, on a log-linear scale, the relationship between wear rate and counterface roughness was linear over the range of roughnesses tested. The specific wear rate increased from 3,4 x 10^{-8} $mm^3.N^{-1}.m^{-1}$ at a roughness of 0,136 micrometers c.l.a. to 3,9 x 10^{-5} $mm^3.N^{-1}.m^{-1}$ at 1,06 micrometers c.l.a., i.e. three orders of magnitude. The graph can be described by the following equation :

$$\text{Specific Wear Rate} = 1{,}096 \times 10^{-8}\ e^{\,7.67\ \text{c.l.a.}}$$

A linear relationship between wear rate and roughness was also reported by Dowson et al (1984) during reciprocating tests with UHMWPE sliding against AISI 316 under water lubrication in the range 0,01 to 1,0 micrometers Ra. The wear rates calculated in these tests varied from approximately 2 x 10^{-6} to 4 x 10^{-5}

$mm^3.N^{-1}.m^{-1}$ in the range 0,1 to 1,0 micrometers Ra. However, these surfaces were prepared with a random surface texture and the greater sensitivity of the wear rates in this study to the increase in surface roughness can be ascribed to the directional nature of the counterface topography. The fact that similar wear rates were calculated at the higher roughnesses (±1,0 Ra) suggests that, at these roughnesses, the mechanism of material removal is independent of the nature of the surface and the wear rate is determined solely by the size of the asperities.

Figure 6.29 shows the variation in the static and kinetic friction coefficients with surface roughness. The values plotted are those recorded after 9 km of sliding.

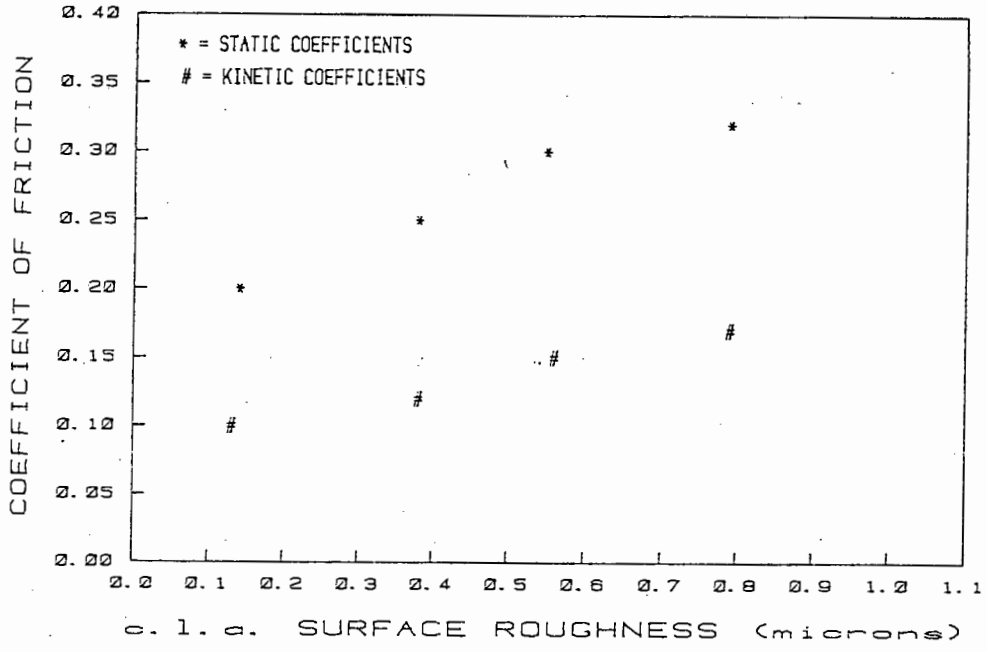

FIGURE 6.29 : The effect of counterface roughness on the friction coefficients of the tests run in water. (The value at 0,38 micrometers c.l.a. is the mean of 5 tests)

Both coefficients displayed a marked dependance on the roughness of the counterface although the static values were more sensitive. The response of the friction coefficients to the increase in roughness may be considered as being linear over the range of roughnesses tested. The relationship between counterface

roughness and the static friction coefficient can be described by an equation of the form :

$\mu = 0{,}180$ c.l.a. + 0,183

The surface temperature values also increased more or less linearly with roughness as illustrated in Figure 6.30. The values plotted are those recorded after 9 km of sliding in each test.

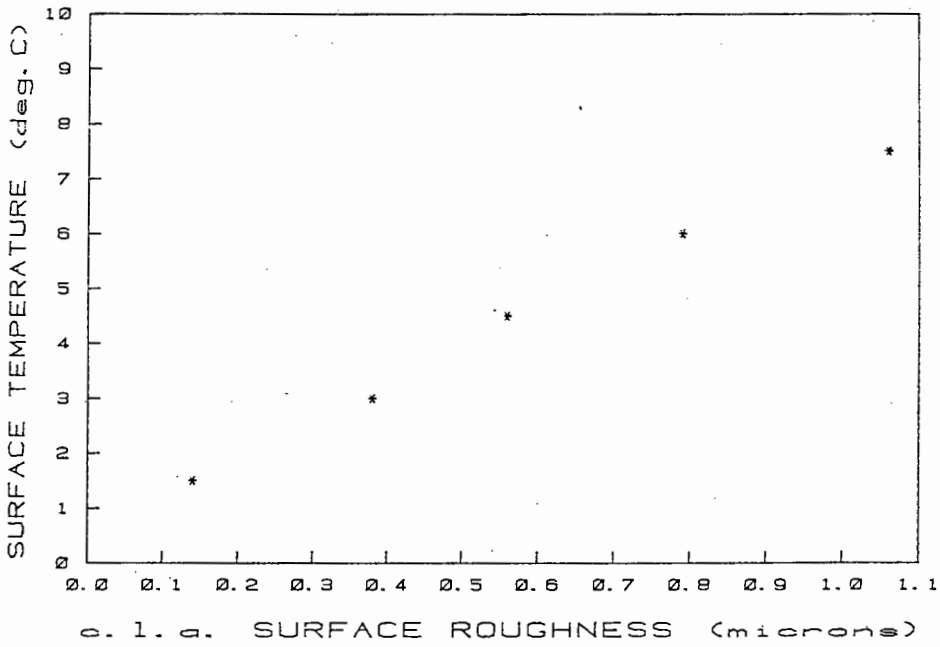

FIGURES 6.30 : Surface temperature as a function of surface roughness for the tests in water. (The value at 0,38 micrometers c.l.a. is the mean of 5 tests)

Scanning electron microscopy revealed that there was a transition in the material removal mechanism as the counterface roughness increased. Figures 6.31(a), (b) and (c) show typical surface topographies of the polymer pins from the 0,136; 0,557 and 0,794 micrometer c.l.a. tests, respectively.

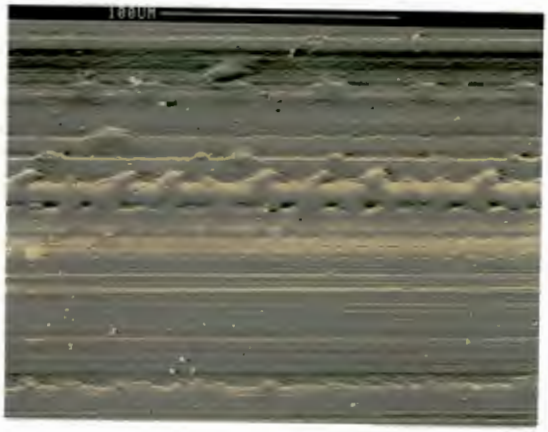

(a) 0,136 c.l.a.

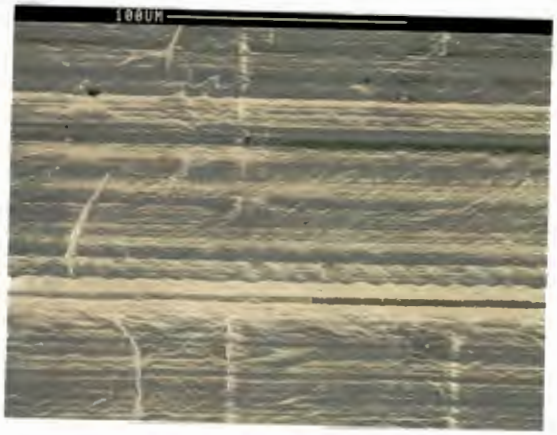

(b) 0,557 c.l.a.

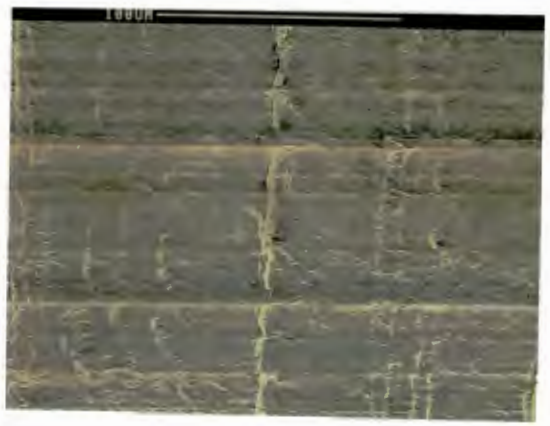

(c) 0,794 c.l.a.

FIGURES 6.31(a),(b) & (c) : Wear morphologies of polymer specimens tested at 0,136; 0,557 and 0,794 micrometers c.l.a., respectively. The arrow indicates the sliding direction

At the low roughness typical abrasive processes dominated, resulting in the formation of long, narrow abrasive grooves. Artifacts of adhesive stick-slip were also observed as illustrated in Figure 6.31(a). As the roughness increased the width and depth

of the abrasive grooves increased. However, from a roughness of approximately 0,4 micrometers c.l.a. abrasive wear was complemented by an additional material removal process. This type of wear was characterised by the appearance on the surface of straight ridges of material lying perpendicular to the sliding direction as shown in Figure 6.31(b). They were formed by a chiselling-type of action, similar to that occurring in machine chatter, of the sharp cutting edges of prominant machining marks. This type of wear mechanism became more and more prominant as the roughness increased until, at 0,794 micrometers c.l.a., it was the primary material removal process as illustrated in Figure 6.31(c).

The transition in the wear mechanism was also observed on the steel counterfaces. At the low roughness value typical 3-body abrasive wear processes and transfer of polymer to the counterface was observed, whilst on the rougher surfaces large chunks of polymer were simply scraped from the sliding surface by the sharp cutting edges of the machining marks. Figures 6.32(a) and (b) are steel counterfaces from the 0,136 and 0,794 micrometer c.l.a. tests, respectively.

FIGURES 6.32(a) & (b) : The counterfaces from the 0,136 and 0,794 micrometer c.l.a. tests, respectively. The arrow indicates the sliding direction

6.3.2 Tests in 5:95

The effect of counterface roughness was also investigated during tests in 5:95. A series of 6 tests were run, under standard conditions of speed (0,25 $m.s^{-1}$) and load (100 kg), against counterfaces whose roughness ranged from approximately 0,1 to 0,9 micrometers c.l.a. Table 6.2 gives the results of the six tests run in 5:95 at the various counterface roughnesses.

TABLE 6.2 : Results of the tests conducted in 5:95 at different surface roughness

TEST	SLIDING SPEED ($m.s^{-1}$)	NORMAL LOAD (kg)	c.l.a. SURFACE ROUGHNESS (μm)	LUBRICANT	TEST DURATION (hours)	LINEAR CORRELATION COEFFICIENT	SPECIFIC WEAR RATE $mm^3.N^{-1}.m^{-2}$
1	0,25	100	0,188 ± 0,029	5:95	25	0,9994	$1,24 \times 10^{-8}$
2	0,25	100	0,339 ± 0,010	5:95	25	0,9971	$4,39 \times 10^{-8}$
3	0,25	100	0,414 ± 0,030	5:95	25	0,9993	$2,05 \times 10^{-7}$
4	0,25	100	0,486 ± 0,025	5:95	25	0,9990	$2,52 \times 10^{-7}$
5	0,25	100	0,734 ± 0,038	5:95	20	0,9977	$1,04 \times 10^{-6}$
6	0,25	100	0,873 ± 0,025	5:95	10	0,9999	4.05×10^{-6}

Appendices B1, 2, 3, 4, 5 and 6 are the cumulative volume loss versus sliding distance curves of the 6 tests. As was the case in the water tests, the effect of running-in became less pronounced as the roughness increased. Figure 6.33 shows the variation of the specific wear rate with surface roughness for the tests in 5:95.

The wear rates of the three separate tests conducted in 5:95 at 0,25 $m.s^{-1}$ during the velocity tests have also been included (c.l.a. surface roughness - ± 0,32 micrometers).

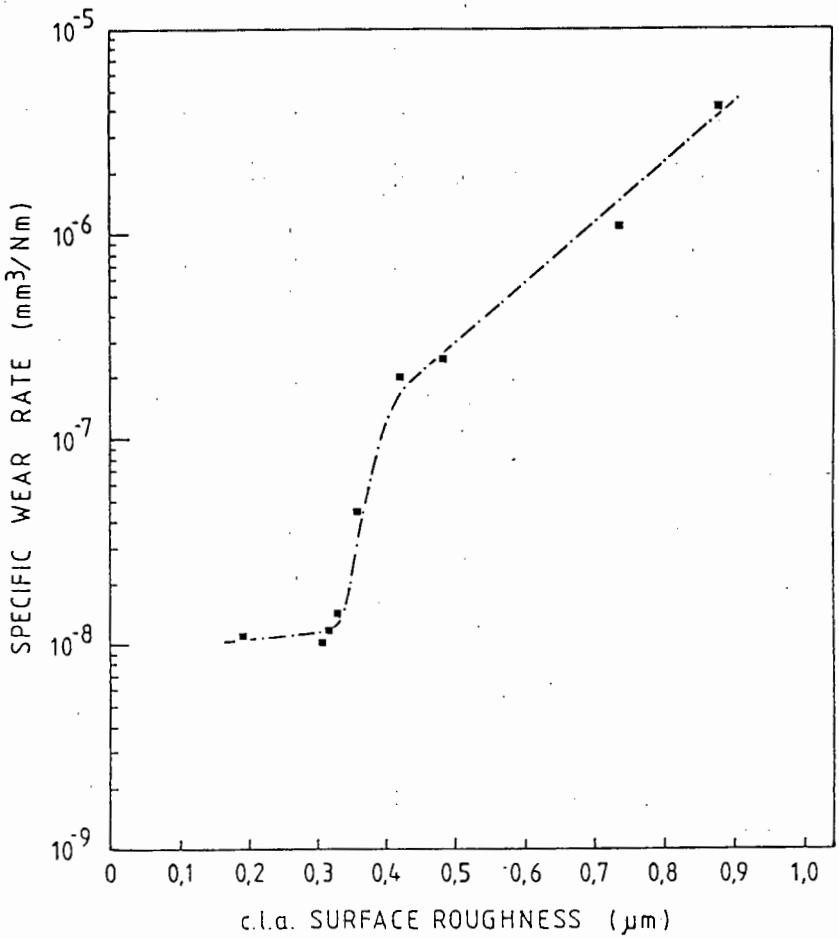

FIGURE 6.33 : The effect of surface roughness on the wear rates of the tests run in 5:95

The figure shows that the increase in roughness from 0,188 to 0,873 micrometers c.l.a. caused the wear rate to increase from 1,2 x 10^{-8} to 4,0 x 10^{-6} $mm^3.N^{-1}.m^{-1}$. However, unlike the water lubricated tests, where the relationship between wear rate and roughness was linear (on a log-linear scale) over the entire range of roughnesses tested, the trend resulting from the tests in 5:95 was more complex.

Below 0,3 micrometers c.l.a. the wear rate was effectively independant of surface roughness. Between 0,3 and 0,4 micrometers c.l.a. there was a rapid transition during which the wear rate increased by an order of magnitude. Above 0,4 micrometers c.l.a. there was a linear response of the wear rate to the increase in roughness, the slope of which was comparable with that resulting from the water tests. This indicates that, at roughnesses greater than approximately 0,4 micrometers c.l.a., wear occurs by the same basic abrasive mechanism which is independant of the type of lubricant.

At the lower values, i.e., below ± 0,3 micrometers c.l.a., the magnitude of the surface asperities are such that good boundary lubricants are able to modify the contact between the surfaces and, consequently, the wear rate.

Figure 6.34 compares the wear rate versus surface roughness curves of the tests in water and 5:95.

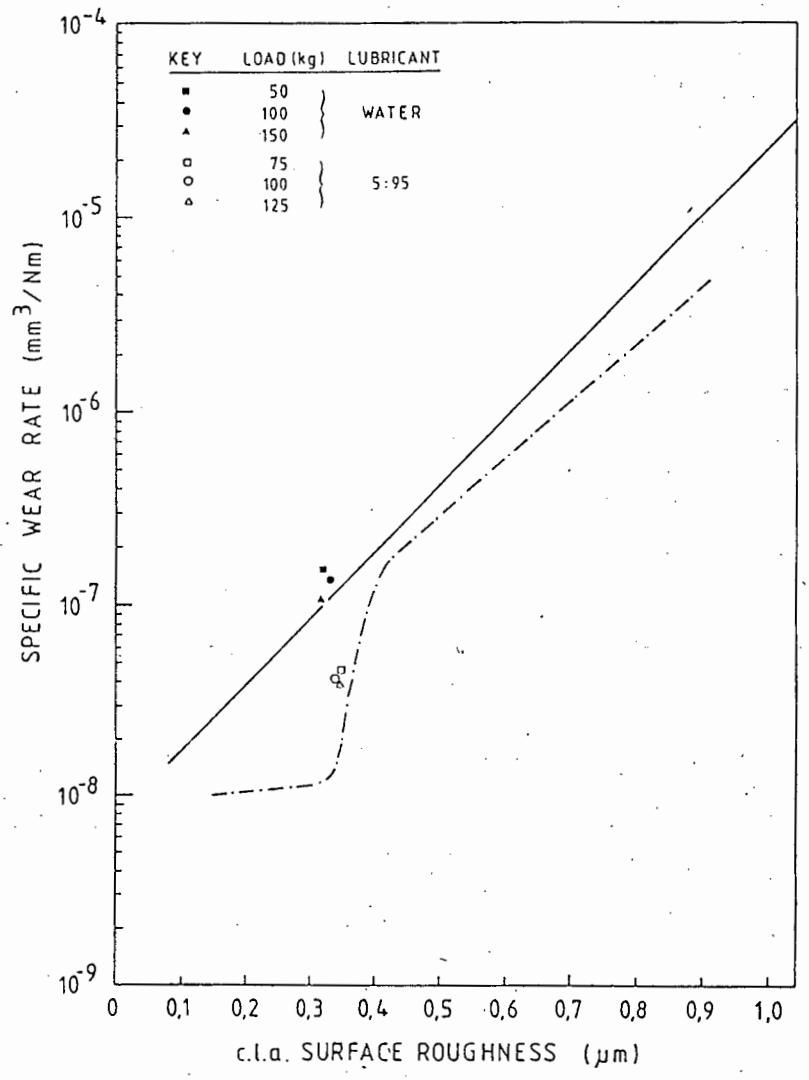

FIGURE 6.34 : A comparision of the effect of surface roughness on the wear rates of the tests run in water and 5:95

The figure shows that the wear rates in 5:95 were lower than those from the water tests over the whole range of roughnesses, especially at the lower roughness values.

As in the water tests, the friction coefficients increased with roughness, as illustrated in Figure 6.35 which shows the static and kinetic coefficients recorded after 9 km of sliding at each roughness. The friction values did not show, clearly, the transition which occurred in the wear rates. Both the static and kinetic friction coefficients increased more or less linearly with roughness.

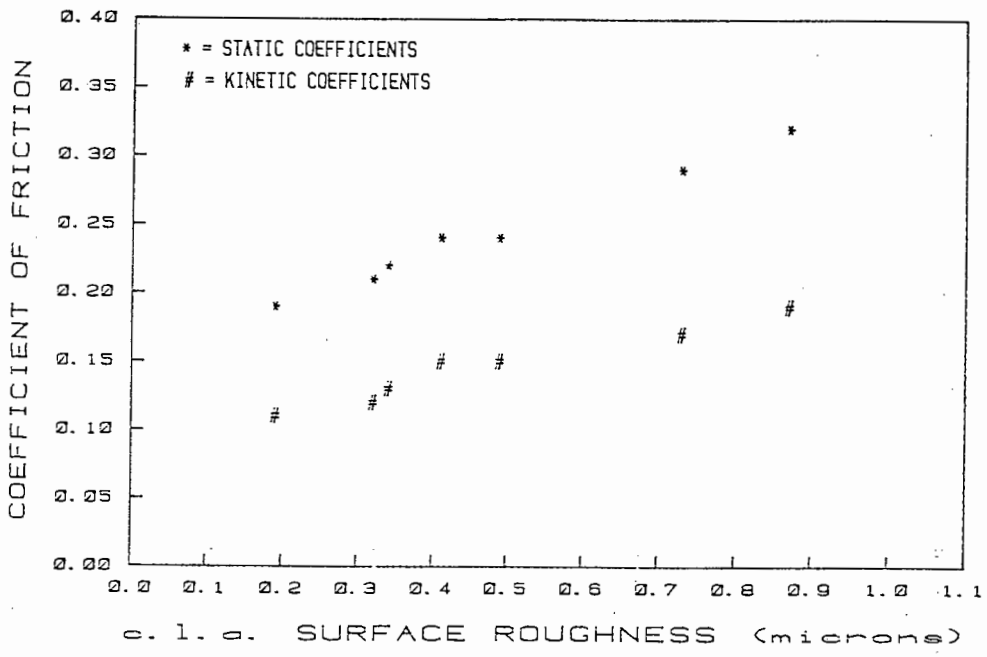

FIGURE 6.35 : Static and kinetic friction coefficients as a function of surface roughness in 5:95

Comparison with the friction data from the water tests showed that the slopes of the friction versus roughness lines, both static and kinetic, were similar in the two lubricating media. However, the static coefficients from the water tests were consistently higher than the 5:95 values. Figure 6.36 shows scatter bands of the friction coefficient data from the tests in water and 5:95 at the different roughnesses.

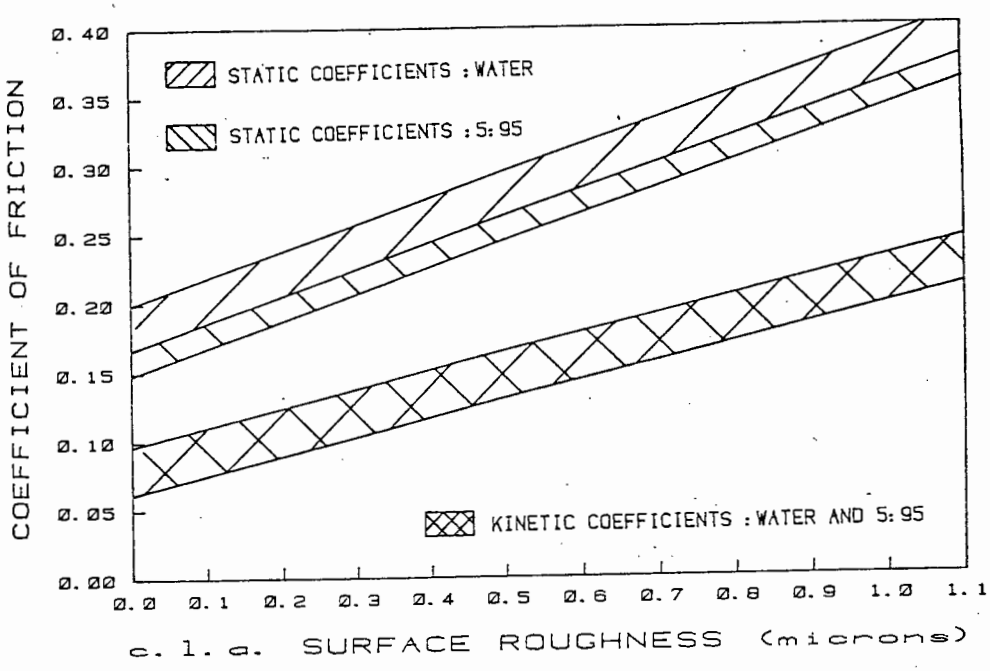

FIGURE 6.36 : Scatter bands showing the variation of the friction coefficients with roughness in water and 5:95

During the tests in 5:95, the surface temperatures increased with surface roughness. The increase was of the same order as that occurring under water lubriction, as illustrated in Figure 6.37. An increase in temperature with roughness was expected because the number of asperity contacts increases with roughness. There is more deformation and ploughing, the static friction coefficient increases and so too does the temperature at the surface.

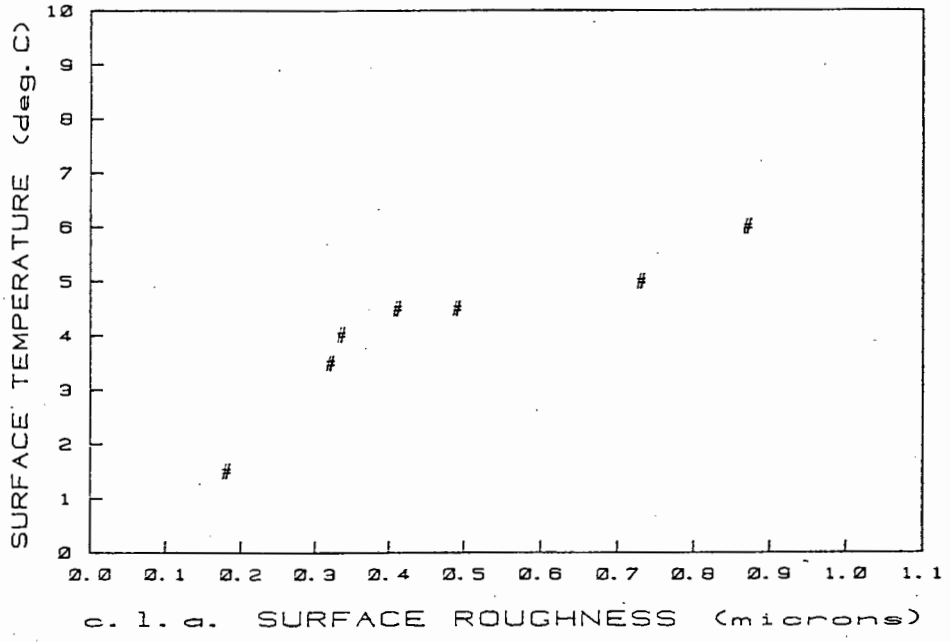

FIGURE 6.37 : The effect of surface roughness on the surface temperatures recorded during the tests in 5:95

Figure 6.38 is a scatter band showing the general increase in temperature with roughness during the tests in both lubricants.

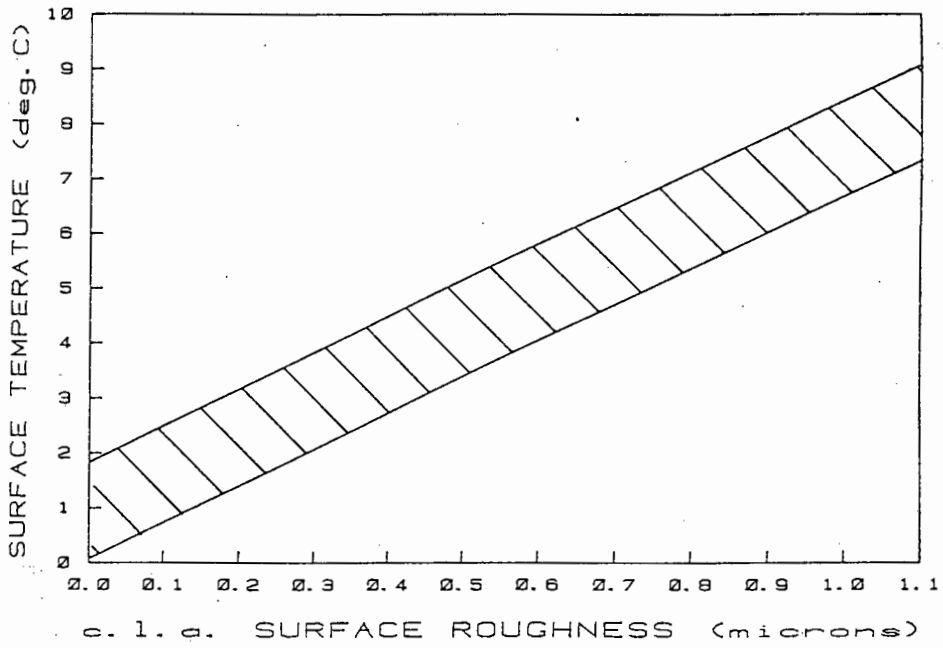

FIGURE 6.38 : The effect of surface roughness on the surface temperatures in water and 5:95

Examination of the worn surfaces in the SEM revealed that a similar change-over in the wear mechanism occurred under 5:95 lubrication. Figures 6.39(a), (b) and (c) are worn polymer surfaces from the 0,188; 0,414 and 0,873 micrometers c.l.a. tests, respectively.

(a) 0,188 c.l.a.

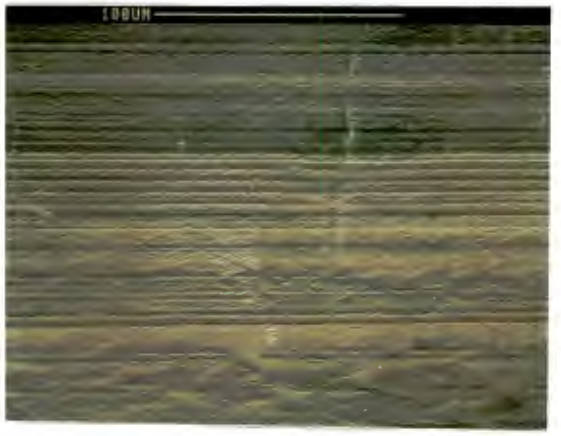

(b) 0,414 c.l.a.

(c) 0,873 c.l.a.

FIGURE 6.39(a),(b) & (c) : Polymer surfaces from the tests in 5:95 on counterfaces with roughnesses of 0,188; 0,414 and 0,873 micrometers c.l.a., respectively. The arrow indicates the sliding direction

The wear mechanism at 0,188 c.l.a. (Figure 6.39(a)) was purely abrasive and was typical of the features observed during the velocity tests (c.l.a. ± 0,32 micrometers). The characteristic chatter marks were observed on the surface of the 0,414 micrometer c.l.a. test (Figure 6.39(b)) which suggests that a transition in the wear mechanism occurred between these two roughness values. The chatter component of the wear became more pronounced as the roughness increased as shown in Figure 6.39(c). The presence of a few small chatter marks on the surface of the specimen from the 0,339 micrometer c.l.a. test confirmed that the change in wear mechanism occurred over an extremely narrow range of roughnesses (between 0,3 and 0,4 micrometers c.l.a.) and could well explain the transition which occurred in the wear rate. Figure 3.40 shows chatter marks on the surface of the 0,339 micrometer c.l.a. specimen.

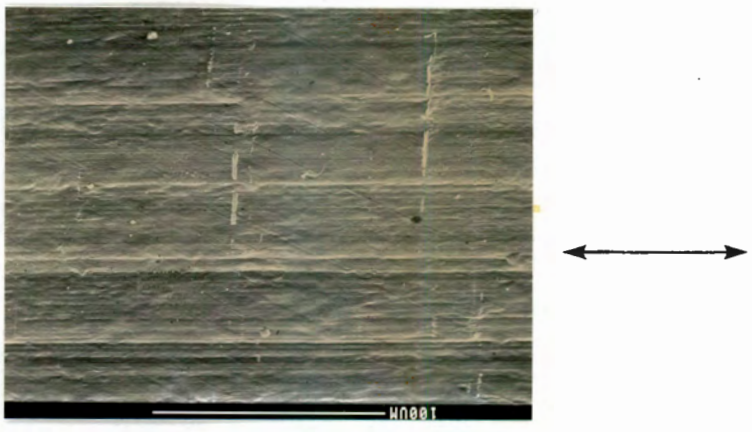

FIGURE 6.40 : The surface of the polymer specimen from the 0,339 micrometer c.l.a. test showing the first signs of chatter marks. The arrow indicates the sliding direction

Figures 6.41(a) and (b) are the counterfaces from the 0,188 and 0,873 micrometer c.l.a. tests, respectively. Abrasive wear tracks were observed on the former whilst large lumps of polymer, up to 100 micrometers wide, were torn from the polymer surface and deposited in the valleys of the rougher surface.

FIGURE 6.41(a) & (b) : Counterfaces from the 0,188 and 0,873 micrometers c.l.a. tests in 5:95. The arrow indicates the sliding direction

The low adhesion occurring between the polymer and the steel, as a result of the presence of the lubricant, lead to back transfer of worn material to the polymer surface as shown in Figure 6.42.

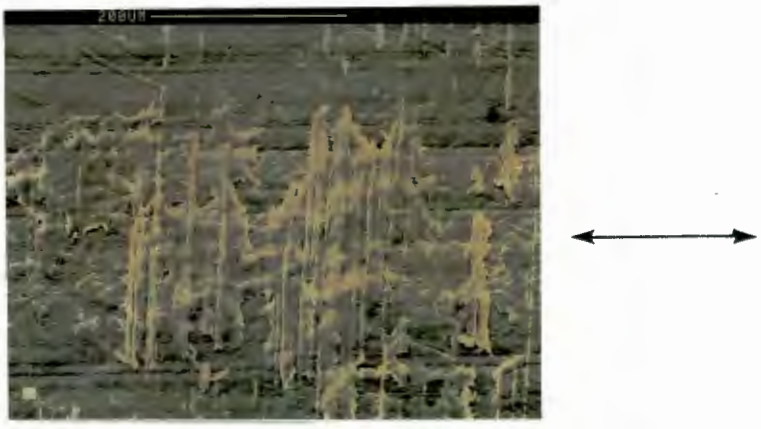

FIGURE 6.42 : Back transfer of polymer wear debris during the 0,874 micrometer c.l.a. test. The arrow indicates the sliding direction

6.4 THE EFFECT OF NORMAL LOAD

6.4.1 Tests in Water

A preliminary study on the effect of normal load on the friction and wear behaviour of UHMWPE under water lubrication was also conducted. Tests were run under normal loads of 50, 100 and 150 kg whilst maintaining a constant sliding velocity of 0,25 $m.s^{-1}$. The average c.l.a. surface roughness of the three counterfaces was

0,325 ± 0,01 micrometers. Figure 6.43 shows the cumulative volume loss versus sliding distance curves for the three tests at the different loads.

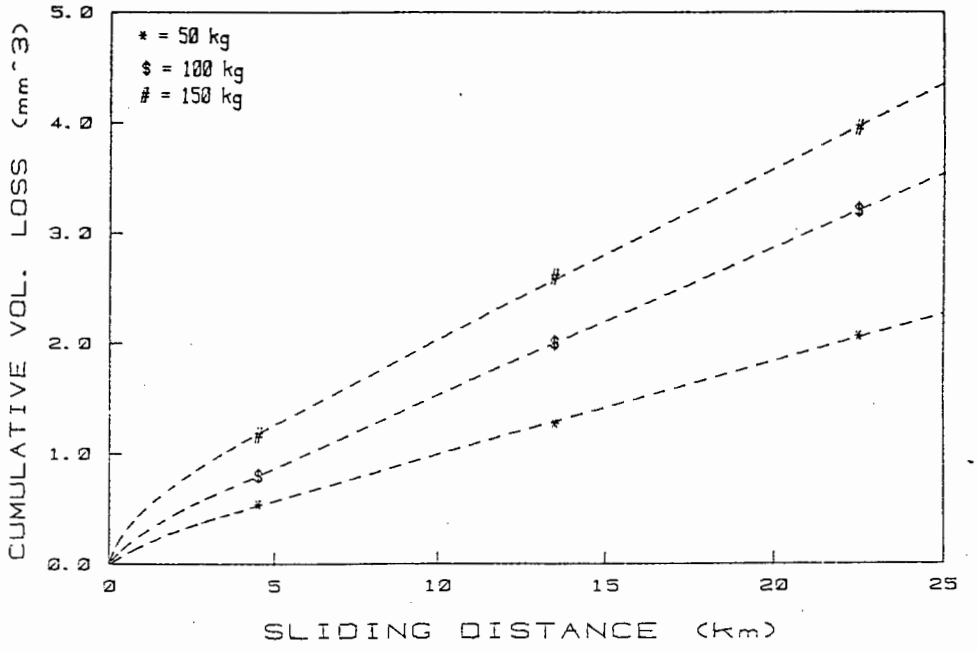

FIGURE 6.43 : The effect of load on the wear rate under water lubrication

As the load increased the volume loss also increased. However, when taking the load into account, the specific wear rates actually decreased as the load increased. However, the decrease was very small and the specific wear rate can, therefore, be considered to be independent of load within the range of loads tested. Table 6.3 gives the results of the tests run at the three different loads.

TABLE 6.3 : The results of the tests at different loads

TEST	SLIDING SPEED ($m.s^{-1}$)	c.l.a. SURFACE ROUGHNESS (μm)	NORMAL LOAD (kg)	LINEAR CORRELATION COEFFICIENT	SPECIFIC WEAR RATE ($mm^3.N^{-1}.m^{-1}$)
1	0,25	0,325 ± 0,022	50	0,9995	$1,62 \times 10^{-7}$
2	0,25	0,334 ± 0,015	100	0,9981	$1,33 \times 10^{-7}$
3	0,25	0,320 ± 0,036	150	0,9998	$1,09 \times 10^{-7}$

Similar behaviour was observed by Dumbleton and Shen (1976) during tests between UHMWPE and AISI 316 in a thrust-washer testing machine. They showed that although the running-in wear increased with load, the specific wear rate was independant of load in the

pressure range 4,6 - 9,1 $N.mm^{-2}$. Evans and Lancaster (1979) and Anderson (1982) showed that, below a critical load the wear rate was independant of load. Above this load, thermal softening of the polymer occurred, leading to a rapid rise in the wear rate.

The change in normal load did, however, have a marked effect on the friction coefficients as shown in Figure 6.44 which plots the static and kinetic friction coefficients as a function of normal load. The values shown were recorded after 9 km of sliding in each test.

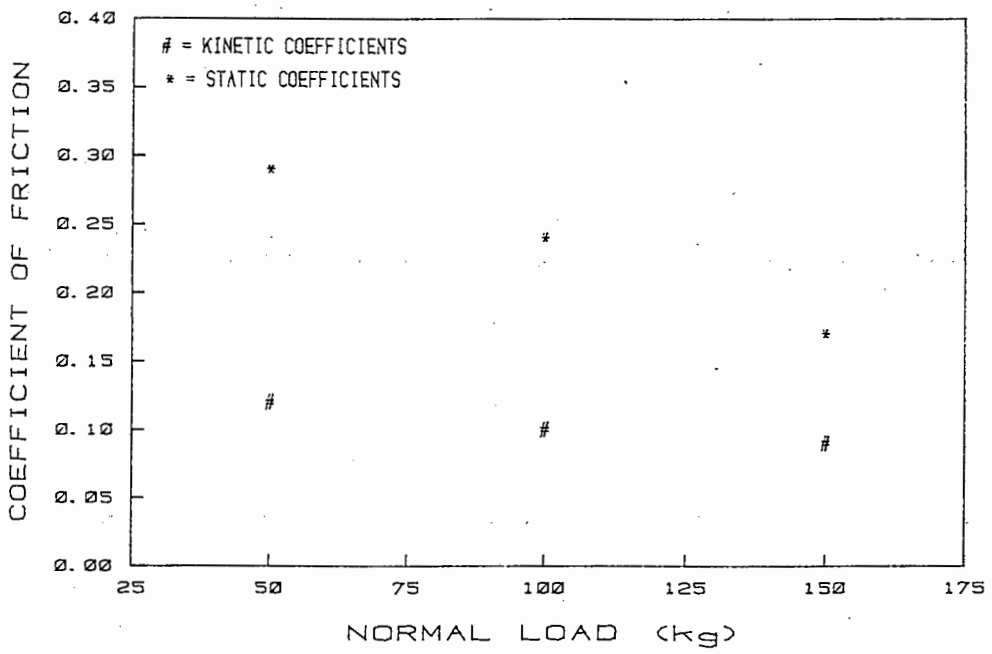

FIGURE 6.44 : Friction as a function of normal load under water lubrication

As the load increased the frictional force at the interface increased. However, the friction coefficients decreased with load. The static coefficients were more sensitive than the kinetic values to the change in load, as shown by the more rapid decrease of the static coefficients. The decrease in friction with load is due to a non-linear increase in the real area of contact with load. Moore (1972) showed that, for elastomers, the area of real contact varied with load according to the relationship $A_r = K\ W^{2/3}$ where K is an elastic constant. The

effect of normal load on the surface temperatures was not clear although there was a general increase in temperature with load as shown in Figure 6.45.

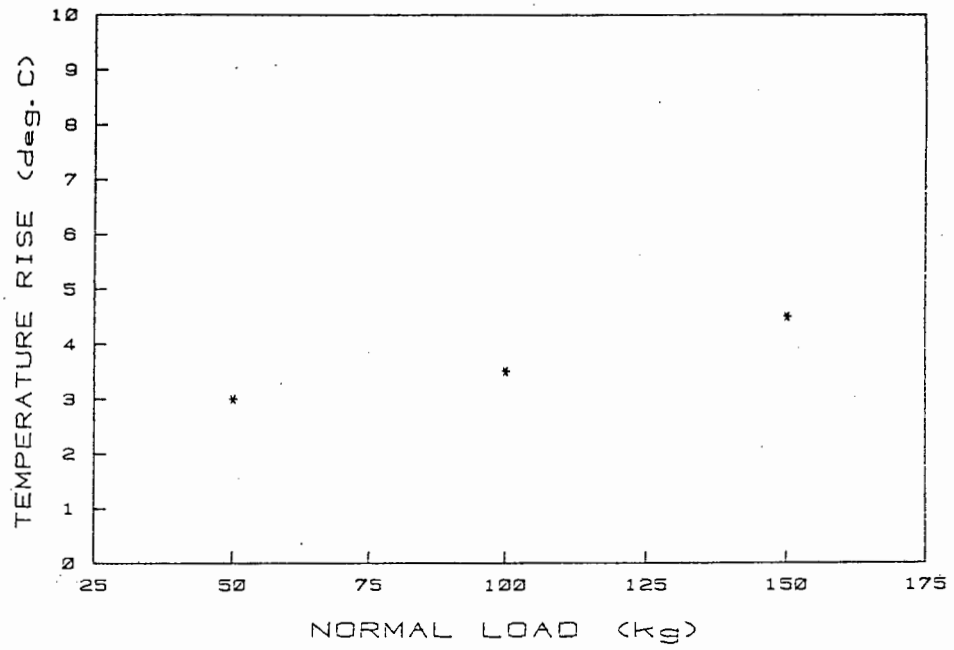

FIGURE 6.45 : The effect of load on the temperatures recorded at the interface during the water tests

Thus, as the load increases the area of contact increases, resulting in a higher temperature at the interface. However, the increase in contact area is not proportional to the load, resulting in a lowering of the friction coefficients and the specific wear rate.

It is clear that more tests at each load are required in order to establish, more accurately, the effect of load on the friction and wear performance of the polymer.

6.4.2 Tests in 5:95

The effect of load was also examined during tests in 5:95. Loads of 75, 100 and 125 kg were applied during these tests. A sliding speed of 0,25 $m.s^{-1}$ was retained and the average surface roughness of the three counterfaces was 0,345 ± 0,05 micrometers c.l.a.

Figure 4.46 shows the cumulative volume loss versus sliding distance curves of the three tests. Identical behaviour to that observed during the water tests resulted, i.e., the volume loss increased with load but the specific wear rates were independant of load. Table 6.4 summarises the results of the three tests.

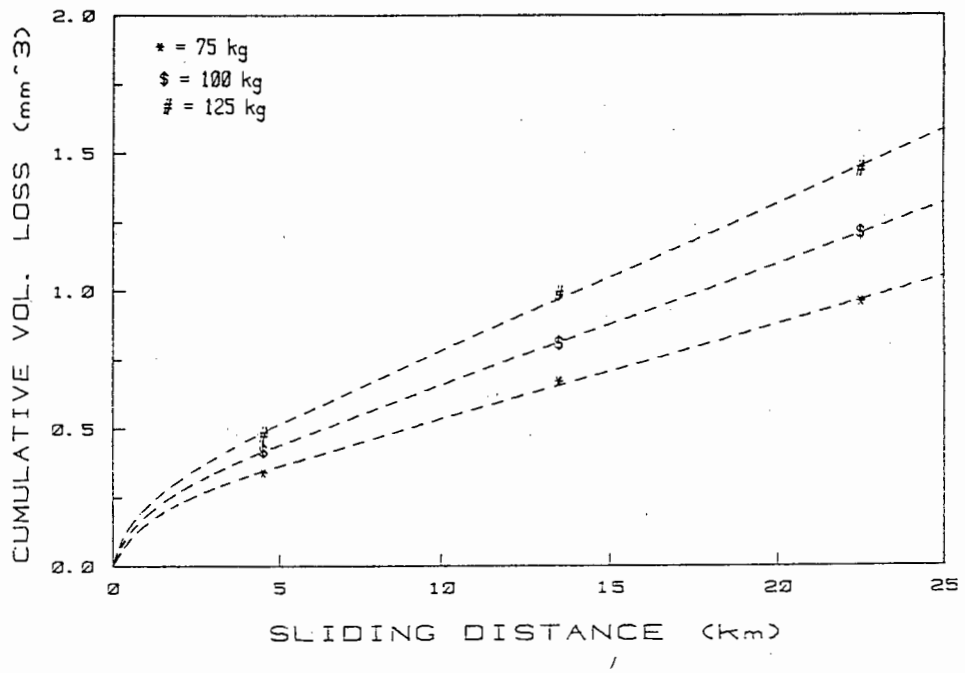

FIGURE 6.46 : The effect of normal load on the wear rate during tests in 5:95

TABLE 6.4 : The wear rates resulting from the tests in 5:95 at different loads

TEST	SLIDING SPEED ($m.s^{-1}$)	c.l.a. SURFACE ROUGHNESS (μm)	NORMAL LOAD (kg)	LINEAR CORRELATION COEFFICIENT	SPECIFIC WEAR RATE ($mm^3.N^{-1}.m^{-1}$)
1	0,25	0,350 ± 0,014	75	0,9976	$4,58 \times 10^{-8}$
2	0,25	0,339 ± 0,010	100	0,9971	$4,39 \times 10^{-8}$
3	0,25	0,346 ± 0,019	125	0,9989	$4,24 \times 10^{-8}$

As in the water tests, the 5:95 tests showed a slight decrease in the specific wear rate as the load increased. It is interesting to note that the load tests were run on counterfaces with roughnesses where the wear transition occurred during the counterface roughness tests in 5:95. The resulting wear rate of $4{,}35 \times 10^{-8}$ $mm^3.N^{-1}.m^{-1}$ for the 100 kg tests fits the existing curve extremely well as illustrated in Figure 6.47 which shows the wear rates of the tests run under the various loads on the graphs plotted from the surface roughness tests.

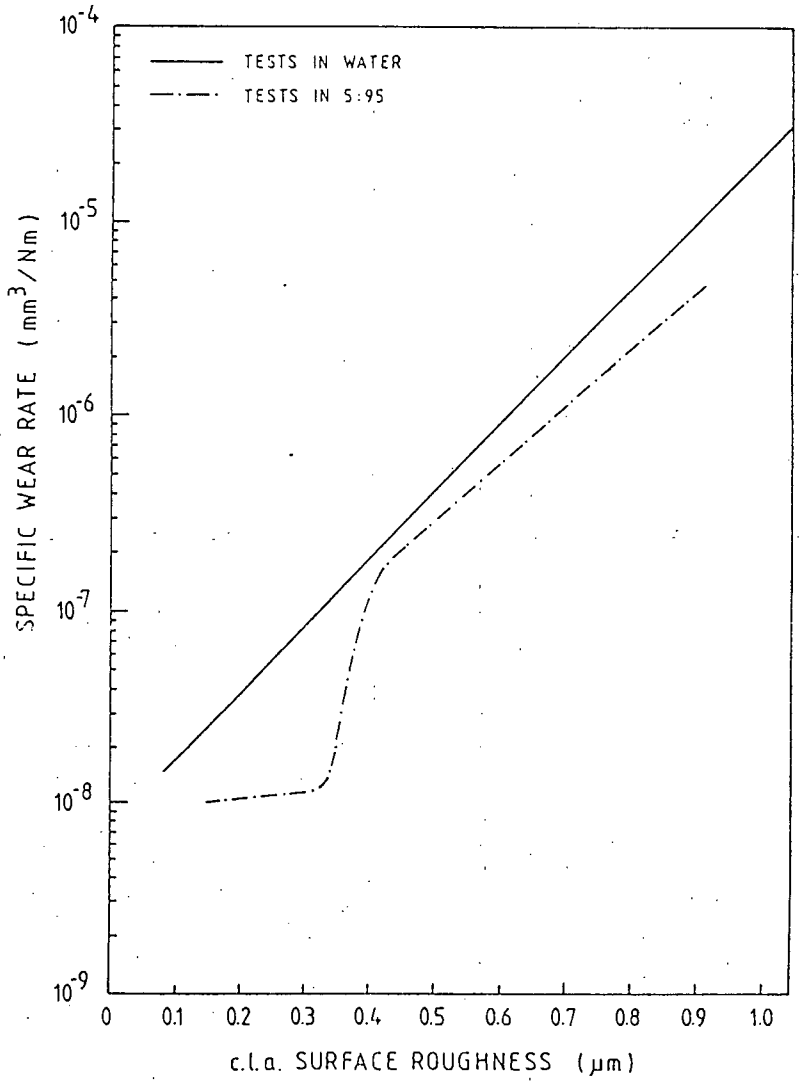

FIGURE 6.47 : The wear rates of the load tests plotted on the curves from the tests in water and 5:95 at the different surface roughnesses

The friction during these tests followed the trends observed during the water tests, i.e., the friction coefficients decreased with increasing load even though the actual friction force was higher at the larger load. Figure 6.48 shows the effect of load on the friction coefficients recorded after 9 km of sliding in each test. This decrease is again ascribed to the non-linear increase in the real contact area with load.

Both friction coefficients were slightly higher than those recorded during the water tests and this is probably due to the higher counterface roughnesses of these tests.

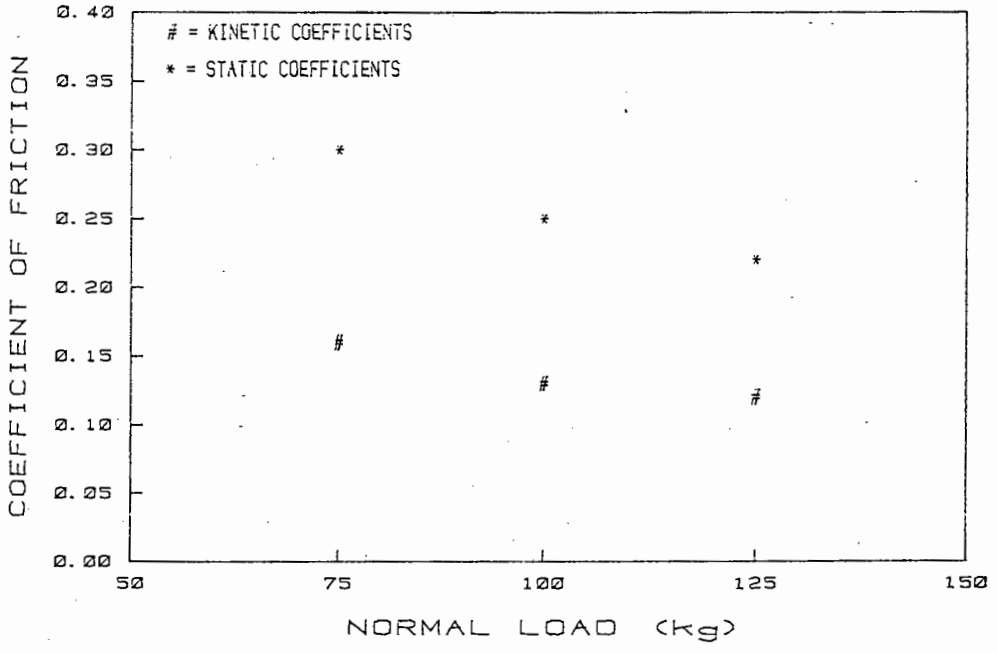

FIGURE 6.48 : Friction coefficients as a function of load for the tests in 5:95

Figure 6.49 shows the surface temperature rise values recorded after 9 km of sliding in each test. There was a steady increase in temperature with load and the temperatures were similar to those recorded during the water tests.

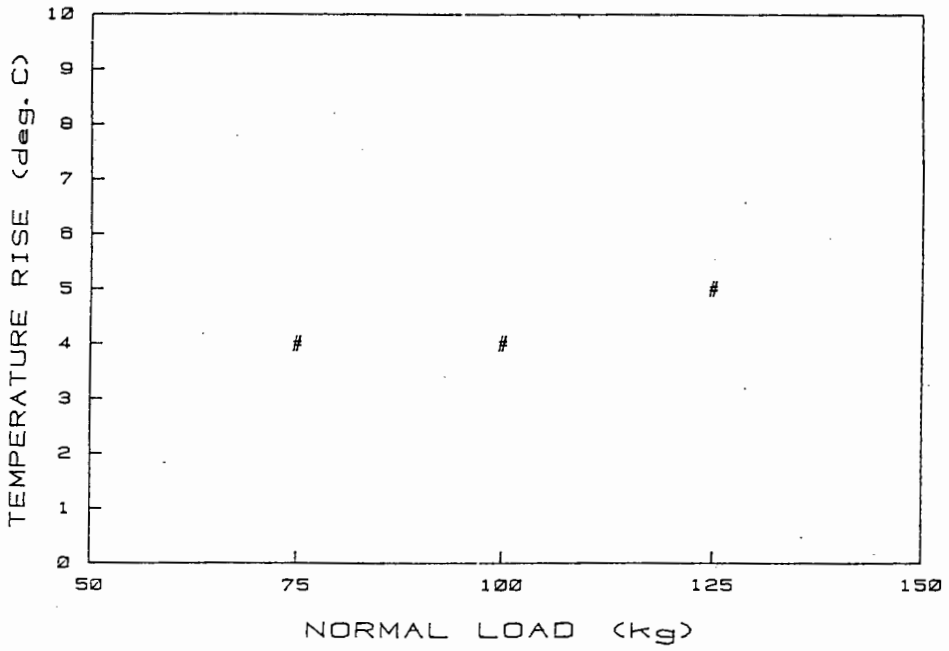

FIGURE 6.49 : Surface temperature as a function of normal load for tests in 5:95

6.5 THE APPLICATION OF THE RESULTS OF THIS STUDY TO THE MINING INDUSTRY

6.5.1 Examination of Worn Polymer Components from Hydraulic Stoping Machines

Abrasion by quartzite particles was the primary process causing degradation of polymer sliding components underground. The size of these particles ranged from a few micrometers up to 1 mm in diameter and are considered to have originated from two sources. The majority entered directly from the stoping environment whilst others were entrained in the hydraulic fluid. The size and concentration of these particles could possibly be reduced by an improved design which will limit the entry of particles from the rockface during drilling/impacting, whilst improved filtering methods would reduce the occurrence of particles in the fluid. There are, however, technical problems associated with filtering of the high-water based fluids but these should be eliminated when the transition is made to pure water.

UHMWPE was seen to act as a "filter" to the abrasive particles by allowing them to embed in the seal surface, thus limiting the passage of the particles to other parts of the machine. UHMWPE does, however, become embrittled by the embedding process, leading to eventual mechanical failure of the seal.

It is believed that most of the wear occurs at the start of each reciprocating cycle when the sliding velocities are low, the friction force is high and the separating effect of the lubricant is negligible, resulting in boundary contact between the sliding surfaces. During the firing stroke, however, a hydrodynamic fluid film forms which reduces the amount of contact and, consequently, reduces wear.

The examination revealed that, above all else, it was the presence of abrasive particles at the sliding interface which determines the service life of polymeric seals and bearings in hydraulic mining machinery. A reduction in the concentration of the particles by improved design and filtering methods should, therefore, result in an appreciable increase in the life of these components.

The question which should be addressed at this stage is, if through improved design and filtering techniques abrasive particles are eliminated, what would be the difference between the wear performance of components running in water and 5:95, and what would be the maximum permissible counterface roughness. It is, however, doubtful that abrasive particles will be totally eliminated from these machines. A reduction in the concentration of abrasive particles will probably result in a decrease in the specific wear rate but the mode of material removal will be unchanged. Therefore, a lowering of the counterface roughness might have little effect on the service life of the polymer components.

6.5.2 The Laboratory Wear Tests

The laboratory tests were conducted without the addition of abrasives to the lubricating medium. The sliding wear performance

of UHMWPE sliding against AISI 431 stainless steel was investigated during tests conducted under a range of operating conditions similar to those encountered in the hydraulic stoping machines. Of particular interest was the effect of changing the lubricating medium from a 5:95 emulsion to pure water. The tests showed that:

(i) The wear rate of UHMWPE was higher in water under all conditions of sliding, i.e. the boundary lubricating properties of water are inferior to those of the emulsion.

It is possible, using the specific wear rates obtained in this study, to make approximate calculations of the effect of counterface roughness on the reduction in thickness of an UHMWPE seal after 20 hours operation in an impact hammer. Table 6.5 shows the results and the calculation is presented in Appendix C.

TABLE 6.5 : The effect of counterface roughness on the reduction in thickness of a UHMWPE seal from an impact hammer operating in water and 5:95 in the absence of abrasive particles

c.l.a. SURFACE ROUGHNESS (μm)	WEAR DEPTH (mm)	
	WATER	5:95
0,1	0,017	0,006
0,3	0,094	0,024
0,5	0,44	0,14
0,9	6,6	2,8

The table clearly illustrates the effect of counterface roughness on the wear rate in both media. The results suggest that, in the absence of abrasive particles, the counterface roughness should be less than approximately 0,5 micrometers c.l.a. if the wear rate is to be maintained within acceptable limits. In fact, hammers operating on water might even be required to operate at roughnesses below 0,3 micrometers c.l.a.

In the presence of abrasive particles a three-body abrasive mechanism predominates and overrides the effect of counterface roughness. Under these conditions a good counterface finish does not improve the wear performance of the seal and surface roughnesses of 0,5 micrometers c.l.a., even in water, are thought to be sufficient.

If the presence of the particles could be reduced by improved design and filtering methods, then by operating at roughnesses below 0,3 micrometers c.l.a. the operating life of the seal will be considerably lengthened.

(ii) The laboratory tests also showed the importance of the coefficient of friction on the wear process. The static friction peak, which occurred at the start of each reciprocating cycle, was very sensitive to changes in operating conditions. The static friction coefficients were significantly higher (approximately 20%) in the water tests which means that the friction force at the start of each impact cycle is higher during water lubrication. An increase in counterface roughness was accompanied by a considerable increase in the static friction coefficients in both lubricants, i.e., in the range 0,2 to 0,9 micrometers c.l.a. the static friction coefficients increased from approximately 0,15 to 0,35 which is an increase of more than 130%. This means that as the surface roughness increases more energy is dissipated at the interface.

This study has served to provide information which can be used to minimise the severe abrasive wear of sliding components in hydraulic mining machinery. The first step in solving this problem is obviously the elimination of abrasive particles from the sliding surfaces. If this can be achieved, the service life of polymer sliding components can be futher lengthened by improving the surface finish of the steel counterfaces. Apart from a slightly higher wear rate in water, there is no fundamental reason preventing the transition from 5:95 to mine service water as the hydraulic power medium.

CHAPTER 7

A SUMMARY OF RESULTS AND CONCLUSIONS

The main objectives of this investigation were:-

i) To determine the wear mechanisms responsible for the degradation of polymer sliding components in newly developed hydraulic stoping machines.

ii) To develop a laboratory test facility which could be used to determine the reciprocating sliding wear performance of material couples from various sliding applications within the mining industry.

iii) To evaluate the reciprocating sliding wear behaviour of UHMWPE against AISI 431 stainless steel under a range of lubricating and operating conditions.

The examination of worn polymer seals and bearings taken from hydraulic impact hammers and hand held rockdrills operating on 5:95 showed that:

Abrasion by quartzite particles is the primary wear mechanism causing degradation of the polymeric sliding components underground. The size of these particles ranged from a few micrometers up to a few millimeters in size and are considered to have originated from two sources. Most of the particles entered the internal workings of the machines directly from the stope face, whilst smaller particles were entrained in the hydraulic fluid. It is envisaged that through careful design and improved filtering methods the size and concentration of these particles could be considerably reduced.

A reciprocating sliding wear testing machine, which essentially simulates the action of a polymer seal sliding against a steel piston in a hydraulic cylinder was successfully commissioned. The rig provides the facilities for measuring the wear rates, friction coefficients and surface temperatures resulting from the sliding of various couples under a range of operating conditions. The reproducibility of the three parameters was shown to be

within acceptable limits. This enabled a detailed study to be carrried out on the wear of UHMWPE sliding against AISI 431 stainless steel under various operating conditions. Of particular interest, however, was the effect of changing the lubricating medium from a 5:95 oil/water emulsion to pure tap water. The laboratory tests showed that:-

1. The wear rate of UHMWPE was higher under water lubrication and the lower wear rates occurring during the tests in 5:95 can be ascribed to the smaller contribution of adhesion to the overall wear process. This was confirmed by the absence of a polymer transfer film on the counterfaces from the 5:95 tests.

2. The friction coefficients decreased steadily throughout the tests in water whilst they remained constant for the duration of the tests in 5:95. This decrease is thought to be the result of modification of the transfer film during the tests in water.

3. An increase in the sliding velocity, in the range where boundary lubrication processes occur, was accompanied by a number of changes at the sliding interface.

   i) An increase in sliding velocity caused the surface temperature to increase. Consequently, the elastic modulus of the polymer decreased locally at the interface, resulting in an increase in the real area of contact.

   ii) As a result of the larger contact area the number of asperity interactions increased, resulting in an increase in the specific wear rate. However, the increase in wear rate was greater in the water tests. This is because, in water, both adhesive and abrasive interactions are affected by the larger contact area, whereas in 5:95, the adhesive component is insignificant and the increase in velocity only affects the deformation component of the wear process.

   iii) The increase in the real area of contact also increased the static friction coefficients in both lubricating media. The increase was larger in the water tests and can be ascribed to the absence of an adhesive contribution to the friction force in 5:95.

4. Abrasive wear, in this case by the asperities of the ground counterfaces, was shown to be the primary material removal mechanism during the laboratory tests. Both two and three-body mechanisms were identified and are considered to occur at surface roughnesses below approximately 0,4 micrometers c.l.a. Three-body wear occurs when steel fragments are detached from the ground counterface by a fatigue process and embed in the sliding polymer surface. The wear damage was less severe under 5:95 lubrication as a result of the low adhesive forces which reduced the probability of forming a third-body at the interface. In the water tests the decrease in the friction coefficient with sliding distance was not accompanied by a decrease in the steady-state wear rate because the mode of material removal was unaffected by the formation of the transfer film.

5. Increasing the surface roughness of the steel counterface in the range 0,1 - 1,0 micrometers c.l.a. caused the wear rate of the polymer to increase markedly in both lubricating media.

   i) In water the increase in the specific wear rate with surface roughness was linear on a log-linear scale and followed the equation:

      $$\text{Specific Wear Rate} = 1{,}096 \times 10^{-8}\, e^{(7{,}67\ \text{c.l.a.})}$$

   ii) In both media, there was a change in the mode of material removal at a surface roughness of approximately 0,4 micrometers c.l.a. Below this value typical ploughing abrasive mehanisms were in operation. Above this value material was removed by the chiselling action of prominent asperities.

   iii) In 5:95 there was a transition in the specific wear rate between 0,3 and 0,4 micrometers c.l.a. which was thought to be associated with the change in the mode of material removal. The wear transition occurred in 5:95 and not in water because the specific wear rate of UHMWPE in 5:95 at surface roughnesses below approximately 0,3 micrometers c.l.a. was considerably lower than in water. The change in the material removal mechanism, therefore, had a more pronounced effect in 5:95. It was the topography of the counterface, not the different lubricant, which brought about the change in the wear mechanism.

iv) An increase in surface roughness also resulted in an increase in the friction coefficients and surface temperatures. At high surface roughnesses a greater percentage of the input energy is dissipated in overcoming the friction force.

6. Varying the normal load in the range 50 - 150 kg had little effect on the respective specific wear rates in each lubricant. An increase in load did, however, lead to a lowering of the friction coefficients because the real area of contact does not increase linearly with load.

7. Tests conducted under dry conditions showed that the wear is dominated by the high surface temperatures reached during sliding. The specific wear rate calculated for these tests was higher than for both of the lubricated tests. Wear occurred by the shearing or extrusion of the molten surface layers.

CHAPTER 8

RECOMMENDATIONS FOR FUTURE WORK

It was not possible, during the course of this study, to cover all aspects of the sliding wear behaviour of UHMWPE against steel. The work covered must, therefore, be seen as a contribution to an ongoing research programme. Apart from providing important empirical data which can be applied in the mining industry, the project also served to improve our understanding of the basic wear mechanisms occurring during polymer/metal sliding.

Future research on sliding wear should, therefore, include work which can be translated into practial terms by mining engineers as well as work of a more fundamental or academic nature.

Laboratory wear tests conducted in the presence of abrasive particles would improve our understanding of the three-body wear mechanisms causing accelerated degradation of components in sliding systems. They would also provide a better simulation of the actual conditions prevailing in the hydraulic mining machines.

Tests between UHMWPE and steel with and without abrasives, should be conducted over a wider range of sliding speeds and normal loads in order that trends in the friction and wear data can be determined. It is important that reproducibility of the results is attained at each value. These trends could then be extrapolated to the real situation where they could be of use to engineers. The tests would also improve our understanding of the change in wear mechanisms accompanying the change in speed or load.

Tests should be run to longer sliding distances in order to monitor any transitions in the friction and wear data as a result of a change in the wear mechanism at the sliding interface.

The effect of sliding against a counterface which had been run-in prior to testing should also be investigated. Similar effects are likely to occur when a seal or piston is replaced during underground operation of the mining machines.

A detailed study of the mode of formation and characteristics of the polymer transfer film would provide a more complete explanation of the wear mechanisms occurring in polymer/metal sliding.

A comparison of the wear processes occurring under dry and lubricated conditions could be carried out by cooling the dry steel specimen to within the range of temperatures generated under lubricated sliding.

Simple tests, in which a loaded conical indenter is drawn across the polymer in the presence of the two lubricants will provide insight into the nature of the asperity interactions occurring in the respective lubricants.

Since a laboratory test rig has already been established, the wear performance of other prospective seal and bearing materials could also be investigated and a ranking table established.

The excellent wear resistance, corrosion resistance and high strength to weight ratio makes ceramic materials an attractive alternative for sliding components in hydraulic mining machinery. Not much literature is currently available on this subject and further research should be directed in this field.

REFERENCES

1. ANDERSON, J.C. (1982a) : "High Density and Ultra-High Molecular Weight Polyethylenes - Their Wear Properties and Bearing Applications", Tribology International, 15, 1, pp 43-47.

2. ANDERSON, J.C. (1982b) : "Wear of Commercially Available Plastic Materials", Tribology International, 15, 1, pp 255-263.

3. ANDERSON, J.C. & ROBBINS, E.J. (1976) : "The Influence of Temperature Generation on the Wear of Some Polymers", The Wear of Non-Metallic Materials, Proc. 3rd Leeds-Lyon Symposium on Tribology, Edited by D. Dowson, M. Godet and C.M. Taylor, MEP, London, pp 94-98.

4. ANDERSON, J.C. & WILLIAMSON, P.K. (1984) : "Relating Laboratory Wear Testing to the In-Service Wear of Polymers", Proc. of the ACS Division of Polymeric Materials : Science and Technology, 50, pp 385-392.

5. ATKINSON, J.R., BROWN, K.J. & DOWSON, D. (1978) : "The Wear of High Molecular Weight Polyethylene. Part I : The Wear of Isotropic Polyethylene Against Dry Stainless Steel in Uni-directional Motion", J. Lubr. Technol., ASME Trans., 100, pp 208-218.

6. ARCHARD, J.F. (1974) : "Surface topography and Tribology", Tribology International, 7, 5, pp 213-220.

7. BAHADUR, S. (1978) : "Wear Research and Development", J. Lubr. Technol., ASME Trans., 100, pp 449-454.

8. BELYI, V.A., SVIRIDYONOK, A.I., SMURUGOV, V.A. & NEVZOROV, V.V. (1977) : "Adhesive Wear of Polymers", J. Lubr. Technol., ASME Trans., 99, pp 396-400.

9. BRISCOE, B.J. (1981) : "The Wear of Polymers : An Essay on Fundamental Aspects", Wear of Materials 1981, S.K. Rhee, A.W. Ruff and K.C. Ludema (eds.), ASME, New York, pp 7-16.

10. BRISCOE, B.J., POOLEY, C.M. & TABOR, D. (1974) : "Friction and Transfer of Some Polymers in Unlubricated Sliding", Advances in Polymer Friction and Wear, L-H. Lee (ed), Polymer Science and Technology Symposium Series, Plenum Press, New York, 5A, pp 191-202.

11. BROWN, K.J. ATKINSON, J.R. & DOWSON, D. (1982) : "The Wear of High Molecular Weight Polyethylene. Part II : The Effects of Reciprocating Motion, Orientation in the Polyethylene, and a Preliminary Study of the Wear of Polyethylene Against Itself", J. Lubr. Technol., ASME Trans., 104, pp 17-22.

12. BUCKLEY, D.H. (1974) : "Introductory Remarks - Friction and Wear of Polymer Composites", Advances in Polymer Friction and Wear, L-H. Lee (ed.), Polymer Science and Technology Symposia Series, Plenum Press, New York, 5B, pp 601-603.

13. CHALLEN, J.M. & DOWSON, D. (1976) : "The Calculation of Interfacial Temperatures in a Pin-on-Disc Machine", The Wear of Non-Metallic Materials, Proc. 3rd Leeds-Lyon Symposium on Tribology, Edited by D. Dowson, M. Godet and C.M. Taylor, MEP, London, pp 25-31.

14. CHAMBER OF MINES RESEARCH ORGANISATION, Annual Report, (1982).

15. CRAWFORD, R.J. (1981) : "Plastics Engineering", Pergamon, Oxford.

16. CREASE, A.B. (1973) : "Design Data for the Wear Performance of Rubbing Bearing Surfaces", Tribology, 6, 1, pp 15-20.

17. CZICHOS, H. (1978) : "Tribology. A systems approach to the Science and Technology of Friction, Lubrication and Wear", Elsevier, Amsterdam.

18. CZICHOS, H. (1983) : "The Influence of Adhesive and Abrasive Mechanisms on the Tribological Behaviour of Thermoplastic Polymers", Wear, 88, pp 27-43.

19. DEUTSCHMAN, A.D., MICHELS, W.J. & WILSON, C.E. (1975) : "Machine Design : Theory and Practice", MacMillan Publishing Co., Inc., New York.

20. DOWSON, D., ATKINSON, J.R., & BROWN, K. (1974) : "The Wear of High Molecular Weight Polyethylene with Particular Reference to it's Use in Artificial Human Joints", Advances in Polymer Friction and Wear, L-H. Lee (ed), Polymer Science and Technology Symposia Series, Plenum Press, New York, 5B, pp 533-551.

21. DOWSON, D., CHALLEN, J.M., HOLMES, & ATKINSON, J.R. (1976) : "The Influence of Counterface Roughness on the Wear Rate of Polyethylene", The Wear of Non-Metallic Materials, Proc. 3rd Leeds-Lyon Symposium on Tribology, Edited by D. Dowson, M. Godet and C.M. Taylor, MEP, London, pp 99-105.

22. DOWSON D., EL-HADY DIAB, M.M., GILLIS, B.J. & ATKINSON, J.R. (1984) : "The Influence of Counterface Topography on the Wear of Ultra-High Molecular Weight Polyethylene Under Wet and Dry Conditions", Proc. of the ACS Division of Polymeric Materials : Science and Engineering, 50, pp 226-232.

23. DUMBLETON, J.H. & SHEN, C. (1976) : "The Wear Behaviour of Ultra-high Molecular Weight Polyethylene ", Wear, 37, pp 279-289.

24. EVANS, D.C. & LANCASTER, J.K. (1979) : "The Wear of Polymers", in Treatise of Materials Science and Technology, Academic Press Inc., 13, pp 86-134.

25. EISS, N.S., WOOD, K.C., HEROLD, J.A. & SMYTH, K.A. (1979) : "Model for the Transfer of Polymer to Rough, Hard Surfaces", J. Lubr. Technol., ASME Trans., 101, pp 212-219.

26. FALKNER, J.E. (1980) : "Introduction to Surface Texture Measurement", FWP Journal, pp 33-45.

27. FULMER MATERIALS OPTIMISER (1981) : "Characterisation and Specification of Thermoplastic Materials", L.M. Wyatt (ed), 3, 1.

28. FURBER, K., ATKINSON, J.R. & DOWSON, D. (1976) : "Wear Mechanisms for Nylon 66", The Wear of Non-Metallic Materials, Proc. 3rd Leeds-Lyon Symposium on Tribology, Edited by D. Dowson, M. Godet and C.M. Taylor, MEP, London, pp 25-31.

29. HALLING, J. (1975a) : "Principles of Tribology", MacMillan Press Ltd, London.

30. HALLING, J. (1976) : "Introduction to Tribology", Wykenham Publications, London.

31. KAR, M.K & BAHADUR, S. (1978) : "Micro-mechanisms of Wear at Polymer-Metal Sliding Interface", Wear, 46, pp 189-202.

32. KAR, M.K. & BAHADUR, S. (1982) : "An Investigation of the Temperature Rise in Polymer-Metal Sliding", Wear, 82, pp 81-92.

33. LANCASTER, J.K. (1969) : "Abrasive Wear of Polymers", Wear, 14, 4, pp 223-239.

34. LANCASTER, J.K. (1971) : "Estimation of the Limiting PV Relationships for Thermoplastic Bearing Materials", Tribology, 4, 2, pp 82-86.

35. LANCASTER, J.K. (1973) : "Dry Bearings : A Survey of Materials and Factors Affecting Their Performance", Tribology, 6, pp 219-251.

36. LEE, L-H., "Effect of Surface Energetics on Polymer Friction and Wear", Advances in Polymer Friction and Wear, L-H. Lee (ed), Polymer Science and Technology Symposia Series, Plenum Press, New York, 5A, pp 31-66.

37. LUDEMA, K.C. & TABOR, D. (1966) : "The Friction and Viscoelastic Properties of Polymeric Solids", Wear, 9, pp 329-348.

38. MAKINSON, K.R. & TABOR, D. (1964) : "The Friction and Transfer of Polytetrafluoroethylene", Proc. R. Soc., London, A281, pp 49-61.

39. MANAGER MAB, CHAMBER OF MINES RESEARCH ORGANISATION (1984) : Private Communication.

40. MATSUBARA, K. & WANATABE, M. (1966) : "The Wear Properties of High Density Polyethylene Irradiated with Gamma-Rays", Wear, 10, 3, pp 214-223.

41. MOORE, D.F. (1972a) : "The Friction and Lubrication of Elastomers", Pergamon Press, Oxford.

42. MOORE, D.F. (1975b) : "Principles and Applications of Tribology", International Series on Materials Science and Technology, 14, Pergamon Press, Oxford.

43. MUSTAFAEV, T.K. DOWSON, D., & GILLIS, B.J. (1976) : "The Lubricated Wear of High Density Polyethylene with Mineral Oil and Stearic Acid", The Wear of Non-Metallic Materials, Proc. 3rd Leeds-Lyon Symposium on Tribology, Edited by D. Dowson, M. Godet and C.M. Taylor, MEP, London, pp 65-71.

44. PLINT, A.G. & PLINT, M.A. (1984) : "A New Technique for the Investigation of Stick-Slip", Tribology International, 18, 4, pp 247-249.

45. POOLEY, C.M. & TABOR, D. (1972) : "Friction and Molecular Structure : The Behaviour of Some Thermoplastics", Proc. R. Soc. (London), A329, pp 251-274.

46. POWELL, P.C. (1983) : "Engineering with Polymers", Chapman & Hall Ltd, London.

47. SUH, N.P. (1973) : "The Delamination Theory of Wear", Wear, 25, pp 111-124.

48. RHEE, S.H. & LUDEMA, K.C. (1978) : "Mechanisms of Formation of Polymeric Transfer Films", Wear, 46, pp 231-240.

49. ROSTOKER, W. & GALANTE, J.O. (1976) : "Some New Studies on the Wear Bahviour of Ultra-High Molecular Weight Polethylene", J. Biomed. Mater. Res., 10, pp 303-310.

50. TABOR, D. (1974) : "Friction, Adhesion and Bourndary Lubrication of Polymers", Advances in Polymer Friction and Wear, L-H. Lee (ed), Polymer Science and Technology Symposia Series, Plenum Press, New York, 5A, pp 5-28.

51. TABOR, D. (1976) : "The Wear of Non-Metallic Materials : A Brief Review", The Wear of Non-Metallic Materials, Proc. 3rd Leeds-Lyon Symposium on Tribology, Edited by D. Dowson, M. Godet and C.M. Taylor, MEP, London, pp 25-31.

52. TABOR, D. (1981) : "Friction - The Present State of Our Understanding", J. Lubr. Technol., ASME Trans., 103, pp 169-179.

53. TANAKA, K. (1979) : "Friction and Wear of Semi-Crystalline Polymers Sliding Against Steel Under Water Lubrication", Wear of Materials 1979, S.K. Rhee, A.W. Ruff and K.C. Ludema (eds.), ASME, New York, pp 563-572.

54. TANAKA, K. (1981) : "The Transfer of Semi-Crystalline Polymers Sliding Against Smooth Steel Surfaces", Wear of Materials 1981, S.K. Rhee, A.W. Ruff and K.C. Ludema (eds.), ASME, New York, pp 98-106.

55. TANAKA, K. & MIYATA, T. (1977) : "Studies on the Friction and Transfer of Semi-Crystalline Polymers", Wear, 41, pp 383-398.

56. TANAKA, K. & UCHIYAMA, Y. (1974) : "Friction, Wear, and Surface Melting of Crystalline Polymers", Advances in Polymer Friction and Wear, L-H. Lee (ed), 5B, pp 199-350.

57. THORPE, J.M. (1982) : "Friction of Some Commercial Polymer-based Bearing Materials Against Steel", Tribology International, 15, 2, pp 69-74.

58. VINGSBO, O. (1979) : "Wear and Wear Mechanisms", Wear of Materials 1979, S.K. Rhee, A.W. Ruff and K.C. Ludema (eds.), ASME, New York, pp 620-635.

59. YUST, C.S. (1985) : "Tribology and Wear", International Metals Reviews, 30, 3, pp 141-154.

APPENDIX A

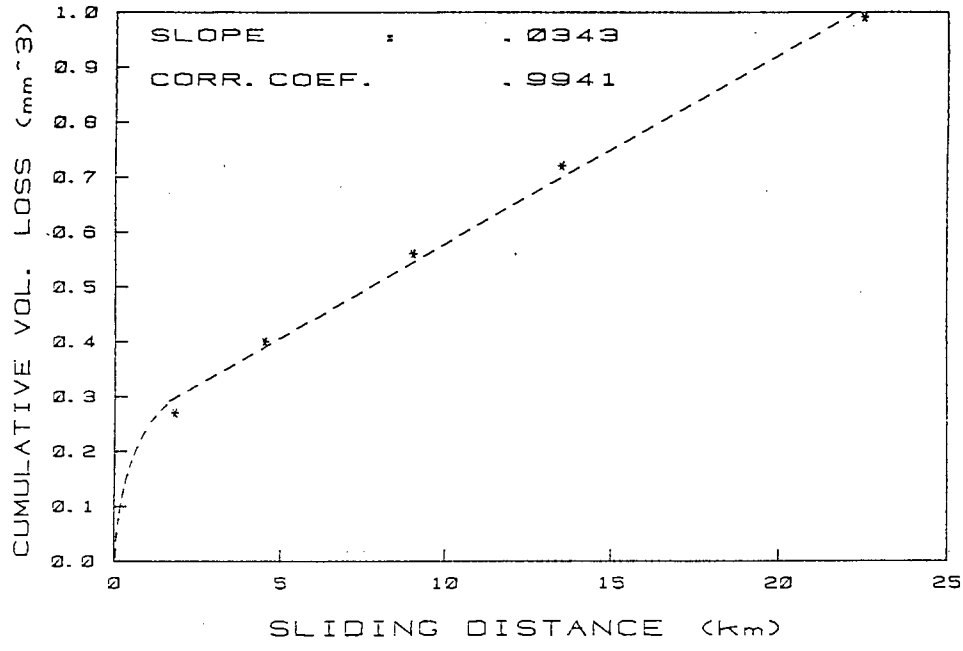

0.136 micrometers c.l.a.

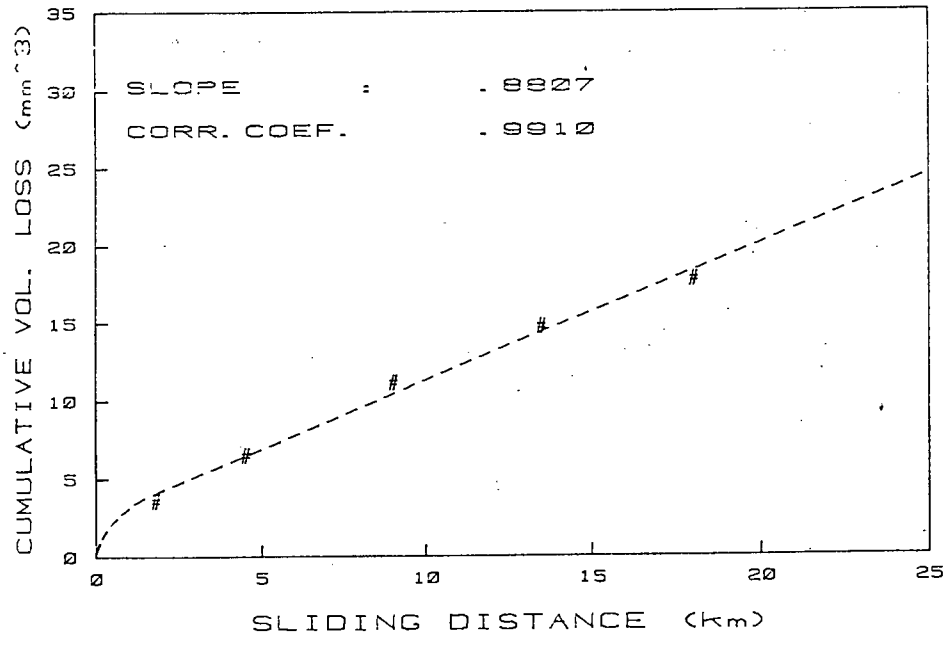

0.557 micrometers c.l.a.

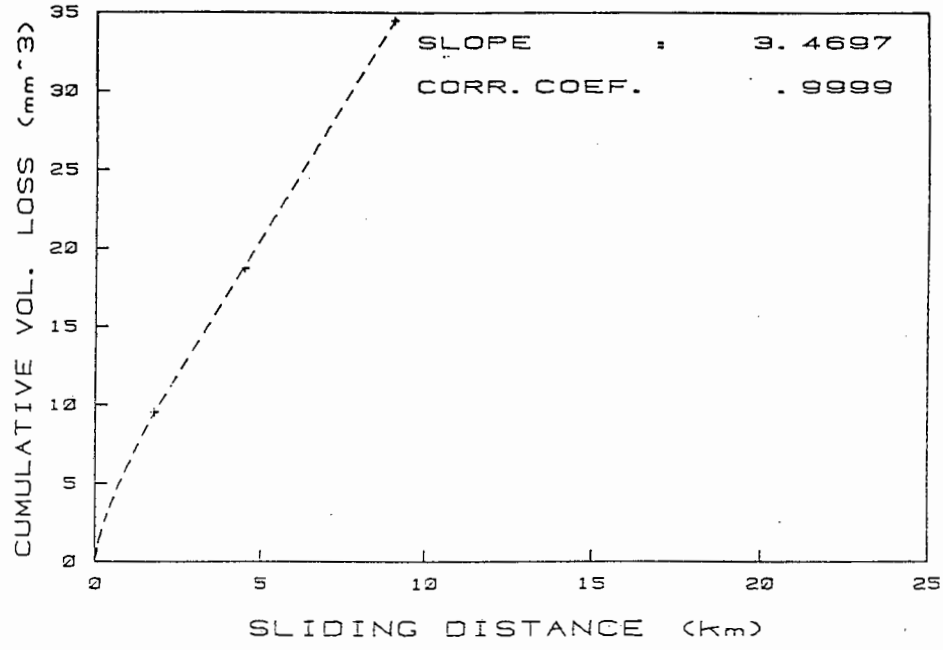

0.794 micrometers c.l.a.

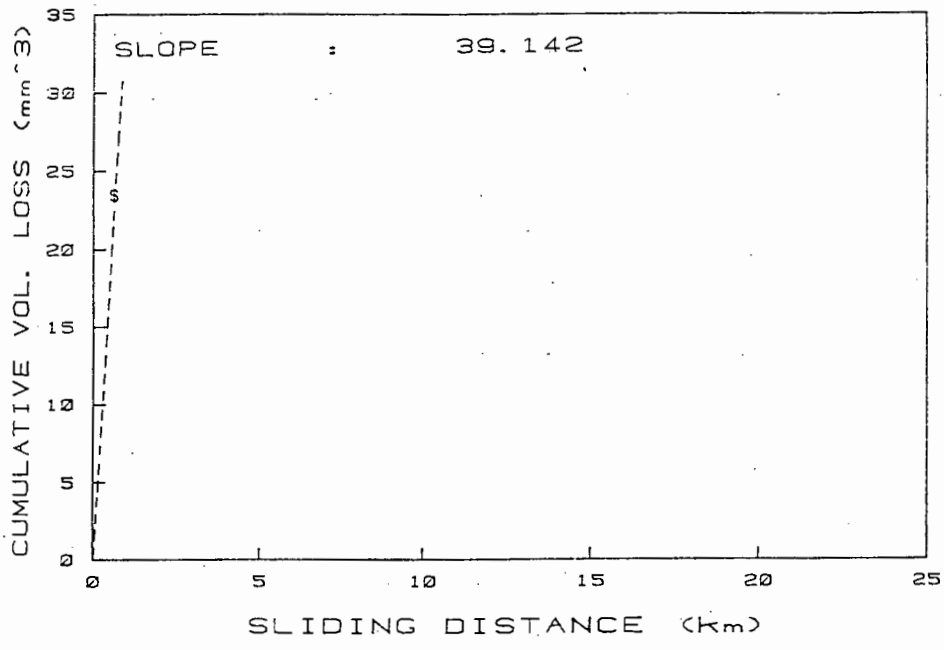

1.06 micrometers c.l.a.

APPENDIX B

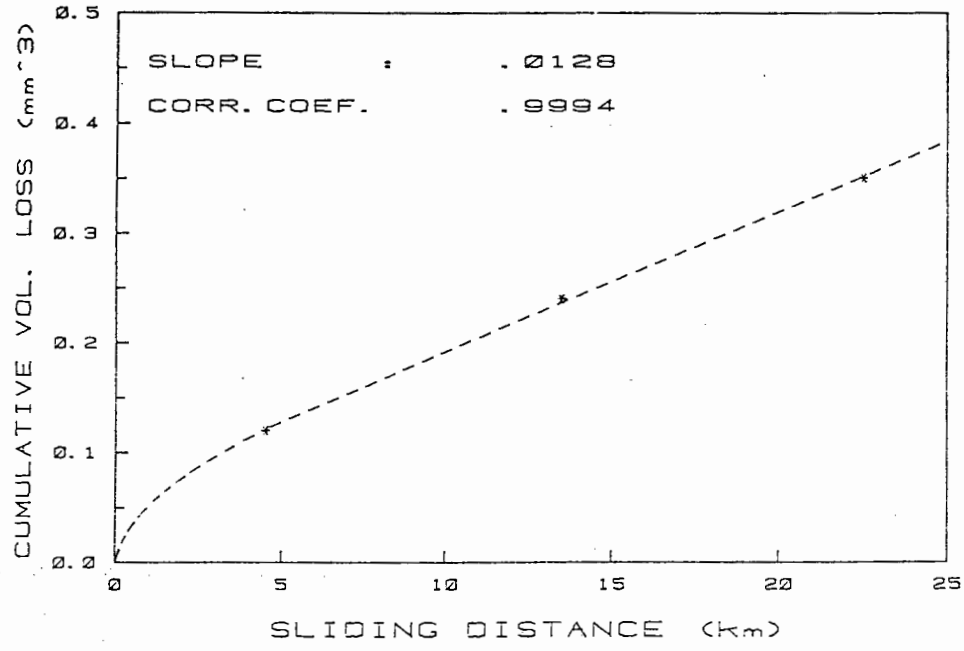

0.188 micrometers c.l.a.

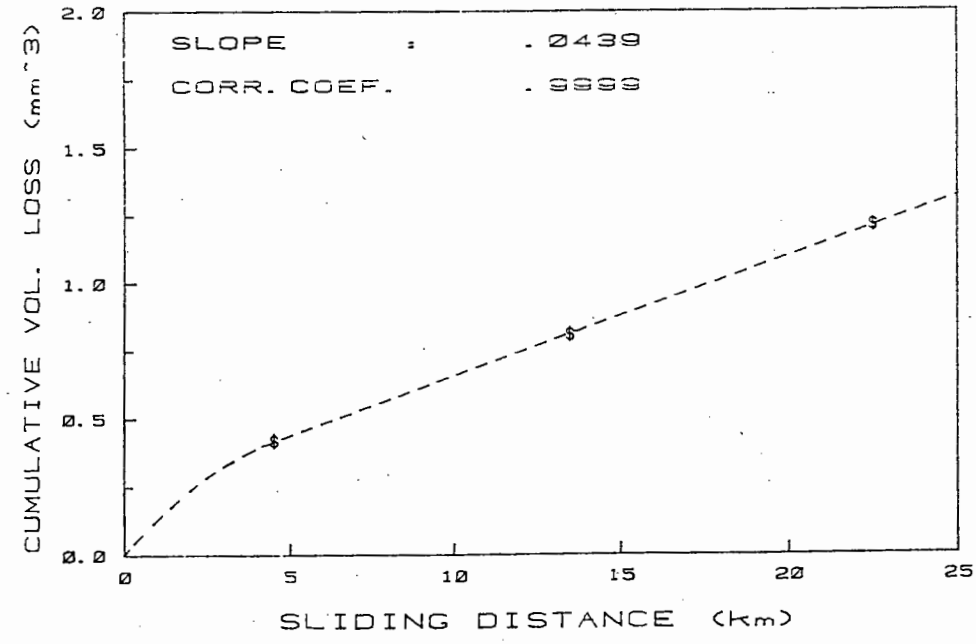

.339 micrometers c.l.a.

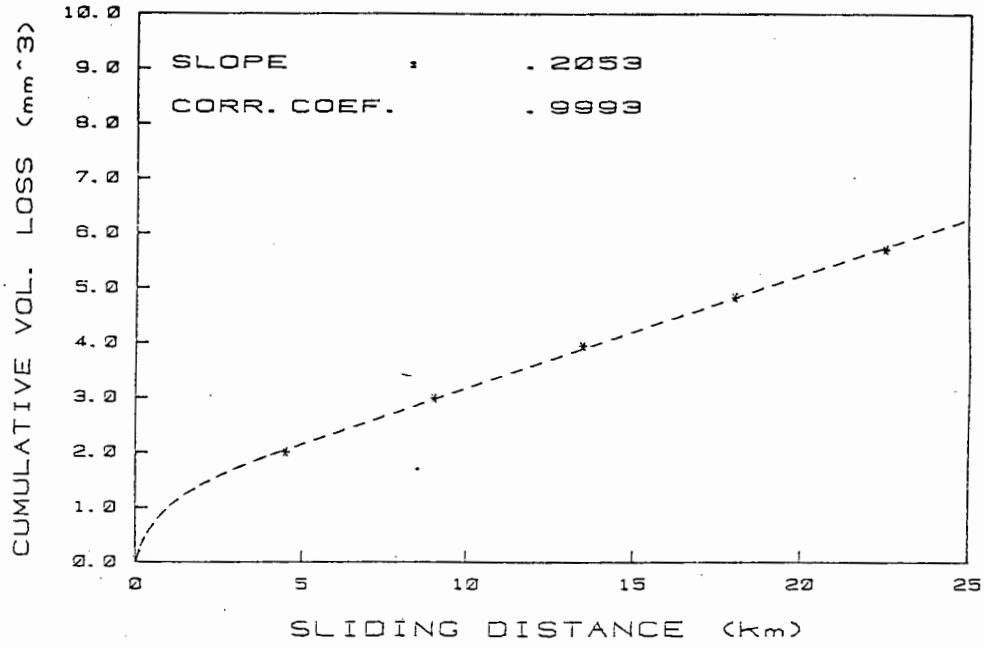

0.414 micrometers c.l.a.

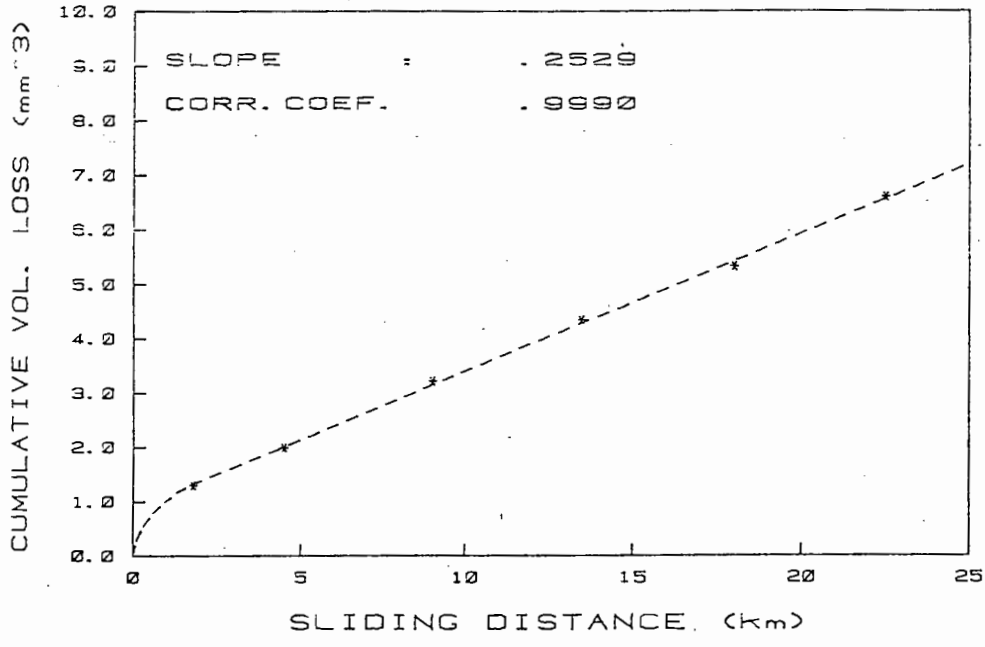

0.486 micrometers c.l.a.

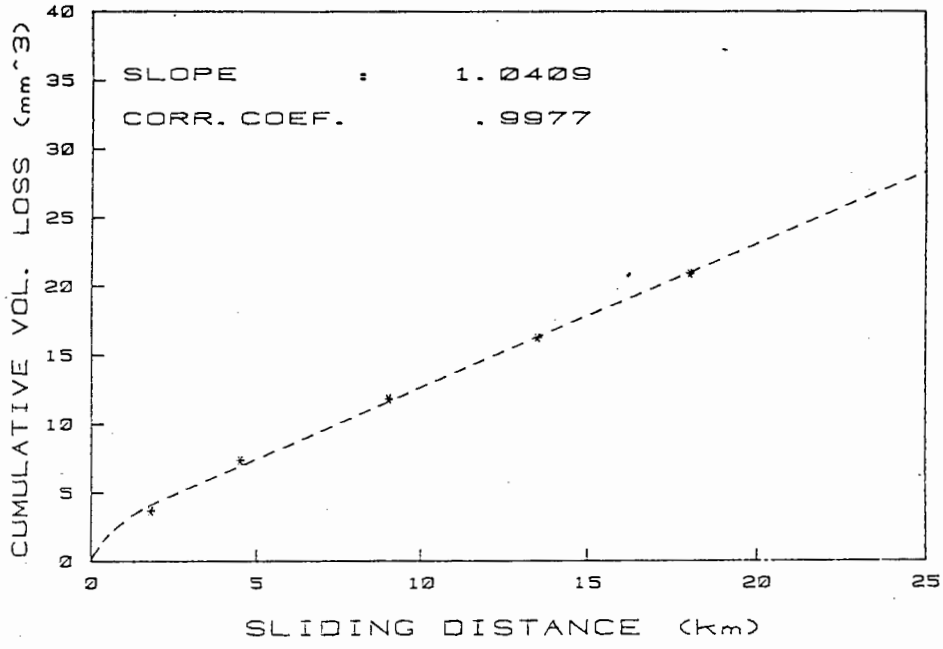

Ø.734 micrometers c.l.a.

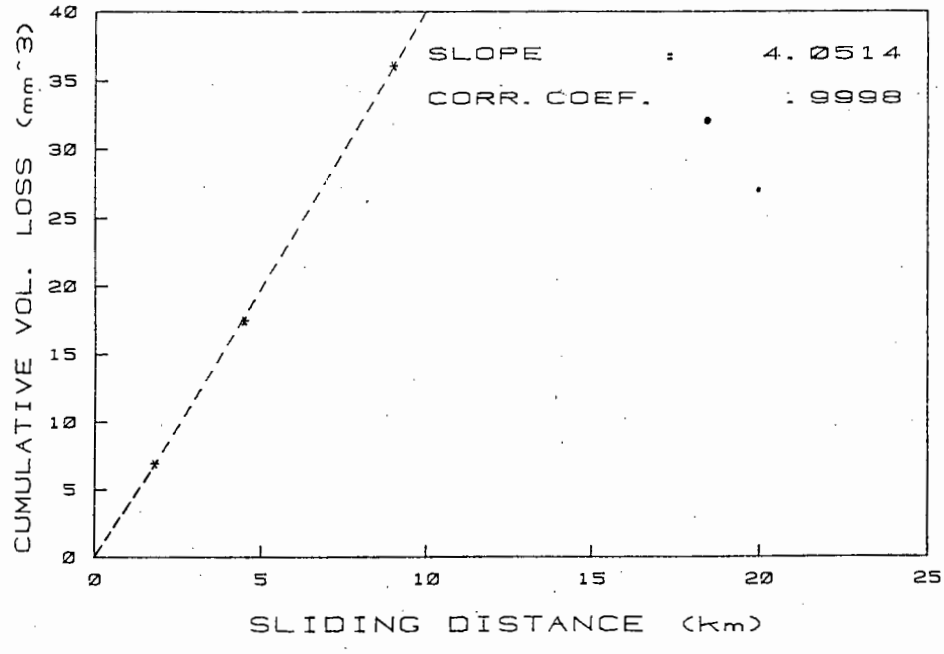

Ø.873 micrometers c.l.a.

APPENDIX C

Calculation of the wear depth of an UHMWPE seal in a hydraulic impact hammer operating continuously for 20 hours under lubricated conditions with no abrasive particles.

Assume 50% boundary contact.

Number of blows per hour = 18 000
Stroke of hammer per blow = 170×10^{-3} m
Pressure = 18 $N.mm^{-2}$

Thus, the distance of actual contact in 20 hours is:

$0,5 \times 20 \times 18\,000 \times 170 \times 10^{-3} = 30\,600$ m

Hence :

Wear depth = Specific wear rate x Pressure x Distance
(mm) = ($mm^3.N^{-1}.m^{-1}$) x ($N.mm^{-2}$) x (m)